AD NUMBER

AD828878

LIMITATION CHANGES

TO:

Approved for public release; distribution is unlimited. Document partially illegible.

FROM:

Distribution authorized to U.S. Gov't. agencies and their contractors; Critical Technology; DEC 1967. Other requests shall be referred to Air Force Cambridge Research Laboratory, CRDM, Hanscom AFB, MA 01730. Document partially illegible. This document contains export-controlled technical data.

AUTHORITY

afcrl ltr, 22 dec 1971

AFCRL-68-0037

STUDY TO OBTAIN DESIGN DATA FOR REENTRY ECM ANTENNA SYSTEMS (U)

Paul E. Bubing, Daniel L. McMenamin, and Arthur K. Jordan

REENTRY SYSTEMS DEPARTMENT
MISSILE AND SPACE DIVISION
GENERAL ELECTRIC COMPANY
P.O. BOX 8555, PHILA., PA. 19101

Contract No. F 19628-67-C-0210
Project No. 8671
Task No. 867100 Work Unit No. 86710001
Third Quarterly Technical Report
VOLUME 1 OF 2
DECEMBER 1967

CONTRACT MONITOR: WALTER ROTMAN
MICROWAVE PHYSICS LABORATORY

GE Report No. 67SD7343

Sponsored By

ADVANCED RESEARCH PROJECTS AGENCY
DEPARTMENT OF DEFENSE
PROJECT DEFENDER
ARPA ORDER NO. 693, AMENDMENT NO.1

Prepared For

AIR FORCE CAMBRIDGE RESEARCH LABORATORIES
OFFICE OF AEROSPACE RESEARCH
UNITED STATES AIR FORCE
BEDFORD, MASSACHUSETTS 01730

AFCRL-68-0037

STUDY TO OBTAIN DESIGN DATA FOR REENTRY ECM ANTENNA SYSTEMS (U)

Paul E. Bisbing, Daniel L. McMenamin, and Arthur K. Jordan

REENTRY SYSTEMS DEPARTMENT
MISSILE AND SPACE DIVISION
GENERAL ELECTRIC COMPANY
P.O. BOX 8555, PHILA., PA. 19101

Contract No. F 19628-67-C-0210
Project No. 8671
Task No. 867100 Work Unit No. 86710001
Third Quarterly Technical Report
VOLUME 1 OF 2
DECEMBER 1967

CONTRACT MONITOR: WALTER ROTMAN
MICROWAVE PHYSICS LABORATORY

GE Report No. 67SD7343

Sponsored By

ADVANCED RESEARCH PROJECTS AGENCY
DEPARTMENT OF DEFENSE
PROJECT DEFENDER
ARPA ORDER NO. 693, AMENDMENT NO.1

Prepared For

AIR FORCE CAMBRIDGE RESEARCH LABORATORIES
OFFICE OF AEROSPACE RESEARCH
UNITED STATES AIR FORCE
BEDFORD, MASSACHUSETTS 01730

ACKNOWLEDGMENT

This research was supported by the Advanced Research Projects Agency, Project DEFENDER, and was monitored by the Air Force Cambridge Research Laboratories, under Contract No. F19628-67-C-0210.

ABSTRACT

This report presents survey material on the effects of the reentry environment on the voltage breakdown characteristics of antennas. Enough is presently known about these effects to indicate their relative importance and to allow meaningful experiments to be designed to diagnose them. Effects of convection are not well understood because of conflicts among various theories and experimental data. High gas temperature effects are not adequately explained and insufficient data presently exist to allow extrapolation with confidence.

Results of some illustrative calculations of flow fields about a typical slightly blunt-nosed body are presented, including an assessment of the vibrational nonequilibrium effect, which is found to be important.

TABLE OF CONTENTS

LIST OF ILLUSTRATIONS

LIST OF ILLUSTRATIONS (Cont)

LIST OF ILLUSTRATIONS (Cont)

SECTION 1
INTRODUCTION

The study of which this report is a part is concerned with the effects of the reentry environment of a slender hypersonic vehicle on the transmission of ECM signals. The most important aspect of this study is the effects of reentry on antenna breakdown. The effort during this reporting period, as well as the last, was concentrated on a survey of reentry effects on antenna breakdown and included visits to the facilities of some of the workers in the field. In addition, illustrative calculations of matched inviscid-boundary layer stagnation line flow field calculations have been performed for three altitudes of reentry of a 0.5 inch radius body, and the effects of vibrational nonequilibrium in the shock layer at 250 kilofeet altitude have been evaluated by a superpositional method.

A phenomenological theory of reentry effects on antenna breakdown is surveyed in terms of the continuity equation and the net ionization frequency. This theory is applied to illustrative calculations and to the generation of constraints on future experimental parameters.

SECTION 2
FLOW FIELD ANALYSIS

2.1 SHOCK LAYER STAGNATION LINE SOLUTIONS

Profiles of the flow properties along the stagnation streamline within the shock layer have been obtained from matched inviscid-boundary layer chemical nonequilibrium pure air solutions for altitudes of 250, 200, and 150 kilofeet. These profiles are required as initial conditions for the nonequilibrium boundary layers which are to be computed during the last quarter of this study; they are, however, of considerable interest in themselves and as such are presented separately from the boundary layer solutions.

In shock layer applications, the stagnation line matched inviscid-boundary layer problem is coupled, i.e., the inviscid solution must be used to provide edge conditions for the boundary layer solution, which in turn must be known to locate the bow shock as influenced by boundary layer displacement. The matched solution must, therefore, be obtained by iteration. The procedure used herein is to first assume the boundary layer profiles necessary to locate the edge at which the inviscid solution is terminated, thereby supplying the necessary edge conditions. The boundary layer solution with these edge conditions is obtained and these profiles are then used to relocate the edge. The process is repeated until the change in the edge is less than a specified small tolerance, after which the solutions are considered matched.

Before proceeding to a description of both the inviscid and boundary layer solutions, it is appropriate to point out that both solutions have identical thermodynamic and nonequilibrium chemical reaction systems, and both assume the condition of thermal equilibrium.

2.1.1 THE INVISCID SOLUTION

In the inviscid region of the shock layer, the solution is provided by the streamtube method of McMenamin and O'Brien[1] which was described in detail in the First Quarterly Technical Report. The governing variable used with the streamtube method is the streamwise velocity obtained from a correlation of data from Burke, Curtis and Boyer[2]; these data are the result

of the inverse shock nonequilibrium inviscid shock layer solution of Cornell Aeronautical Laboratory. The correlation which reproduces the data of Reference 2 to within $\pm$ 8 % is given by:

$$v = v_s (1 - s/\Delta)^b \qquad (2.1.1.-1)$$

in which v is the streamwise velocity, v_s is the velocity behind the shock wave, s is the distance from the shock wave, Δ is the shock detachment distance, and the exponent is given by:

$b = 1$ for $v_s \leq 1670$ ft/sec

$b = 0.000596\, v_s$ for $v_s > 1670$ ft/sec

The nonequilibrium shock detachment distance required for the inviscid shock layer solution is obtained in the following manner. By examining a multitude of shock detachment distances from equilibrium air and perfect gas ($1 \leq \gamma \leq 5/3$) flow field solutions for spherical noses, Storer[3] found that all cases could be correlated with excellent agreement by the formula

$$\frac{\Delta}{R_N} = 0.75 \left(\frac{\rho_\infty}{\rho_s}\right) + 1.543 \left(\frac{\rho_\infty}{\rho_s}\right)^{3.571} \qquad (2.1.1\text{-}2)$$

in which R_N is the sphere radius, ρ_∞ is the free stream density and ρ_s is the density behind a normal shock wave corresponding to either the equilibrium air or perfect gas shock solution as the case may be. Since the gas density in the stagnation region for either equilibrium air or a perfect gas is nearly constant, it might be expected that the shock detachment distance could be essentially specified by the density behind the normal shock. This cannot be true for the nonequilibrium flow, however, because the density varies from the frozen value ($\gamma = 7/5$) at the shock wave to the equilibrium value at the stagnation point. Nevertheless, because Storer's formula applies equally well to both the extremes of nonequilibrium flow, it might be expected to apply also in the nonequilibrium case if the density behind the

shock were replaced by a suitable average density along the stagnation streamline. Indeed, this has been found to be the case and good agreement with the nonequilibrium shock detachment data of Reference 2 has been obtained when ρ_s in Storer's formula is replaced by

$$\rho = \frac{1}{\Delta_{FROZ}} \int_{0}^{\Delta_{FROZ}} \rho \, ds \qquad (2.1.1\text{-}3)$$

in which Δ_{FROZ} is the frozen shock detachment distance, and ρ is the density from the nonequilibrium streamtube solution which is obtained using the velocity correlation with $\Delta = \Delta_{FROZ}$.

2.1.2 BOUNDARY LAYER SOLUTION

In the boundary layer region of the shock layer the solution is provided by the implicit finite difference method of Blottner[4]. At the stagnation point the boundary layer equations degenerate to a set of ordinary nonlinear differential equations with two-point boundary conditions. After a transformation to the Howarth-Dorodnitsyn coordinates system, Blottner solves the linearized set of governing equations by an implicit finite difference scheme which requires the successive inversions of a tridiagonal matrix. The governing equations which must be solved are of the form

$$\frac{d^2H}{d\eta^2} + \alpha_1 \frac{dH}{d\eta} + \alpha_2 H + \alpha_3 = 0 \qquad (2.1.2\text{-}1)$$

in which η is the transverse Howarth-Dorodnitsyn coordinate and H represents the longitudinal velocity ratio u/u_e, the temperature ratio T/T_e, the species mass fractions C_i, or the element mass fractions C^j depending on whether the momentum, energy, species continuity, or element conservation equation is being considered. Because of the linearization process the coefficients α_1, α_2, α_3 and α_4 depend on the unknown variables H. Thus, to start the solution, initial profiles of the dependent variables must be provided from which to calculate

the coefficients. The set of governing finite difference equations forms a tridiagonal matrix which yields the solution of the dependent variables after inversion. Based on these values of the dependent variables, the coefficients are recalculated and the process repeated until the change in the dependent variables for successive iterations is less than a specified small tolerance.

Calculations for a 0.5-inch-nose-radius body at velocities of 22.1, 22.0, and 21.95 kilofeet/second at altitudes of 250, 200, and 150 kilofeet, respectively, have been done. The results of the matched inviscid-boundary layer stagnation line solutions are presented in Figures 2.1.2-1 through 2.1.2-10, where successively, in groups of three, the inviscid and boundary layer solutions are compared at altitudes of 250, 200 and 150 kilofeet for the gas temperature, density, electron density, and pressure. In all cases the boundary layer edge was arbitrarily defined as the point where the derivative of the longitudinal velocity ratios equaled 1/10, i.e., at the point where

$$\frac{d\, u/u_e}{d\, \eta} = 1/10 \qquad (2.1.2\text{-}2)$$

The rather large mismatch in the solutions at 250 kilofeet is due to a convergence tolerance which is too large, an effect which was corrected for the lower altitudes. In all three cases the boundary layer displacement thickness is negative due to the cold wall condition and, with the exception of the highest altitude, it is so small as to be unnoticeable in the results. Also, in all three cases the catalytic wall condition (thermodynamic equilibrium) is imposed.

It should be noted that the rapid decrease in temperature and corresponding increase in density for the inviscid solution near the wall is caused by the equilibrium condition which is intrinsically required by reacting inviscid flows at a stagnation point.

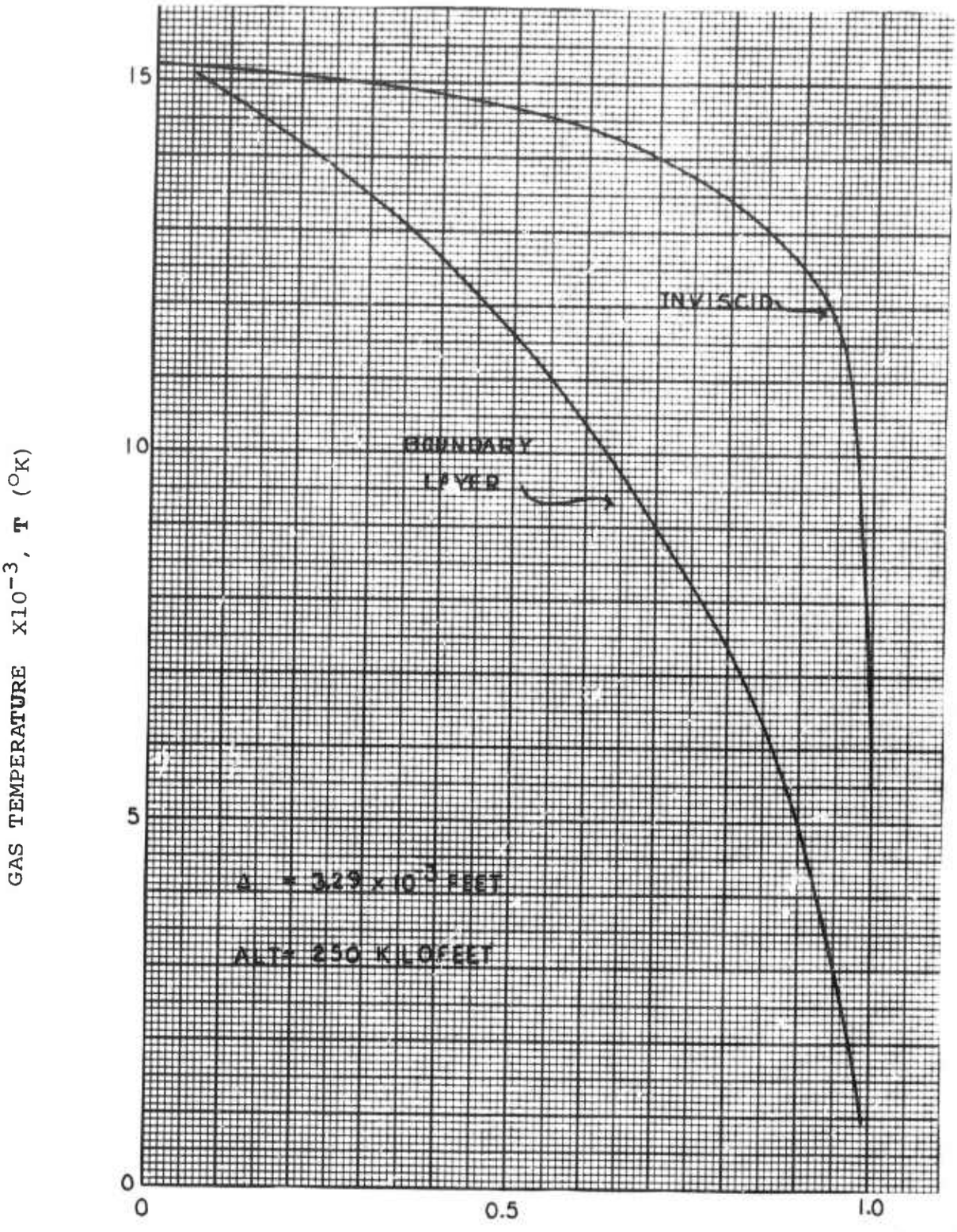

Figure 2.1.2-1. Matched Inviscid-Boundary Layer Solutions; Gas Temperature vs Normalized Distance from Shock Wave (250 kilofeet Altitude)

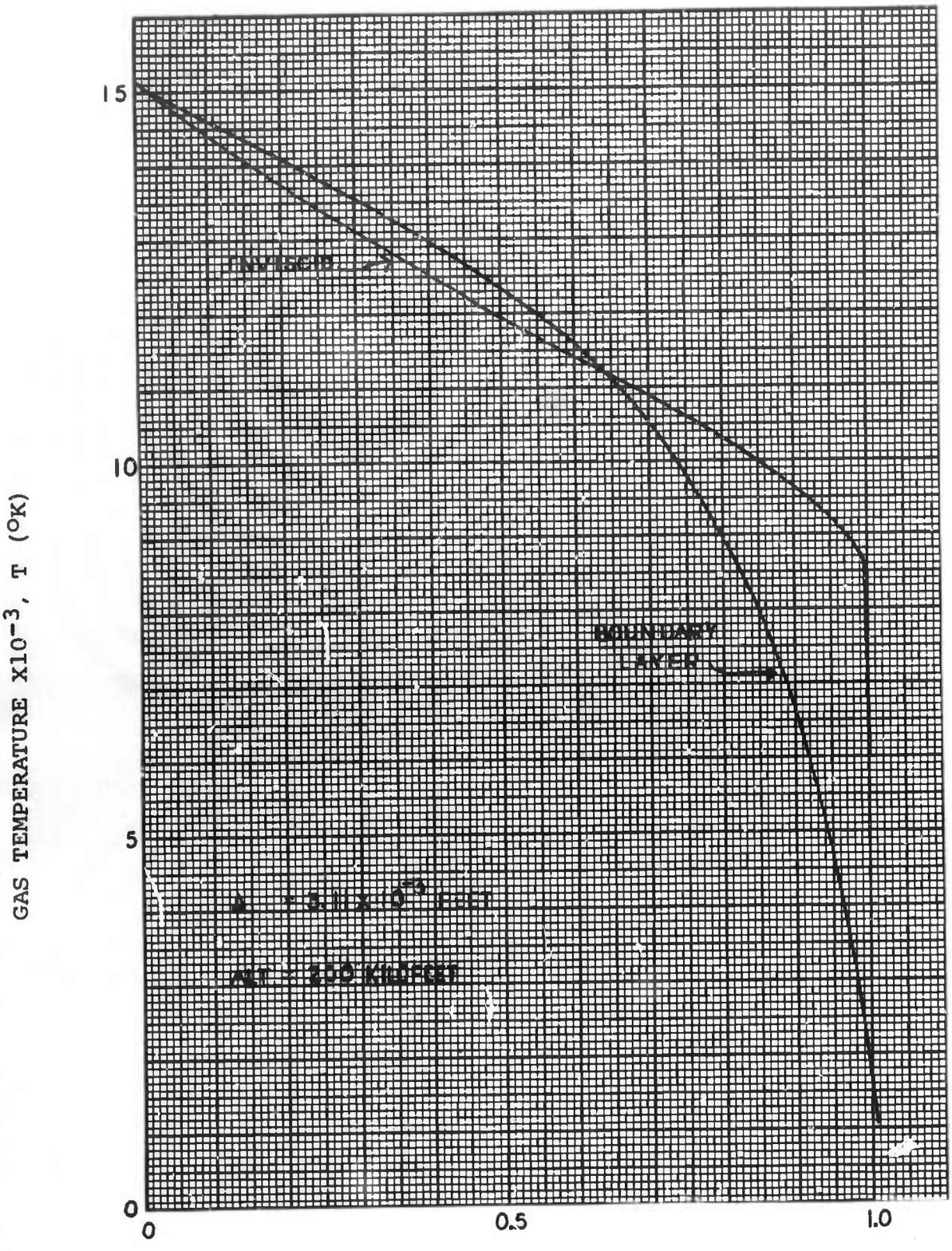

Figure 2.1.2-2. Matched Inviscid-Boundary Layer Solutions; Gas Temperature vs Normalized Distance from Shock Wave (200 kilofeet Altitude)

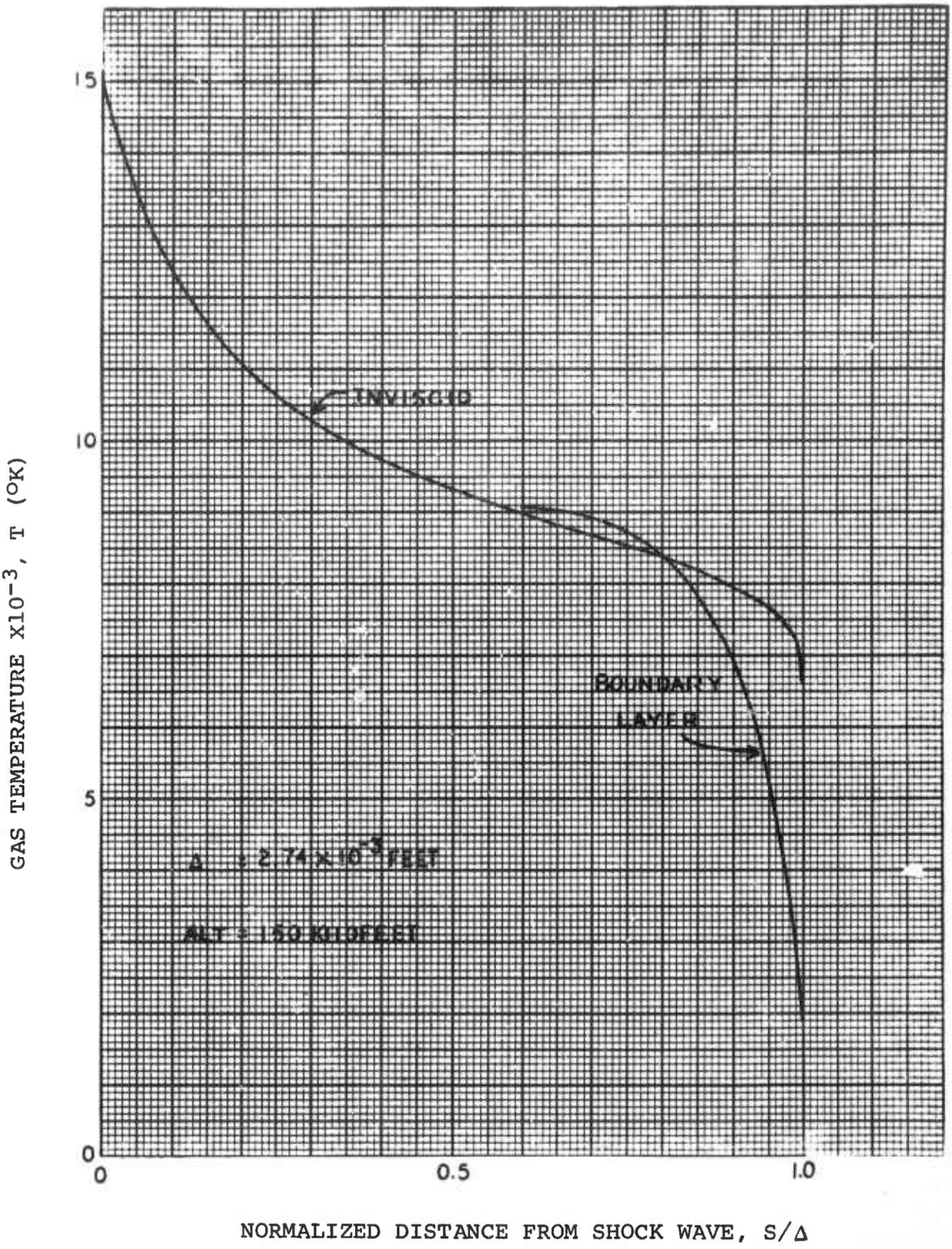

Figure 2.1.2-3. Matched Inviscid-Boundary Layer Solutions; Gas Temperature vs Normalized Distance from Shock Wave (150 kilofeet Altitude)

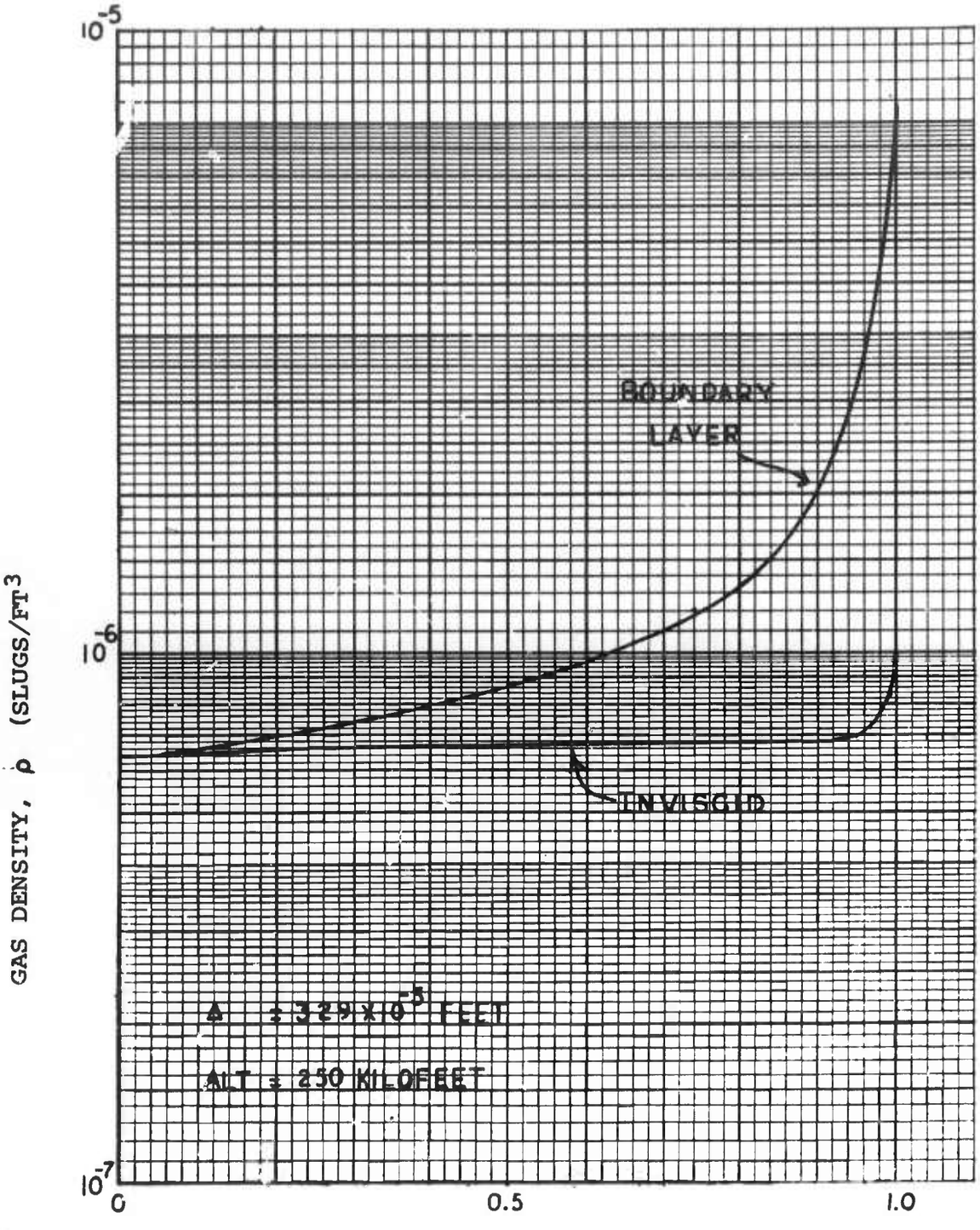

Figure 2.1.2-4. Matched Inviscid-Boundary Layer Solutions; Gas Density vs Normalized Distance from Shock Wave (250 kilofeet Altitude)

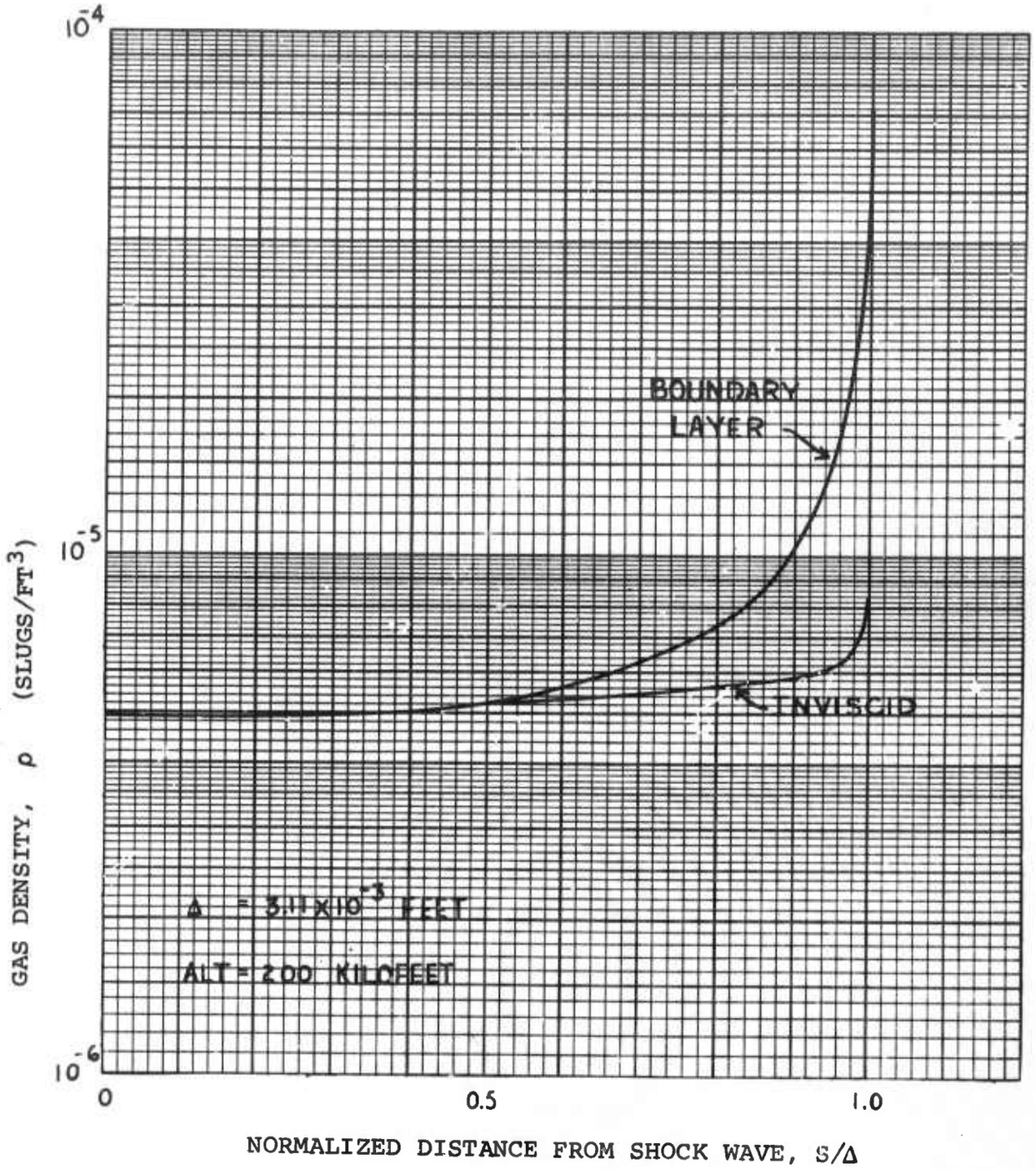

Figure 2.1.2-5. Matched Inviscid-Boundary Layer Solutions; Gas Density vs Normalized Distance from Shock Wave (200 kilofeet Altitude)

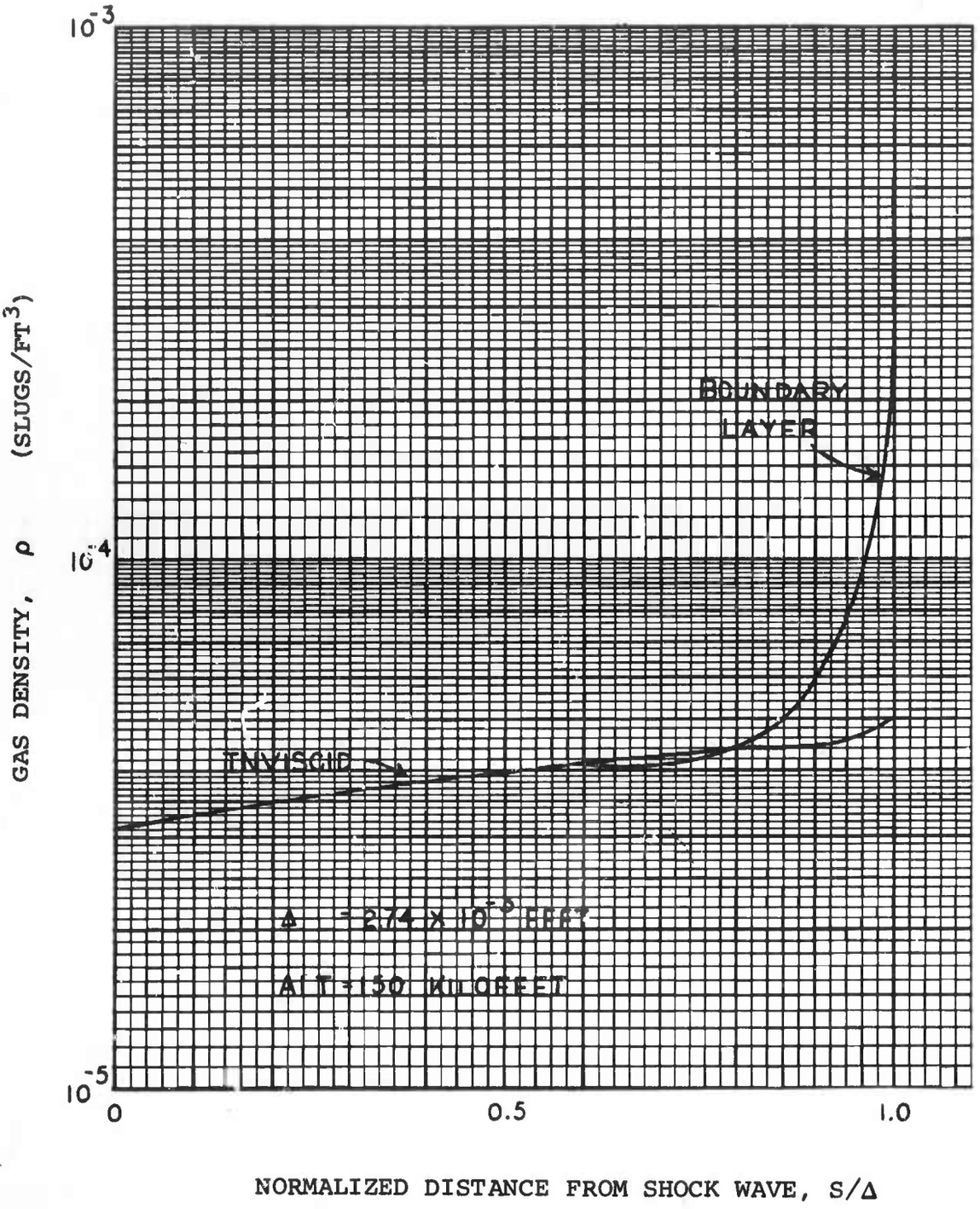

Figure 2.1.2-6. Matched Inviscid-Boundary Layer Solutions; Gas Density vs Normalized Distance from Shock Wave (150 kilofeet Altitude)

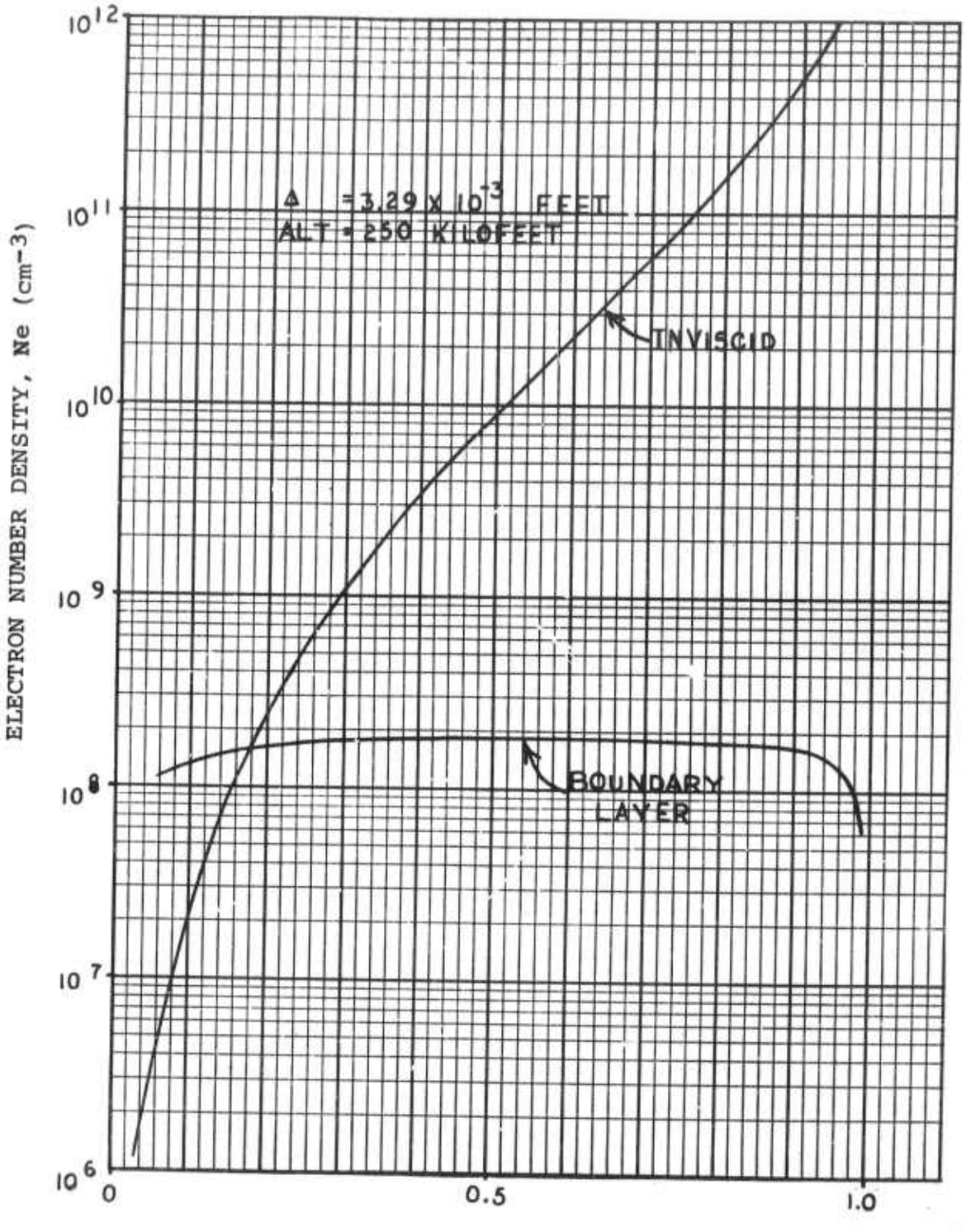

Figure 2.1 2-7. Matched Inviscid-Boundary Layer Solutions; Electron Density vs Normalized Distance from Shock Wave (250 kilofeet Altitude)

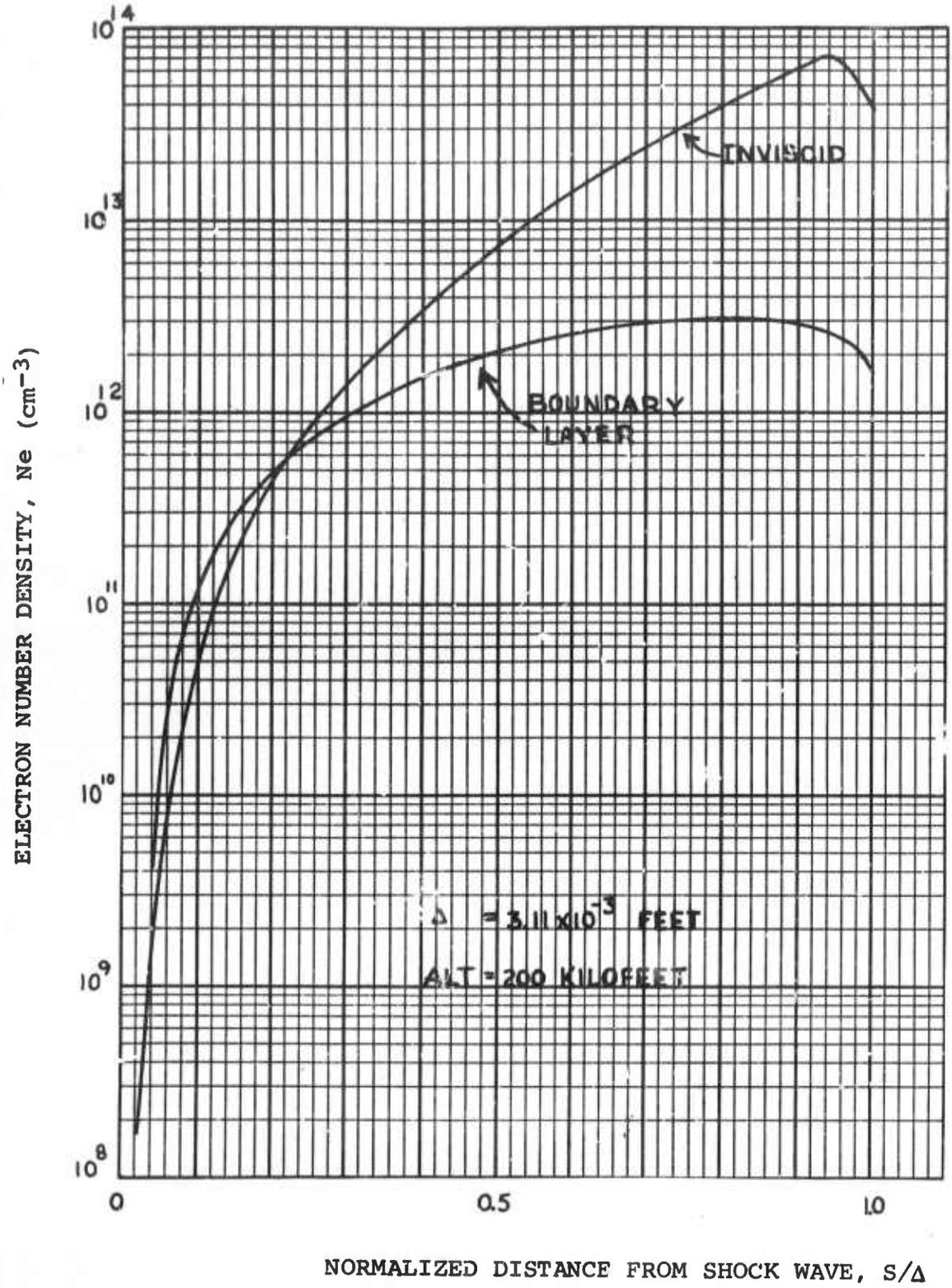

Figure 2.1.2-8. Matched Inviscid-Boundary Layer Solutions; Electron Density vs Normalized Distance from Shock Wave (200 kilofeet Altitude)

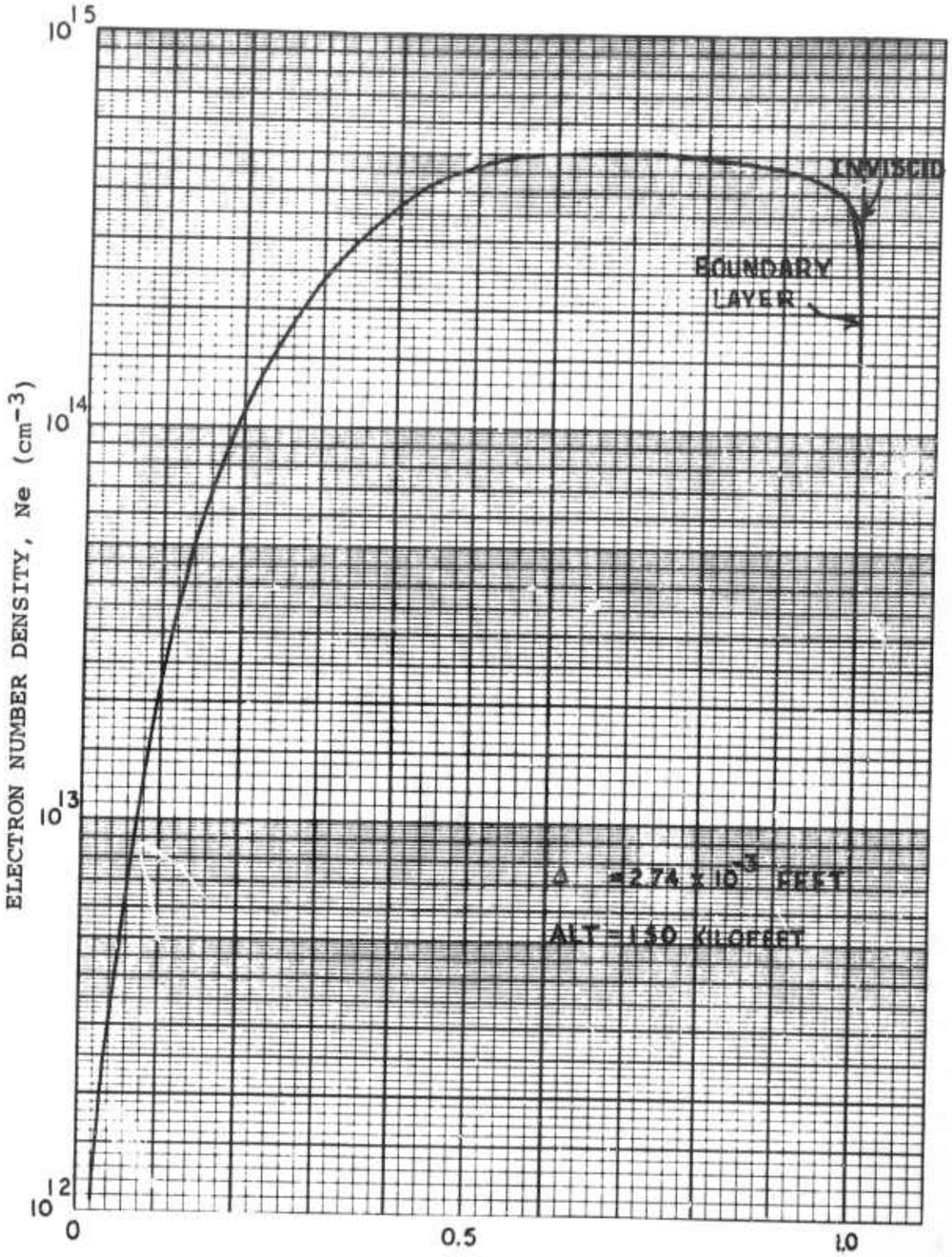

Figure 2.1.2-9. Matched Inviscid-Boundary Layer Solutions; Electron Density vs Normalized Distance from Shock Wave (150 kilofeet Altitude)

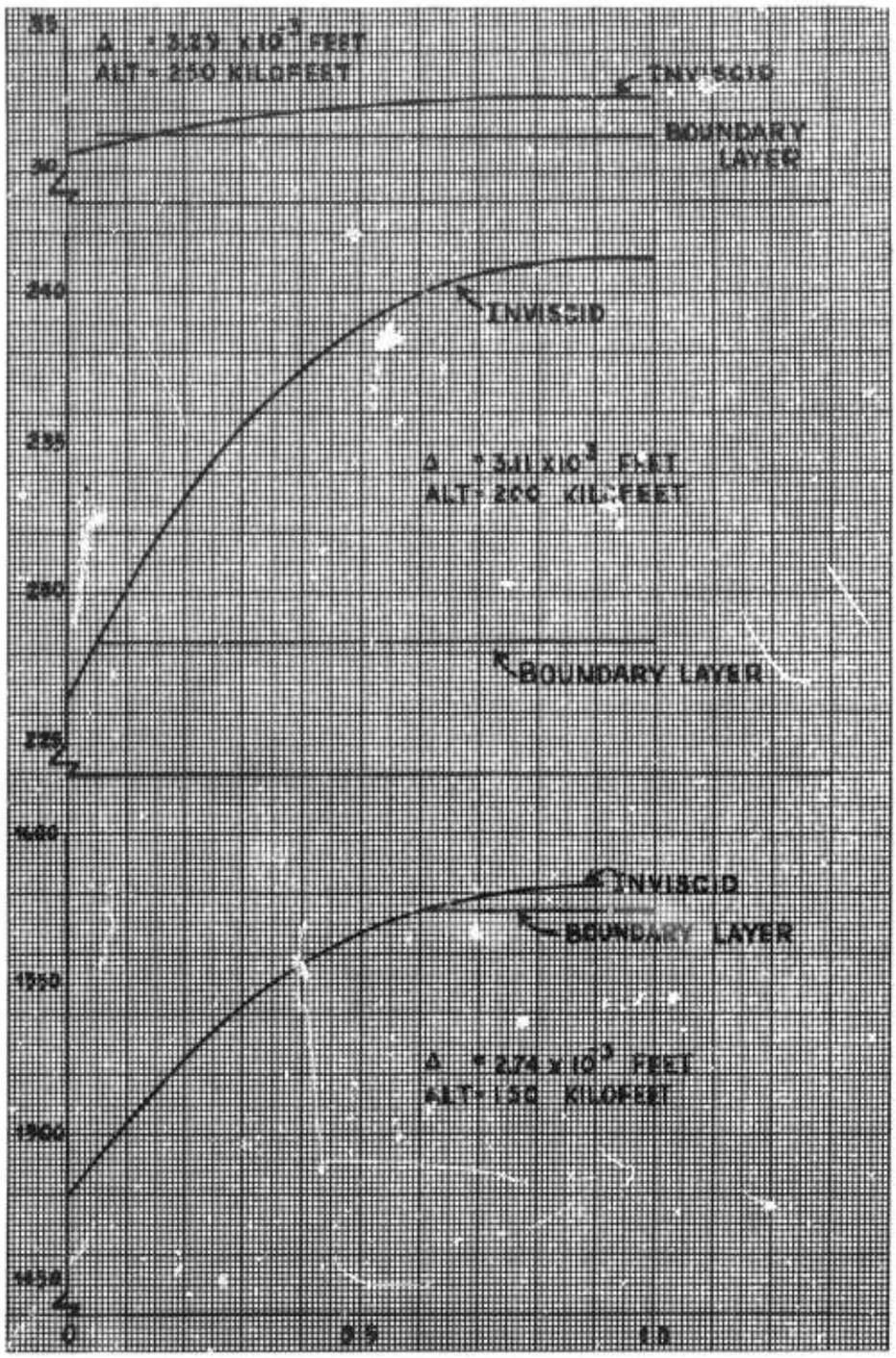

Figure 2.1.2-10. Matched Inviscid-Boundary Layer Solutions; Gas Pressure vs Normalized Distance from Shock Wave

2.2 VIBRATIONAL NONEQUILIBRIUM

The relative importance of vibrational nonequilibrium on the shock layer flow properties has been investigated by applying the superpositional method described in the Second Quarterly Technical Report to the inviscid flow field at 250 kilofeet. The highest altitude flow field was selected for investigation because, since vibrational relaxation times vary inversely with pressure, conditions for vibrational nonequilibrium are most favorable at higher altitudes. Based on this simplified, order-of-magnitude analysis it is concluded that vibrational nonequilibrium can cause substantial changes in the flow properties, particularly the gas temperature and density, and consequently must be taken into account to accurately predict the shock layer properties at higher altitudes. The analysis and the results which form the basis for this conclusion are discussed below.

The superpositional method used in this investigation consists of solving the uncoupled streamwise vibrational relaxation equation using superposition with the thermal equilibrium chemical nonequilibrium inviscid flow field to provide the values of the gas pressure and temperature required to calculate the local relaxation time and vibrational equilibrium energy. Only the primary molecular constituents N_2 and O_2 were considered, and the relaxation times for each of these species were obtained from Millikan and White[5]:

$$\tau_{O_2} = \frac{1}{p} e^{(129T^{-1/3} - 22.3)} \qquad (2.2\text{-}1)$$

$$\tau_{N_2} = \frac{1}{p} e^{(220T^{-1/3} - 24.8)} \qquad (2.2\text{-}2)$$

where the relaxation times τ_{O_2} and τ_{N_2} are in seconds, p is the gas pressure in atmospheres, and T is the gas temperature in degrees Kelvin. The harmonic oscillator model is used to define the vibrational temperature corresponding to the vibrational energy obtained from the solution of the relaxation equation and, therefore, is given by

$$T_v = \theta_v / \ell n \, (1 + R\theta_v/\epsilon_v) \qquad (2.2\text{-}3)$$

In the above expression T_v and ϵ_v are the vibrational temperature and energy, R is the universal gas constant and θ_v is the characteristic vibrational temperature which has a value of $2239^{\circ}K$ for oxygen and $3395^{\circ}K$ for nitrogen.

Some typical results of the analysis are shown in Figures 2.2-1 through 2.2-3 for streamlines which intersect the bow shock at shock angles of 89, 70, and 46 degrees, respectively. In these figures the streamwise variation of the vibrational temperatures of O_2 and N_2, as well as the gas temperatures obtained from solutions for thermal equilibrium chemical nonequilibrium and for perfect gas with $\gamma = 7/5$ (undissociated air with no vibrational excitation), are given as functions of the normalized distance along the body surface. In all cases the vibrational temperatures of both oxygen and nitrogen are characterized by an initial rapid rise from the free stream value at the shock. However, as the streamline continues to expand around the body, the drop in the gas pressure and temperature causes a rapid increase in the local relaxation time with a corresponding rapid leveling off ("freezing") of the vibrational temperature. If at this point the vibrational temperature is less than the equilibrium temperature, vibrational temperature will continue to rise gradually until the two are equal, which for this application, particularly for nitrogen, requires a considerable distance along the body. If the vibration temperature at the leveling off point is greater than the equilibrium temperature, the vibration temperature will decrease gradually until the two are equal. It can be seen that this latter situation is the case for the 89 degree shock angle streamline, whereas the former situation applies for the other two streamlines. Also, for the 89 degree streamline it may be noticed that the difference between the no-vibrational-excitation temperature and the thermal equilibrium temperature back on the conical portion of the body is about $2500^{\circ}K$ or about 45% of the equilibrium temperature. In this case, however, this temperature difference should not be interpreted as indicative of the extent of vibrational nonequilibrium effects because both the oxygen and nitrogen vibrational temperatures are above the thermal equilibrium temperature. As a result of this, if, in the solution of the coupled problem, gas temperature changes from thermal equilibrium do not significantly affect the chemical activity,

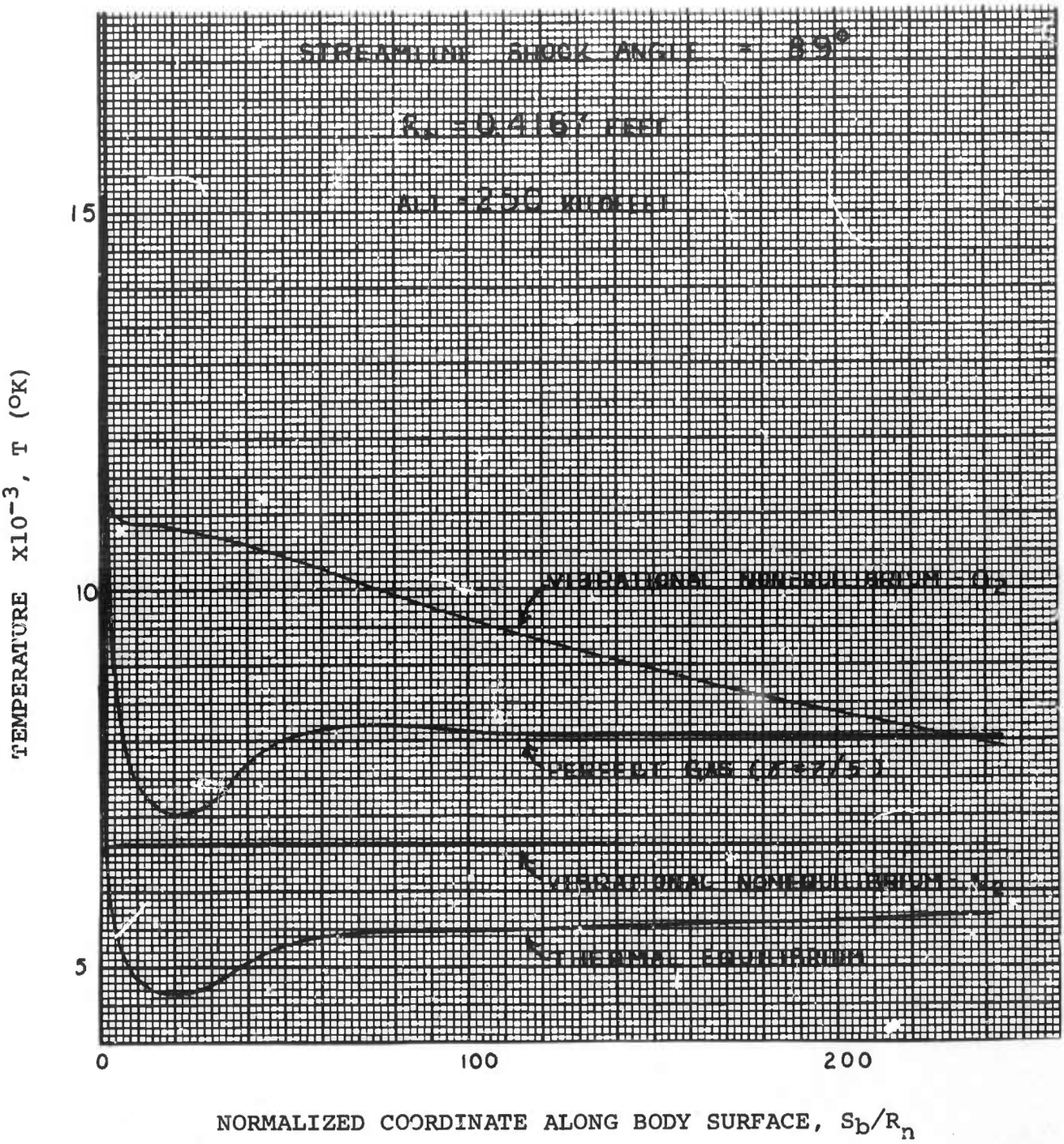

Figure 2.2-1. Vibrational Nonequilibrium; Streamwise Variation of Temperature vs Normalized Coordinate Along Body Surface (Streamline Shock Angle = 89 Degrees)

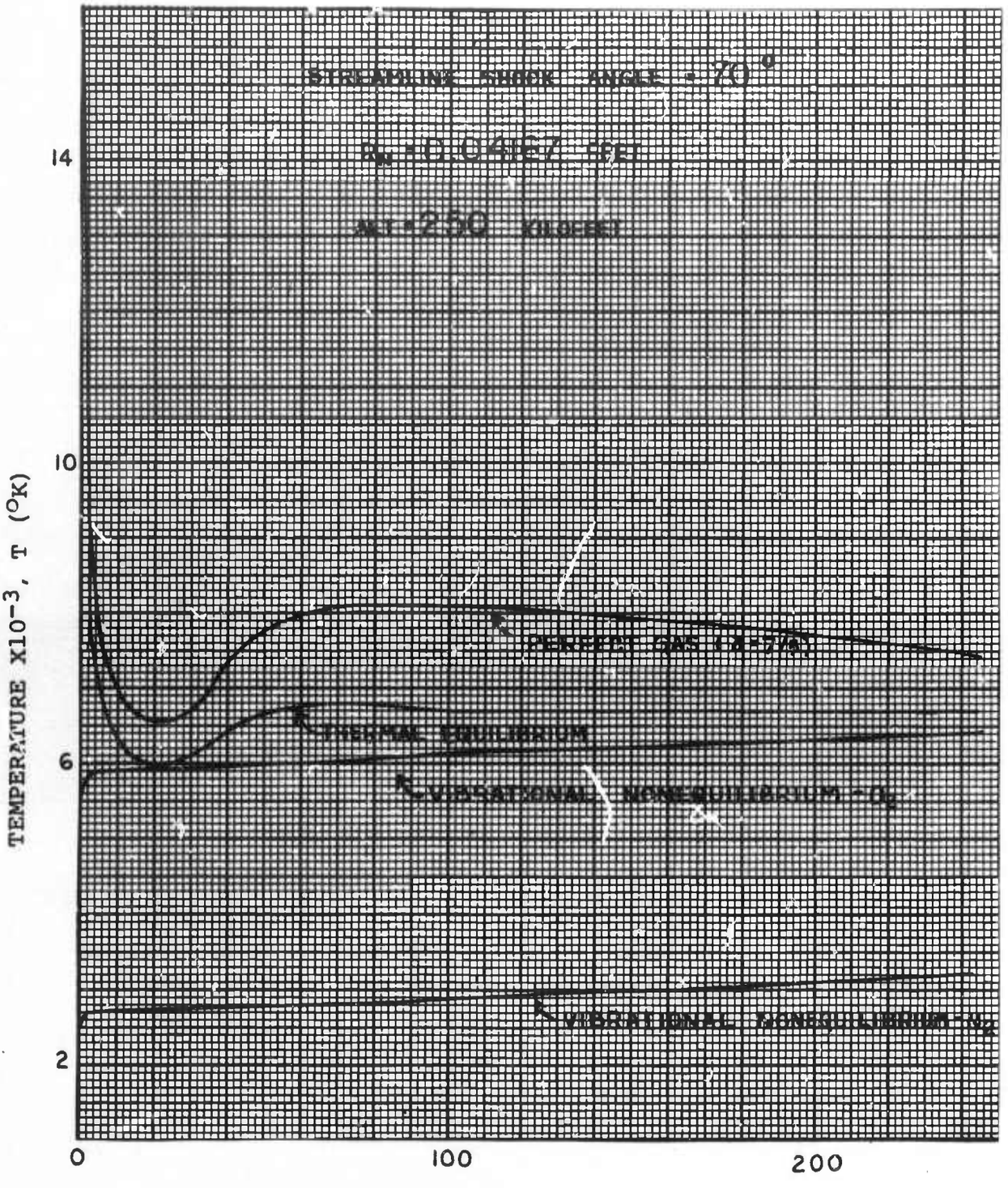

Figure 2.2-2. Vibrational Nonequilibrium; Streamwise Variation of Temperature vs Normalized Coordinate Along Body Surface (Streamline Shock Angle = 70 Degrees)

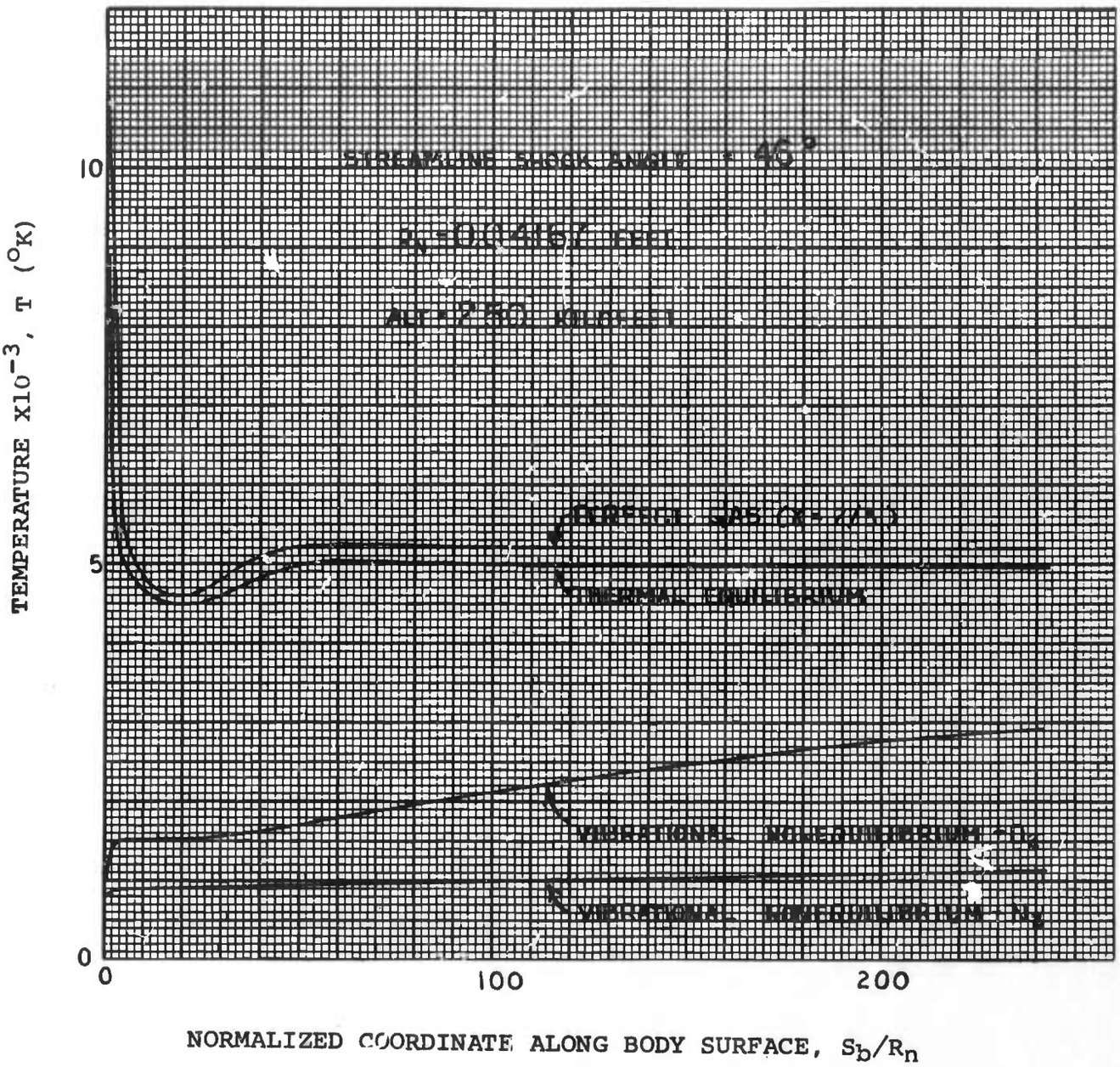

Figure 2.2-3. Vibrational Nonequilibrium; Streamwise Variation of Temperature vs Normalized Coordinate Along Body Surface (Streamline Shock Angle = 46 Degrees)

the gas temperature from the coupled solution would be below the equilibrium temperature shown in Figure 2.1.2-1. To evaluate the extent of vibrational nonequilibrium effects in this case would require a comparison with the gas temperature from a perfect gas solution with $\gamma = 9/7$ (full vibrational excitation). In the other two cases, however, where the vibrational temperatures are below the thermal equilibrium temperature, the gas temperature from the coupled solution would be between the $\gamma = 7/5$ curve and thermal equilibrium curve and, consequently, the difference between these two curves would indicate the extent of the vibrational nonequilibrium effects.

SECTION 3

REENTRY EFFECTS ON ANTENNA BREAKDOWN

The subject of this section is the effects of the hypersonic reentry environment of a slender cone body on voltage breakdown of an antenna mounted on the body. The discussion surveys ideas and data taken from written reports and private discussions with a number of researchers in the field. As indicated in a previous report in this series[6], the various slender cone vehicle flow field characteristics which can affect antenna breakdown may be listed as follows: convection, gas particle number density, gas temperature, ionization, chemical additives, and gradients of all flow field quantities.

The prediction of the effect of these flow field characteristics on the breakdown field of a given antenna can, in principle, be accomplished by either the kinetic theory method or the phenomenological method. The latter method is more instructive in a general survey and also it can fairly readily be applied to reentry phenomena using presently available theoretical and experimental data. Hence the discussion which follows treats the phenomenological theory of reentry effects on antenna breakdown. Accordingly the treatment will follow the development of the electron continuity equation, which describes the average rates of electron number density gains and losses.

Some of the effects of reentry enter into the continuity equation directly in explicit terms; others are implicit in various terms of the equation. An important term in the continuity equation is the ionization frequency in terms of its dependence on the microwave field intensity, which allows the breakdown field to be related to the solution of the continuity equation. Also, the antenna near-field distribution has an important implicit effect on the solution of the continuity equation, through the dependence of ionization frequency on local field intensity. Local gas temperature apparently has a strong effect on the ionization frequency at the temperatures induced by hypersonic reentry.

3.1 THE CONTINUITY EQUATION

The basic starting point in the phenomenological theory of antenna breakdown is the electron continuity equation:

$$\nabla \cdot \Gamma + \frac{\partial n}{\partial t} = \frac{dn}{dt} \qquad (3.1\text{-}1)$$

In this equation the electron flux vector Γ is related to the rate of change of electron density n with time t. The total derivative term on the right-hand side is meant to represent only the net effects of sources and sinks, such as ionization and attachment rates for collisions of electrons with neutral particles. If only electron-neutral collisions are included as electron sources or sinks, the continuity equation can be written in the following form:

$$\nabla \cdot \Gamma + \frac{\partial n}{\partial t} = \nu_n n \qquad (3.1\text{-}2)$$

where ν_n is the average net ionization frequency, including ionization minus attachment. (We omit the conventional bar over the symbol for average frequencies of reactions, since we will discuss only averages, implicitly assuming that the effects of the velocity distribution can be properly included in the average in a phenomenological way.)

Before one can proceed to the next step in the analysis, the effect of convection must be considered. The fact that the gas which is being subjected to the high near-fields of the antenna is moving fairly rapidly past the antenna means that either the electron flux must include a convective term or the frame of reference for time variations must move with the flowing gas. These two alternative views of convection give rise to the two prevalent classes of convection theories.

3.1.1 FINITE TIME THEORY

In the frame of reference of an observer moving with the gas velocity past the antenna, the local electric field intensity appears to vary with time in the same way as the variation of

antenna near-field along a streamline of the flow. In the very simple situation of uniform flow with velocity V through a region of uniform field of length L, the gas will be affected by the field for a length of time equal to L/V. In this case the analysis can be performed in exactly the same way as pulsed signal breakdown of a nonflowing gas, where the pulse duration is taken as L/V. (Of course, for pulsed signals in such a situation the effective pulse duration is either L/V or the actual pulse duration, whichever is shorter.) This is Kelly and Margenau's method[7]. The preceding simple finite time result is not strictly rigorous even under the simple uniform field, uniform flow conditions postulated, since the diffusion losses in the presence of the flow are not the same as those in the absence of flow. For example, in a uniform field region bounded by parallel plates, the electron density distribution is symmetrical about the midplane (the lowest order mode gives the well known result for the diffusion length L/π). But as shown in Figure 3.1.1-1, in the presence of gas flow between the plates the electron density distribution must be unsymmetrical, with the peak shifted toward the downstream side, since the gas on the downstream side has been under the influence of the field for the longest period of time. Note that this case is discussed only to illustrate, in the most fundamental way possible, how convection affects diffusion, so that the finite time result does not give the complete answer. We do not wish to imply that the situation depicted in Figure 3.1.1-1 is representative of the reentry problem.

The above objection to the finite time theory of convection is fundamentally related to the problem of coupling between convection and diffusion. This objection alone may not be very serious except in terms of the Cottingham theory (see below), but it will be true that the reentry flow field environment makes it particularly difficult to follow the breakdown process in the frame of reference of the flowing gas. Velocity gradients, or shear effects, will unduly complicate the problem mathematically. Also, the antenna nonuniform near-field distribution, even in the presence of uniform flow, would present a difficult problem, since it would be analogous to the problem of breakdown of a nonrectangular pulse.

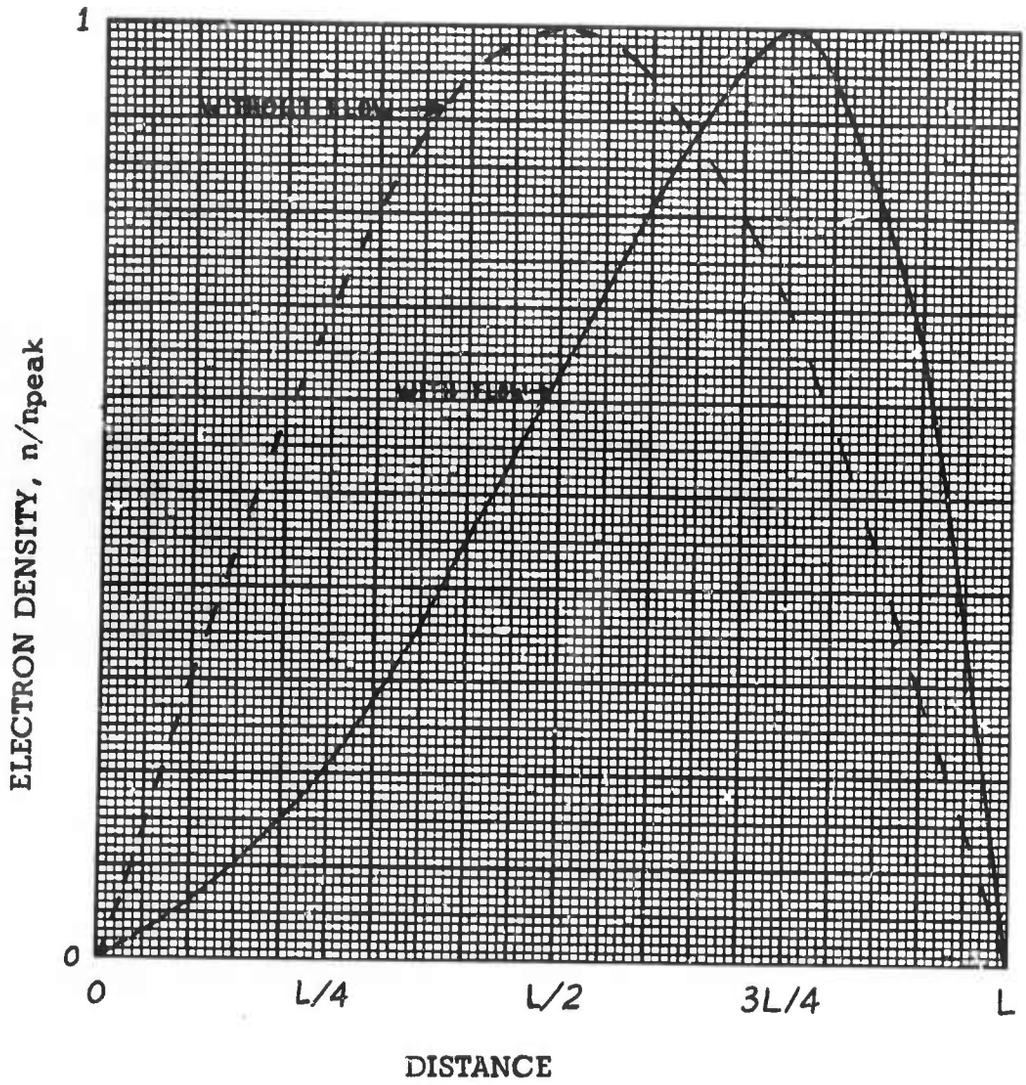

Figure 3.1.1-1. Effect of Gas Flow on the Electron Density Distribution in a Uniform Field Region, with Flow Normal to the Walls

3.1.2 COUPLED CONVECTION-DIFFUSION THEORY

The class of convection theories which couple the convection and diffusion phenomena is based on the use of the following equation for the electron flux vector:

$$\Gamma = nV - \nabla (Dn) \qquad (3.1.2\text{-}1)$$

where V is velocity and D is the diffusion coefficient. When this expression is substituted in Equation 3.1.2-2, the continuity equation becomes

$$\frac{\partial n}{\partial t} = \nu_n n + \nabla^2 (Dn) - \nabla \cdot (nV) \qquad (3.1.2\text{-}2)$$

Covert[8] has suggested a change of variable which eliminates the term in the divergence from the continuity equation. This change of variable may be generalized to allow for spatial variation of the diffusion coefficient.

Let

$$D_n = \psi \exp \left(\int \frac{V}{2D} \cdot dr \right) \qquad (3.1.2\text{-}3)$$

where r is the radius vector from an arbitrary origin. The exponent in this expression is proportional to the integral along a streamline of the ratio of the diffusion time to the convection time. The resulting form of the continuity equation is

$$\nabla^2 \psi + \left[\frac{\nu_n}{D} - \frac{1}{Dn} \frac{\partial n}{\partial t} - \nabla \cdot \left(\frac{V}{2D} \right) - \left(\frac{V}{2D} \right)^2 \right] \psi = 0 \qquad (3.1.2\text{-}4)$$

If separation of variables in space and time can be accomplished, this equation represents a homogeneous differential equation with, in general, a nonconstant coefficient.

Compare the form of Equation 3.1.2-4 with the equation which would result if convection were absent.

$$\nabla^2 (Dn) + \left[\frac{\nu_n}{D} - \frac{1}{Dn} \frac{\partial n}{\partial t} \right] Dn = 0 \qquad (3.1.2\text{-}5)$$

This equation is of exactly the same form, implying that the net ionization frequency with convection is given by

$$\frac{\nu_n}{D} = \left(\frac{\nu_n}{D} \right)_o + \nabla \cdot \left(\frac{V}{2D} \right) + \left(\frac{V}{2D} \right)^2 \qquad (3.1.2\text{-}6)$$

where the subscript o represents the absence of convection. This result actually can be true only at one point in the case of nonuniform electric field, but then it can be interpreted in terms of a breakdown criterion at the peak field point. With the exception of the more general term permitting compressible flow, Equation 3.1.2-6 is identical with the results of Romig[9] and Fante[10], which were derived without the aid of Covert's transformation, but with the use of boundary conditions and separation of variables. Thus the transformation allows the coupling between diffusion and convection to be displayed directly in the form of the ratio V/(2D) without the necessity of invoking boundary condition or separation of variables.

The example cited above of the simple one-dimensional situation of uniform gas flow between two parallel plates bounding a uniform field region offers a simple illustration of the result of the coupled convection-diffusion theory. The lowest order solution of Equation 3.1.2-4, for the condition of vanishing electron density at the boundaries and the steady state condition of vanishing $\partial\psi/\partial t$, is the following:

$$\psi = \psi_1 \sin \frac{\pi x}{L} \qquad (3.1.2\text{-}7)$$

$$\frac{\nu_n}{D} = \left(\frac{V}{2D}\right)^2 + \left(\frac{\pi}{L}\right)^2 \qquad (3.1.2\text{-}8)$$

where ψ_1 is the maximum value of ψ and x is the distance between the plates. Thus the electron density distribution is

$$n = n_1 \exp\left[(x - x_1)\frac{V}{2D}\right] \frac{\sin\frac{\pi x}{L}}{\sin\frac{\pi x_1}{L}} \qquad (3.1.2\text{-}9)$$

where n_1 is the peak electron density, occurring at the point x_1.

$$\tan\frac{\pi x_1}{L} = -\frac{2\pi D}{VL} \qquad (3.1.2\text{-}10)$$

This result has been plotted in Figure 3.1.1-1 for the case of $x_1 = 3L/4$. The value of V for this case is $2\pi D/L$, which would be on the order of 20,000 feet/second for air near the breakdown minimum using the free diffusion coefficient. Also, the value of ν_n is twice its value without flow in this example.

The above simple calculation, besides illustrating how the theory is applied, shows the magnitude of the results which it predicts. It will be seen below that the breakdown field varies as a relatively low power of the ionization frequency, so that the convection of air at 20,000 feet/second is predicted to increase the minimum breakdown power by only about 1 db. Of course, a greater effect would be observed in the presence of ionization, since the ambipolar diffusion coefficient is much less than the free diffusion coefficient, but it will be seen that the breakdown criterion then becomes an important consideration which modifies the result.

There are a few fine points which have been left out of the above discussion, since it was meant only as a very simple example. Equation 3.1.2-8 follows directly as a condition for the existence of a solution; but Equation 3.1.2-9 contains an arbitrary constant, the peak electron density, implying that the solution is not unique. The solution of Fante[10] for the problem of breakdown between parallel plates with flow parallel to the plates is just the opposite. There the electron density distribution is a unique function of the net ionization frequency; and the value of ν_n given by Equation 3.1.2-8 is a threshold above which the solution fails to exist. Of course, the one-dimensional flow problem solved above is physically impossible to realize without having the boundaries be perfectly porous to all particles but electrons. However, it may approximate the situation in which the afterglow decay beyond a uniform field region is extremely rapid.

W. C. Taylor (Stanford Research Institute, private communication) has pointed out that Fante's result applies only if the breakdown criterion is that the electron density becomes infinite. He finds that the peak electron density at lower values of ν_n is actually increased by orders of magnitude over the initial value,and that the finite time theory is a good approximation to the exact results if the breakdown criterion is relaxed to require only a significant rise from the initial electron density. This result makes the convection effect even weaker than it has been represented above. In other words, the coupled convection-diffusion theory represents an upper limit for the net ionization frequency at breakdown,and the finite time theory is a good approximation if a finite electron density is used as a breakdown criterion. Private communications with various investigators reveal that this viewpoint apparently agrees with shock tube experiment results for single pulse breakdown. These latter considerations probably apply only to the case of significant flow field ionization, which causes ambipolar diffusion and the modification of the breakdown criterion. But convection has a minor effect in the presence of free diffusion.

3.1.2.1 Space Charge Coupled Convection

The preceding discussion might lead to the conclusion that the convection effect is relatively unimportant, except for a theory of W. B. Cottingham (Purdue University, private

communication). This theory takes account of the coupling between space charge field and convection and diffusion of both ions and electrons. It is very similar in form to the simple coupled convection-diffusion theory discussed above, but it predicts a much different result for the effect of convection on breakdown field. Cottingham has verified this theory in experiments on multiple pulse breakdown in pipe flow.

The derivation starts with expressions for the electron and ion flux which resemble those of Allis and Rose[11].

$$\Gamma = nV - \nabla (D_- n) - \mu E n \qquad (3.1.2.1\text{-}1)$$

$$\Gamma_+ = n_+ V - \nabla (D_+ n_+) + \mu_+ E n_+ \qquad (3.1.2.1\text{-}2)$$

where D_- is the electron free diffusion coefficient, μ is the electron mobility, E is the space charge field, and the subscript + refers to the positive ions. In the steady state the electron flux is equal to the ion flux and the space charge field may be eliminated between these equations:

$$\Gamma = \frac{(\mu + \mu_+) n n_+ V - \mu_+ n_+ \nabla (D_- n) - \mu n \nabla (D_+ n_+)}{\mu n + \mu_+ n_+} \qquad (3.1.2.1\text{-}3)$$

According to Allis and Rose, the free diffusion of electrons at low electron densities is equivalent to the condition

$$D_+ n_+ = D_- n \qquad (3.1.2.1\text{-}4)$$

which gives

$$\Gamma = \frac{\mu + \mu_+}{\mu D_+ + \mu_+ D_-} D_- nV - \nabla (D_- n)$$

$$= \left(\frac{D}{D_a} \right) nV - \nabla (D_- n) \qquad (3.1.2.1\text{-}5)$$

where D_a is the ambipolar diffusion coefficient. Also, according to Allis and Rose, the ambipolar diffusion of electrons at high electron densities corresponds to equal electron and ion densities, giving

$$\Gamma = nV - \frac{\mu_+}{\mu + \mu_+} \nabla (D_- n) - \frac{\mu}{\mu + \mu_+} \nabla (D_+ n) \qquad (3.1.2.1\text{-}6)$$

Under the reasonable assumption that the ratio of electron and ion mobilities is independent of position, this gives

$$\Gamma = nV - \nabla (D_a n) \qquad (3.1.2.1\text{-}7)$$

It follows from Equations 3.1.2.1-5 and 3.1.2.1-7 that the electron flux vector is given by the following equation at the limits of either free or ambipolar diffusion.

$$\Gamma = \left(\frac{D_s}{D_a} \right) nV - \nabla (D_s n) \qquad (3.1.2.1\text{-}8)$$

where D_s is the transitional electron diffusion coefficient. This is Cottingham's equation. Under the "constant ratio approximation" (see below) this equation would apply to the transition from free to ambipolar diffusion as well as to just either limit, as derived above. The true form of this equation can be determined only by simultaneous solution of

Equations 3.1.2.1-1 and 3.1.2.1-2 with Poisson's equation, as done by Allis and Rose for the case of no convection; but, as pointed out by Allis[12], an equation like 3.1.2.1-8 is approximately correct when the transitional diffusion coefficient is related to the electron density by the proper criterion.

It is immediately apparent that the last equation is of the same form as Equation 3.1.2-1. Thus the space charge coupled convection theory can be viewed as a generalization of the simple diffusion coupled convection theory given above. Then the generalized continuity equation is

$$\nabla^2 \psi + \left[\frac{\nu_n}{D_s} - \frac{1}{D_s n} \frac{\partial n}{\partial t} - \nabla \cdot \left(\frac{V}{2D_s} \right) - \left(\frac{V}{2D_s} \right)^2 \right] \psi = 0 \qquad (3.1.2.1\text{-}9)$$

$$\psi = D_s n \exp \left(- \int \frac{V}{2D_s} \cdot dr \right) \qquad (3.1.2.1\text{-}10)$$

where V is to be interpreted as the flow velocity v in the ordinary coupled diffusion-convection theory and as $D_s v/D_a$ in the coupled space charge theory.

A simple physical interpretation of the latter theory can be made as follows. The convection of ions in the background of flowing gas creates a space charge force on the electrons which, because of the greater mobility of the electrons, makes convection more efficient by the ratio of the (transitional) diffusion coefficient to that for ambipolar diffusion. In fact if it is noted that the gas convection acts directly only on the ions, because the electron energy far exceeds the kinetic energy of convective motion, then the convective term in Equation 3.1.2.1-1 should be dropped. The first term in the numerator of Equation 3.1.2.1-3 would then involve only μ and not also μ_+, but this involves no difference in the results, since μ is much greater than μ_+ and is negligibly different from their sum.

Now the predicted result of convection is not negligible, especially when the the diffusion is free, since D_s/D_a can be as large as 100. This means that the result shown in Figure 3.1.1-1 can correspond to a velocity on the order of only 200 feet/second. Also, Equation 3.1.2-8 in the space charge coupled theory takes the form

$$\frac{\nu_n}{D_s} = \left(\frac{V}{2D_a}\right)^2 + \left(\frac{\pi}{L}\right)^2 \qquad (3.1.2.1\text{-}11)$$

And Equation 3.1.2-6 is

$$\frac{\nu_n}{D_s} = \left(\frac{\nu_n}{D_s}\right)_o + \nabla \cdot \left(\frac{V}{2D_a}\right) + \left(\frac{V}{2D_a}\right)^2 \qquad (3.1.2.1\text{-}12)$$

Therefore, a velocity of 20,000 feet/second could increase the ionization frequency by a factor of 10^4. But if this much increase in ionization frequency were to occur, it would probably create ambipolar diffusion, in which case Equation 3.1.2.1-12 would be, neglecting the divergence.

$$\nu_n = \nu_{n_o} \frac{D_a}{D_-} + \frac{V^2}{4D_a} \qquad (3.1.2.1\text{-}13)$$

where ν_{n_o} is the ionization frequency without flow under free diffusion conditions. This predicts that a flow velocity of 20,000 feet/second would increase the ionization frequency by a factor on the order of 100, which corresponds to about 4 db increase in the minimum breakdown power of air.

3.1.3 SEPARATION OF VARIABLES

Up to this point the time derivative of the electron density has been retained in the expression for the coefficient of the unknown function in the continuity equation. The discussion in the

previous section was based on the steady state assumption of vanishing time derivative, which corresponds to continuous wave (CW) breakdown. In order to obtain a solution for pulsed signal breakdown it is necessary to separate variables with respect to space and time.

It is customary, though not always explicitly stated, to assume that the quantities ν_n and D_s in Equation 3.1.2.1-9 are independent of time and, at most, functions only of position. This assumption is implicitly equivalent to assuming that the electron energies relax to their steady state distribution much more rapidly than the electron density distribution does. The time independence of D_s also implies that the electron density does not vary sufficiently widely to change the value of the transitional diffusion coefficient over an appreciable fraction of the time for onset of breakdown. Of course, V is an external parameter determined by the flow field properties and it is, at most, a function of position. Equation 3.1.2.1-9 separates as follows:

$$D_s \frac{\nabla^2 \psi}{\psi} + \nu_n - D_s \nabla \cdot \left(\frac{V}{2D_s}\right) - \frac{V^2}{4D_s} = \frac{1}{n} \frac{\partial n}{\partial t} = \gamma \qquad (3.1.3\text{-}1)$$

where γ is a separation constant.

$$n = n_o e^{\gamma t} \qquad (3.1.3\text{-}2)$$

where n_o is the initial electron density. Also for a pulsed signal

$$\gamma = \frac{1}{\tau} \ell n \frac{n_B}{n_o} \qquad (3.1.3\text{-}3)$$

where n_B is the electron density at breakdown and τ is the pulse time. The continuity equation in spatial coordinates is now

$$\nabla^2 \psi + \left[\frac{\nu_n - \gamma}{D_s} - \nabla \cdot \left(\frac{V}{2D_s} \right) - \left(\frac{V}{2D_s} \right)^2 \right] \psi = 0 \qquad (3.1.3\text{-}4)$$

Since γ vanishes in CW breakdown, the above result shows that the breakdown criterion for the ionization frequency for pulsed signals is:

$$\nu_{n_{pulse}} = \nu_{n_{CW}} + \frac{1}{\tau} \ell n \frac{n_B}{n_o} \qquad (3.1.3\text{-}5)$$

which is the result found by Gould and Roberts[13].

3.1.4 EFFECTS OF THE REENTRY ENVIRONMENT

The continuity equation generally leads naturally to a breakdown criterion involving the bracketed terms comprising the coefficient of ψ in Equation 3.1.3-4 in addition to a term involving a characteristic length determined by the geometry of the particular problem. The effects of the reentry environment appear implicitly in each of these terms, besides the already discussed explicit appearance of the convective velocity. Now consider each reentry phenomenon in terms of its effect on these terms.

3.1.4.1 Gas Density

The classical theory of microwave breakdown expresses breakdown criteria in terms of proper variable such as ν_n/p and Dp, where p is the pressure in torrs. These quantities generally normalize in approximately this way because of the dependence of collision frequencies on number density of gas particles. In voltage breakdown experiments under standard laboratory conditions, the practice is to express the state of the gas being tested in terms of pressure, since this is a directly measurable quantity. However, pressures in the reentry induced shock layer are often orders of magnitude higher than in the free stream. Also, because of increased gas temperature, shock layer density is not generally the same as in the free stream. Whitmer and MacDonald[14] have noted that the physically important parameter for breakdown is the gas density rather than pressure, since it is the number of gas particles per unit volume which determines the rates for all the processes which control

breakdown. Thus the use of either the free stream pressure or the shock layer pressure in predicting breakdown at a given altitude would give erroneous results. The distribution of gas density in the high field intensity region is the correct determining factor.

In order to give a quantity which is commensurable with the classically used parameter of pressure, most authors define a reduced pressure p*. Reilly[15] defines the reduced pressure in torrs in terms of the gas number density N in particles per cubic centimeter:

$$p^* = 2.9 \times 10^{-17} N \qquad (3.1.4.1\text{-}1)$$

Light and Taylor[16] define the reduced pressure in an equivalent way in terms of temperature T in ^{o}K:

$$p^* = 273\ p/T \qquad (3.1.4.1\text{-}2)$$

These corrections have the effect of shifting the curve of breakdown field versus altitude about 30,000 feet higher in altitude at velocities of the order of 22,000 feet/second, according to Whitmer and MacDonald[14].

Gas density effects have been observed in reentry flight experiments. Bisbing[17] showed that the observed period of breakdown of a slot antenna on a conical vehicle agreed with laboratory data in cold air when the air density corresponding to the inviscid flow region was used as the independent variable. Nanevicz[18] also showed that when the vhf breakdown data from Nike-Cajun flights is corrected for local density, it agrees roughly with laboratory measurements in cold air.

The gas density affects all the terms of the continuity equation in their proper variables form in terms of the reduced pressure p*, but the remaining reentry environmental factors affect only one or two terms each. Therefore, the remainder of the discussion of the effects of reentry on the continuity equation treats each of these terms in turn.

3.1.4.2 The Diffusion Coefficient

It is conceivable that the diffusion coefficient will be affected by flow field ionization, gas temperature, and chemical composition. The ionization effect on the diffusion coefficient is well known and has been discussed by many authors. As indicated above, it is necessary to recognize this fact by writing the diffusion coefficient as D_s, denoting transitional diffusion. The magnitude of the transitional diffusion coefficient can be calculated only by solving the boundary value problem constituting the separate electron and ion continuity equations, with space charge, and Poisson's equation. The result depends on the geometry of the boundaries as well as on the ionization level.

Allis and Rose[11] have performed calculations for hydrogen and found that the transition from free to ambipolar diffusion takes place over five orders of magnitude of electron density. Moreover, their results indicate that the constant ratio approximation is nearly correct if the electron density used in this approximation is decreased from its actual value by a constant factor. From Figure 4 of their paper it appears that this factor should be about 20, but Allis[12] indicates a factor of five in another calculation. A factor of ten may be reasonable. The constant ratio approximation consists of assuming that the ratio of electron and ion densities is constant throughout the discharge. Allis[12] has derived an expression for the transitional diffusion coefficient which follows:

$$\frac{D_s}{D_- D_a} = \frac{\ell_D^2 + \Lambda^2 \left(1 + \frac{\mu_+ n_+}{\mu n}\right)}{D_a \ell_D^2 + D_- \Lambda^2 \left(1 + \frac{\mu_+ n_+}{\mu n}\right)} \qquad (3.1.4.2\text{-}1)$$

where Λ is the diffusion length (see below), ℓ_D is the Debye length, μ is mobility, n is particle density (+ refers to ions), D_- is the electron free diffusion coefficient and D_a is the ambipolar diffusion coefficient:

$$D_a = \frac{\mu_+ D_- + \mu D_+}{\mu_+ + \mu} \qquad (3.1.4.2\text{-}2)$$

$$\ell_D^2 = \frac{\epsilon_o D_-}{ne\mu} \qquad (3.1.4.2\text{-}3)$$

where ϵ_o is the permittivity of free space and e is the electronic charge. In practice, the ratio $\mu_+ n_+ / (\mu n)$ is generally small compared with unity, except possibly when the Debye length is very large, in which case the ratio is not important. Thus a good approximation which depends only on the electron density is the following equation.

$$\frac{D_s}{D_- D_a} = \frac{\ell_D^2 + \Lambda^2}{D_a \ell_D^2 + D_- \Lambda^2} \qquad (3.1.4.2\text{-}4)$$

In the limits of low and high electron density the value of D_s approaches D_- and D_a respectively. In order to allow the above constant ratio approximation formula to reproduce approximately the actual transition situation, apply the factor of ten recommended above.

$$\frac{D_s}{D_- D_a} = \frac{10\,\ell_D^2 + \Lambda^2}{10\,D_a \ell_D^2 + D_- \Lambda^2} \qquad (3.1.4.2\text{-}5)$$

Thus the transition from free to ambipolar diffusion in this approximation occurs when the Debye length is about one third of the diffusion length.

Two simplified approximations to the ambipolar diffusion coefficient are possible, considering the fact that μ is much greater than μ_+. In an active discharge, $D_- \mu_+$ is much greater than $D_+ \mu$, so that the ambipolar diffusion coefficient is given approximately by the following equation:

$$D_a = \frac{\mu_+}{\mu} D_- \qquad (3.1.4.2\text{-}6)$$

But in the case of an isothermal plasma, $D_- \mu_+$ is equal to $D_+ \mu$:

$$D_a = \frac{2\mu_+}{\mu} D_- = 2D_+ \qquad (3.1.4.2\text{-}7)$$

It is important to note that the latter result applies only to the afterglow plasma, for example the decaying plasma which exists between pulses in multiple pulse breakdown. Also, there is not actually a factor of two difference between these two results, because D_-/μ is much greater in the active discharge than in the isothermal plasma, while μ_+ is practically constant.

It is apparent that one needs values for the parameters D_- and μ_+/μ to apply these equations and also one needs a value of D_-/μ in order to calculate the Debye length for Equation 3.1.4.2-5. The latter problem is accurately enough handled for the purposes of the transitional diffusion in the constant ratio approximation by casting Equation 3.1.4.2-3 in the following form:

$$\ell_D^2 = \frac{\epsilon_o kT_e}{ne^2} \qquad (3.1.4.2\text{-}8)$$

where k is Boltzmann's constant and T_e is the electron temperature. In the isothermal, afterglow plasma T_e is equal to the gas temperature; and in an active discharge in air kT_e is on the order of a few electron volts. At breakdown in air, a commonly used value of D_- is given by Kelly and Margenau[7]:

$$D_- p = 1.6 \times 10^6 \text{ cm}^2 \text{ torr sec}^{-1} \qquad (3.1.4.2\text{-}9)$$

But MacDonald[19] prefers to use a value which depends on the microwave field intensity E.

$$10^{-4} D_- p = 29 + 0.9 E_e/p \text{ cm}^2 \text{ torr sec}^{-1} \qquad (3.1.4.2\text{-}10)$$

where E_e is the effective field (see below).

Various values of μ/μ_+ (or D_-/D_a) for breakdown in air have appeared in the literature, including Kelly and Margenau's[7] value of 100 and Whitmer and MacDonald's[14] value of 40. But these are not actually inconsistent, since the latter authors applied Equation 3.1.4.2-7 to the data on mobilities for nonisothermal plasmas. Thus the value of 40 is actually 80 and it seems reasonable to assume that for breakdown of air:

$$\frac{D_-}{D_a} = \frac{\mu}{\mu_+} \cong 100 \qquad (3.1.4.2\text{-}11)$$

The discussion of the diffusion coefficient so far has concentrated on the effects of flow field ionization. It was mentioned above that gas temperature and composition can conceivably affect diffusion. The gas composition effects are fairly obvious, it being apparent that molecular dissociation of the air and the formation of products of ablation in the flow field surrounding a reentry vehicle would require one to obtain basic data on the mobilities of electrons and ions in the product gases, some of which are undoubtedly available in the literature. The gas temperature effect is probably not too significant, since data by Mentzoni[20] indicate a maximum factor-of-two effect at relatively low temperature.

3.1.4.3 Pulsed Signal Breakdown

Flow field ionization can affect pulsed signal breakdown in terms of the separation constant γ, which is logarithmic in the initial electron density. The relative importance of this effect is somewhat difficult to define, since it depends on two arbitrary parameters, the initial and final electron density. The final electron density level usually used in the

breakdown criterion is the critical electron density, which in units of cm^{-3} is approximately equal to 10^{-8} times the square of the microwave frequency (for example, see References 14 and 15). Most authors generally state that when the initial ionization from the flow field is already equal to or greater than the critical value, then the breakdown field is essentially zero, since the gas may already be considered to be broken down and there can be no penetration of the microwave field through the plasma.

On the other hand, the CW breakdown criterion normally used does not depend on the electron density level, but only on the rate of increase of electron density from the microwave field. Thus no such critical electron density effect as above appears. But the two physical situations cannot be this different merely because one is for pulsed signals and the other is for CW. The difficulty is obviously a result of the arbitrary criteria used in defining breakdown.

In the case of the reentry induced flow field of a slender cone body, it is possible to have greater than critical electron density in a thin layer, such that total signal blackout does not occur. Thus there will be a significant transmission of power through the plasma which will increase linearly with input power until breakdown is approached, when the transmitted power will attenuate nonlinearly due to the thickening of the plasma layer by the breakdown process. This indicates that the only physically meaningful way to calculate breakdown in the presence of strong flow field ionization is to calculate signal transmission as a function of input power level, taking into account the increased level of ionization induced by the field, as has been suggested by Epstein[21].

A careful consideration of the form of the breakdown criterion is not only necessary for pulsed signal breakdown in the presence of ionization but also for breakdown with convection, as pointed out in the discussion at the end of Section 3.1.2. A meaningful prediction of breakdown in the presence of flow field ionization with convection requires one to calculate the electron density distribution over the antenna and the power transmitted through this plasma

as functions of the input power. The importance of this consideration lies mainly in its effect on the breakdown criterion and not so much in the phenomenon of alteration of the antenna near-field and impedance by the plasma, although the latter may be important considerations if the electron density is initially very high.

3.2 THE NET IONIZATION FREQUENCY

The net ionization frequency is the most important term in the continuity equation for microwave breakdown. This quantity, through its dependence on the microwave field intensity, determines the breakdown field. In practice the breakdown field is obtained by first solving the continuity equation for the net ionization frequency under the appropriate breakdown criterion. Then the dependence of the net ionization frequency on the electric field determines the breakdown field.

3.2.1 DEPENDENCE ON MICROWAVE FIELD

Unfortunately, the ionization frequency has never been measured directly except for hydrogen, for which it was done by an optical method by Cottingham and Buchsbaum[22]. The data for air have been inferred from either diffusion controlled or pulse controlled breakdown fields, using some form of phenomenological theory.

Two representations of the data for air exist. MacDonald[23] has reduced the data of Herlin and Brown[24] to the form of curves of $\nu_n \lambda$ versus $p\lambda$ with $E\lambda$ as a parameter, where λ is the wavelength and E is the electric field. In the MacDonald method of predicting breakdown, one uses these curves in conjunction with Equation 3.1.4.2-10, using the following expression for the effective field E_e:

$$\left(\frac{E}{E_e}\right)^2 = 1 + \left(\frac{36}{p\lambda}\right)^2 \qquad (3.2.1\text{-}1)$$

Scharfman and Morita[25] have obtained data by a focused pulsed microwave technique. They

have interpreted their data in terms of a single curve of net ionization frequency as a function of E_e/p, including in the results the data of several other investigators also reduced to this form. Their results are shown in Figure 3.2.1-1 along with a simple power law approximation given by the following equation:

$$\frac{\nu_n}{p} = 4 \times 10^7 \left(\frac{E_e}{100\ p}\right)^{5.34} - 6.4 \times 10^4 \qquad (3.2.1\text{-}2)$$

This function has advantages in terms of nonuniform electric field problems (see below).

3.2.2 HIGH GAS TEMPERATURE

At the present time the effect of high gas temperature on the net ionization frequency is not well understood theoretically, but there is enough experimental data to indicate the existence of an effect in shock heated air (see References 16, 26, 27, and 28). Some of the more pertinent data are shown in Figure 3.2.2-1.

Light and Taylor[16] have proposed a model for the high temperature effect on the ionization frequency which relates phenomenologically to the dependence of the electron energy distribution on vibrational excitation of oxygen molecules. Their equation is as follows:

$$\frac{\nu_n}{p^*} = F\left[\left(1 - e^{\frac{-2200}{T}}\right) \frac{X}{X_o} \left(\frac{E_e}{p^*}\right)^2\right] \qquad (3.2.2\text{-}1)$$

where T is the gas temperature in ^oK, X/X_o is the ratio of the mole fraction of oxygen molecules to their mole fraction in cold air and $F\left[(E_e/p^*)^2\right]$ is the net ionization frequency function in cold air. The above equation represents the apparent trends of the

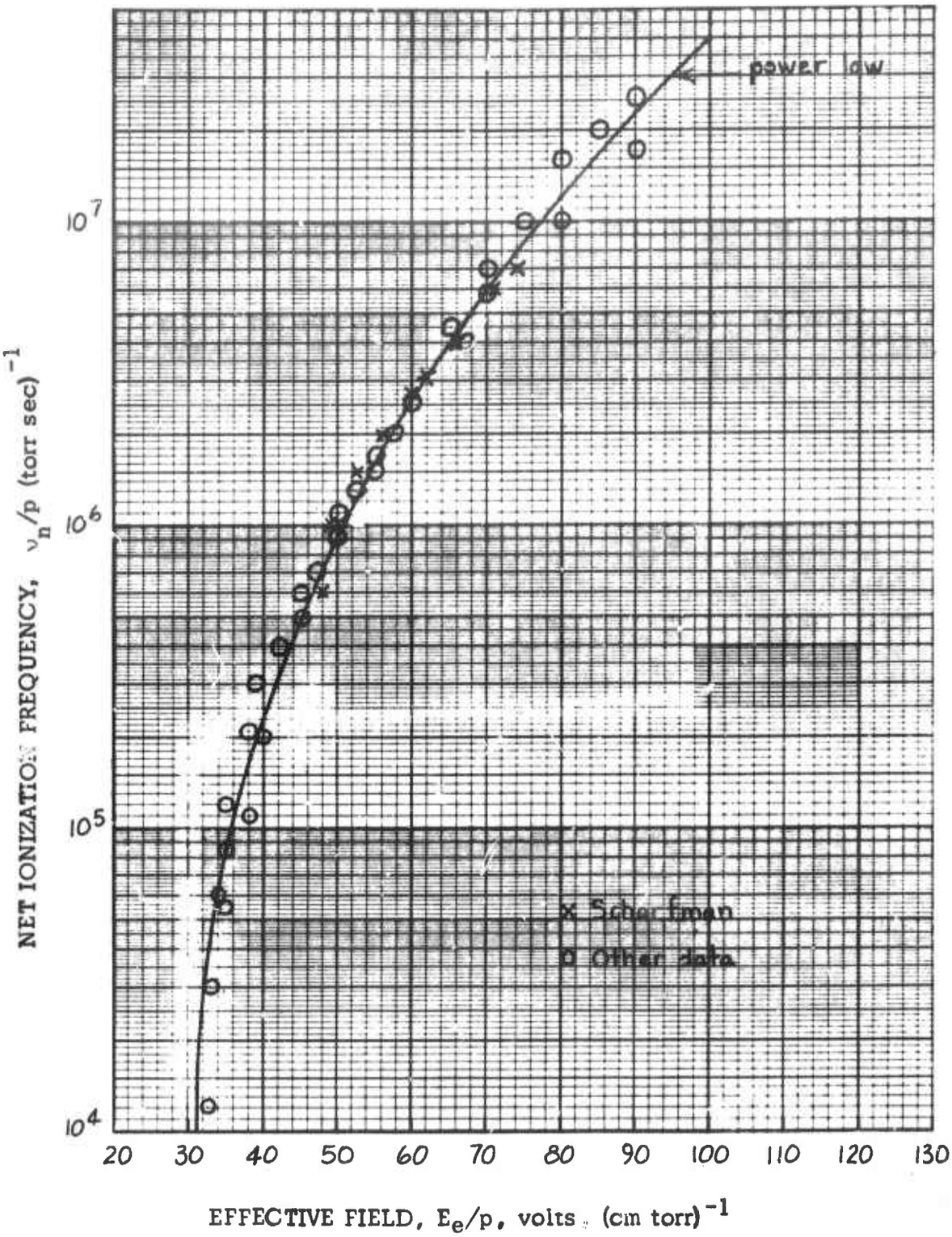

Figure 3.2.1-1. Dependence of Net Ionization Frequency on Microwave Field

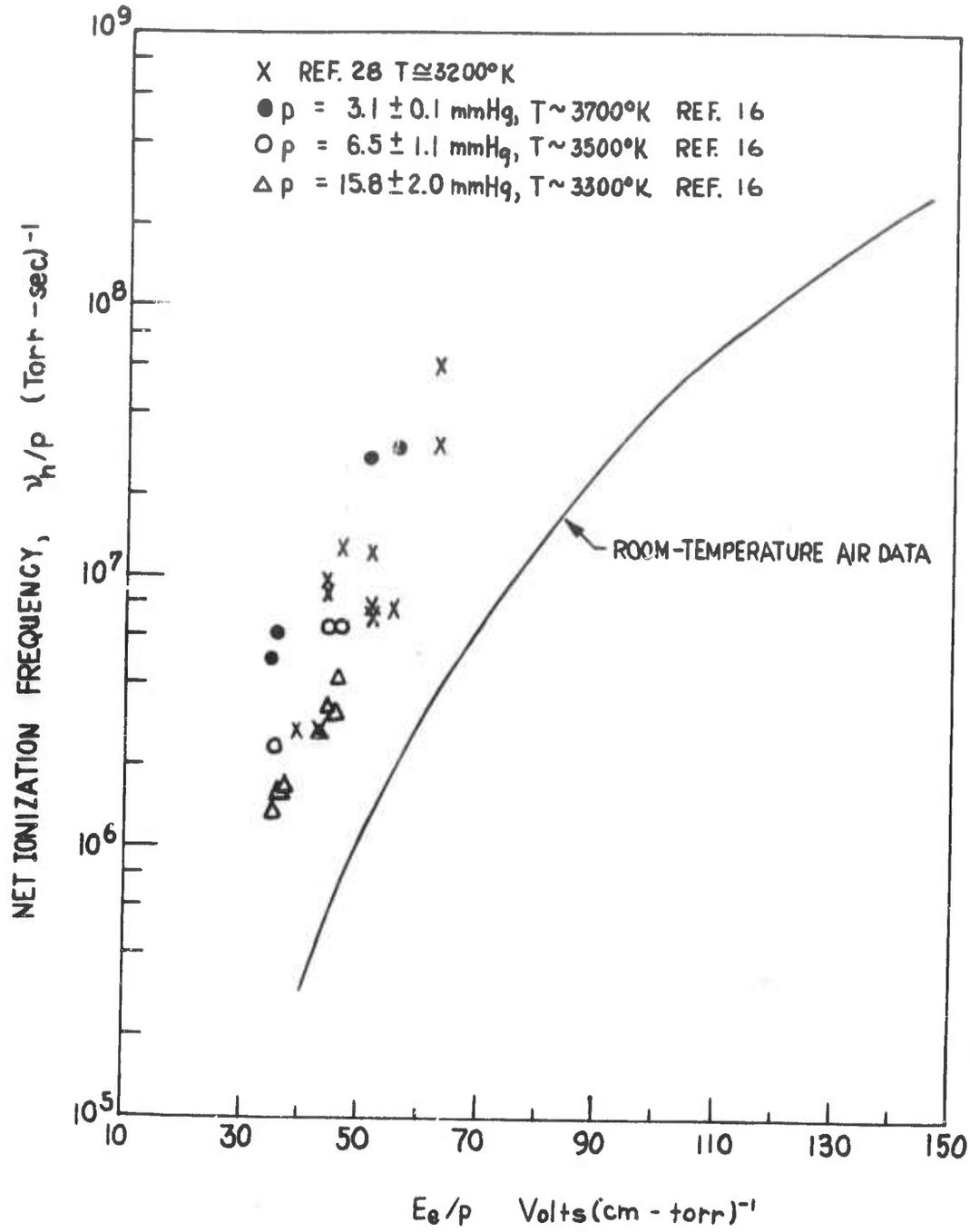

Figure 3.2.2-1. Effect of High Gas Temperature on the Ionization Frequency

data fairly well if the dissociation of oxygen is relatively complete* at the higher temperatures in Light and Taylor's experiment; however, the range of temperatures and field strengths is rather small for the high temperature data.

3.2.3 CHEMICAL COMPOSITION EFFECTS

It is obvious that the net ionization frequency as a function of electric field (and temperature) must depend on the gas composition, for several reasons. The ionization potentials of many gases are lower than air and there are also possibilities of many additional mechanisms for energy and charge transfer, all of which affect the ionization frequency. The attachment frequency can be affected very significantly also with either the addition of electrophilic materials acting to enhance it or the dissociation of oxygen molecules acting as a damper. (See the previous report[6] in this series for a brief discussion of some of the more recent data on these effects.)

3.3 GRADIENTS OF ANTENNA FIELDS AND FLOW FIELD PROPERTIES

The continuity equation discussed in detail above is, in general, an elliptic partial differential equation of second order involving both time and space derivatives and possessing nonconstant coefficients. It is apparent from this fact and from some of the discussions above that the mathematical criterion used in defining breakdown in terms of a solution of this equation will have a significant influence on the results. Moreover, the physical effects of gradients of the antenna near-field and the flow-field properties will be significant in the problem of reentry antenna breakdown. Thus these gradients must be taken into account in solving the continuity equation to predict breakdown.

3.3.1 ANTENNA NEAR-FIELDS

The problem of nonuniform antenna near-fields has been discussed by Brown and MacDonald[29] in terms of a limiting boundary on the region of validity of the diffusion theory of breakdown.

---

* The thermodynamic equilibrium concentrations of O_2 are needed to explain the data.

Within this region of validity the continuity equation (in the absence of convection) supposedly can be solved as a homogeneous differential equation with constant coefficient, giving as a solution the eigenvalue ($-1/\Lambda^2$), where Λ is the diffusion length. Brown and MacDonald assume that the uniform field assumption is correct in the parallel plate situation if the plate separation is less than or equal to a half wavelength, so that no more than a single loop of a standing wave of electric field would be maintained. This gives the result that the uniform field assumption works if Λ is less than $\lambda / (2\pi)$.

Herlin and Brown[30,31] and MacDonald[32] have calculated breakdown in nonuniform fields by a method which is discussed fully by MacDonald[33], using the following form of continuity equation:

$$\nabla^2 \psi + \left(\frac{\nu_n}{D}\right)_o \left(\frac{E}{E_o}\right)^{\beta} \psi = 0 \qquad (3.3.1\text{-}1)$$

where β is held constant throughout the gas volume. The results for cylindrical cavities depend on the geometry and they indicate that the effective height of the cavity can be much less than its actual height if the radius is relatively small. For a spherical cavity the effective size of the cavity can be reduced by a factor of two or three by this effect. Of course for the case of antenna breakdown, boundaries such as exist in cavities are absent and one must solve an equation similar to Equation 3.3.1-1 for the conditions imposed by the antenna near-field. Most investigators of antenna breakdown assume a diffusion length either by analogy with parallel plate breakdown or by fitting experimental breakdown data to diffusion theory.

The determination of the magnitude of the antenna near-fields is necessary for prediction of the breakdown condition shown in Equation 3.3.1-1. We consider three antennas:

a. Electric dipole
b. Magnetic dipole (electric current loop)
c. Conical equiangular-spiral antenna (CESA)

The electric dipole has been used in previous analyses[34] and is a useful approximation to several radiating configurations. The magnetic dipole is used in the analyses of slots on planes[35]. The CESA is of interest in ECM applications for its broadband characteristics and practical geometry[36], although polarization diversity may be a problem[37].

The analysis of the fields of electric and magnetic dipoles provides useful and simple approximations to the near-fields of more complicated antennas. As indicated in the first quarterly report[38], the electric field $\vec{E}$, is found from the vector potential, $\vec{A}$:

$$\vec{E} = \frac{-j}{\omega\mu\epsilon} \nabla \cdot \nabla \cdot \vec{A} \qquad (3.3.1\text{-}2)$$

with

$$\vec{A} = \frac{1}{4\pi} \int_{\tau'} \vec{J}(r', \theta', \phi') \frac{e^{-jK \left| \vec{r} - \vec{r}' \right|}}{\left| \vec{r} - \vec{r}' \right|} d\tau' \qquad (3.3.1\text{-}3)$$

where

$\vec{J}(r', \theta', \phi')$ = Antenna source current density

K = $2\pi/\lambda$

λ = Radiated wavelength

r', θ', ϕ' = Spherical components of source current elements

$d\tau'$ = Source volume element

$$\left| \vec{r} - \vec{r}' \right| = r = \left[(X - X')^2 + (Y - Y')^2 + (Z - Z')^2 \right]^{1/2} \qquad (3.3.1\text{-}4)$$

For the electric dipole (Figure 3.3.1-1) we use $I_o e^{-j\omega t}$ as a source current I and we have

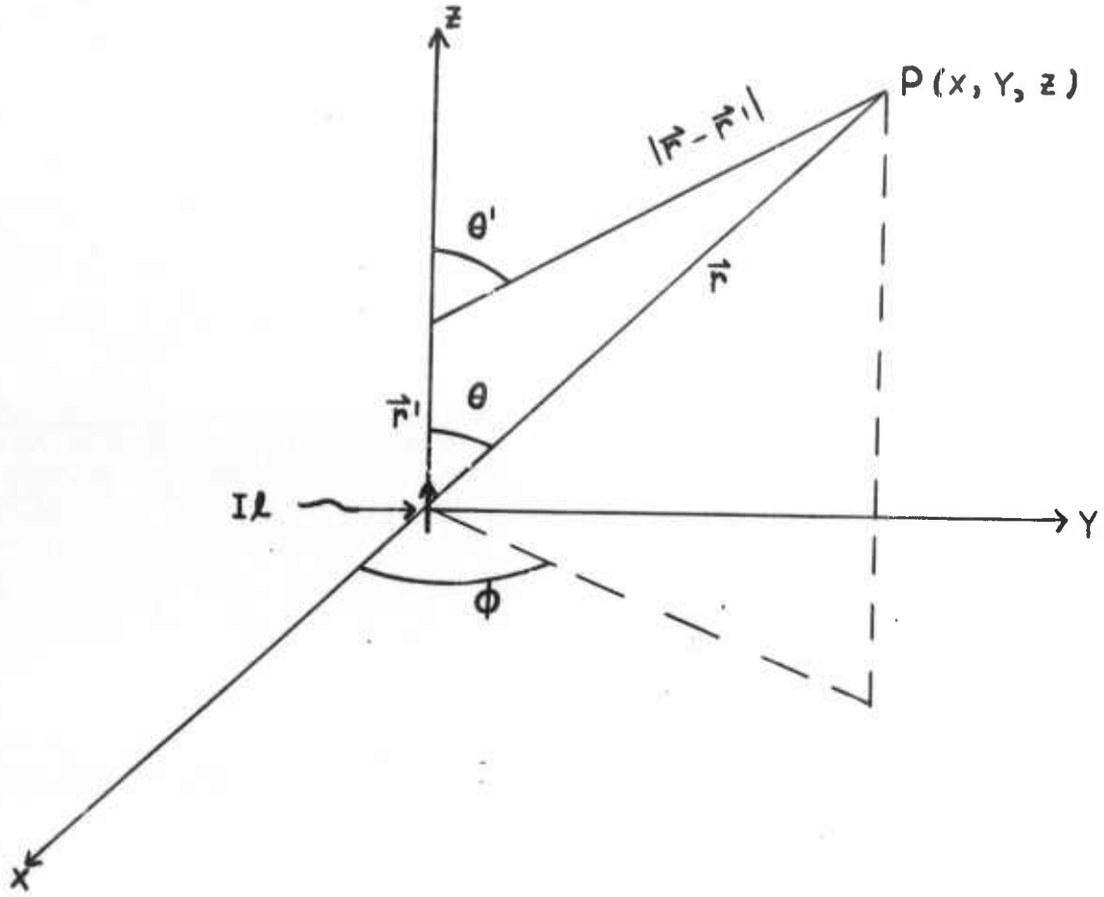

Figure 3.3.1-1. Configuration of Electric Dipole

$$\vec{A} = \hat{K} A_z = \frac{\hat{K} I \ell e^{-jKr}}{4\pi r} \qquad (3.3.1\text{-}5)$$

where ℓ is the length of the dipole.

$$\vec{E} = \hat{r} E_r + \hat{\theta} E_\theta \qquad (3.3.1\text{-}6)$$

$$E_r = \frac{I\ell}{4\pi} e^{-jKr} \left(\frac{Z}{r^2} + \frac{1}{j\omega\epsilon r^3} \right) \cos\theta \qquad (3.3.1\text{-}7)$$

$$E_\theta = \frac{I\ell}{4\pi} e^{-jKr} \left(\frac{j\omega\mu}{r} + \frac{Z}{r^2} + \frac{1}{j\omega\epsilon r^3} \right) \sin\theta \qquad (3.3.1\text{-}8)$$

where $Z = \sqrt{\mu/\epsilon}$. Plots of E_r, E_θ, and $E = \sqrt{E_r^2 + E_\theta^2}$ versus r and θ in the near-field are shown in Figures 3.3.1-2 through 3.3.1-7.

The magnetic dipole (see Figure 3.3.1-8) is characterized by its strength $KS = I \pi a^2$.

$$\vec{A} = \hat{\phi} A_\phi \qquad (3.3.1\text{-}9)$$

$$A_\phi = \frac{I\pi a^2}{4\pi} \left(\frac{jK}{r} + \frac{1}{r^2} \right) e^{-jKr} \sin\theta, \qquad (3.3.1\text{-}10)$$

$$\vec{E} = \hat{\phi} E_\phi$$

$$E_\phi = \frac{\phi\eta I\pi a^2}{4\pi} \left(\frac{K^2}{r} - \frac{jK}{r^2} \right) e^{-jKr} \sin\theta \qquad (3.3.1\text{-}11)$$

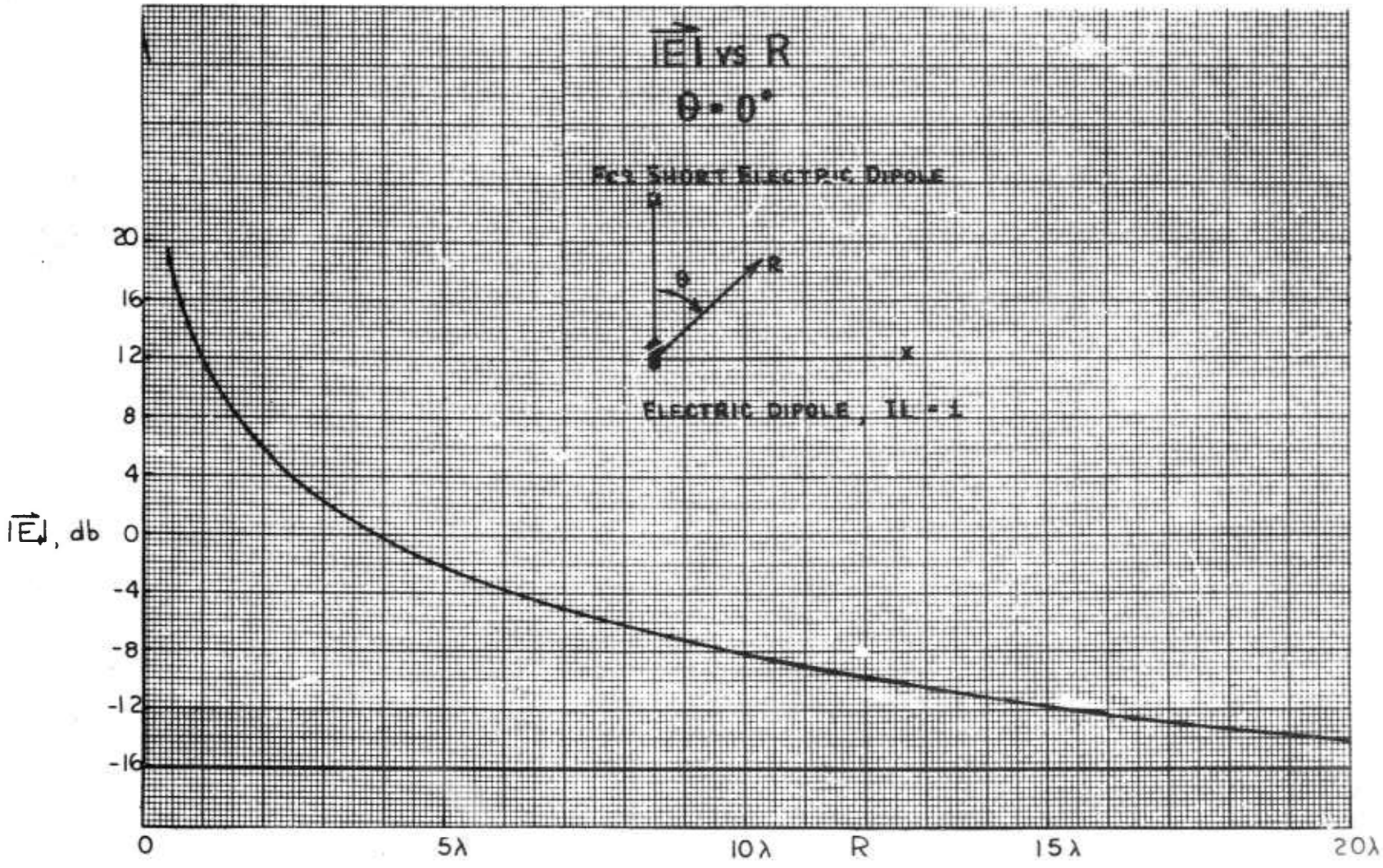

Figure 3. 3. 1-2. Magnitude of Electric Field of Short Electric Dipole, Normalized to Magnitude of Field at $R = \lambda\sqrt{2}$, $|E| = \sqrt{E_r^2 + E_\theta^2}$; Axial Radiation

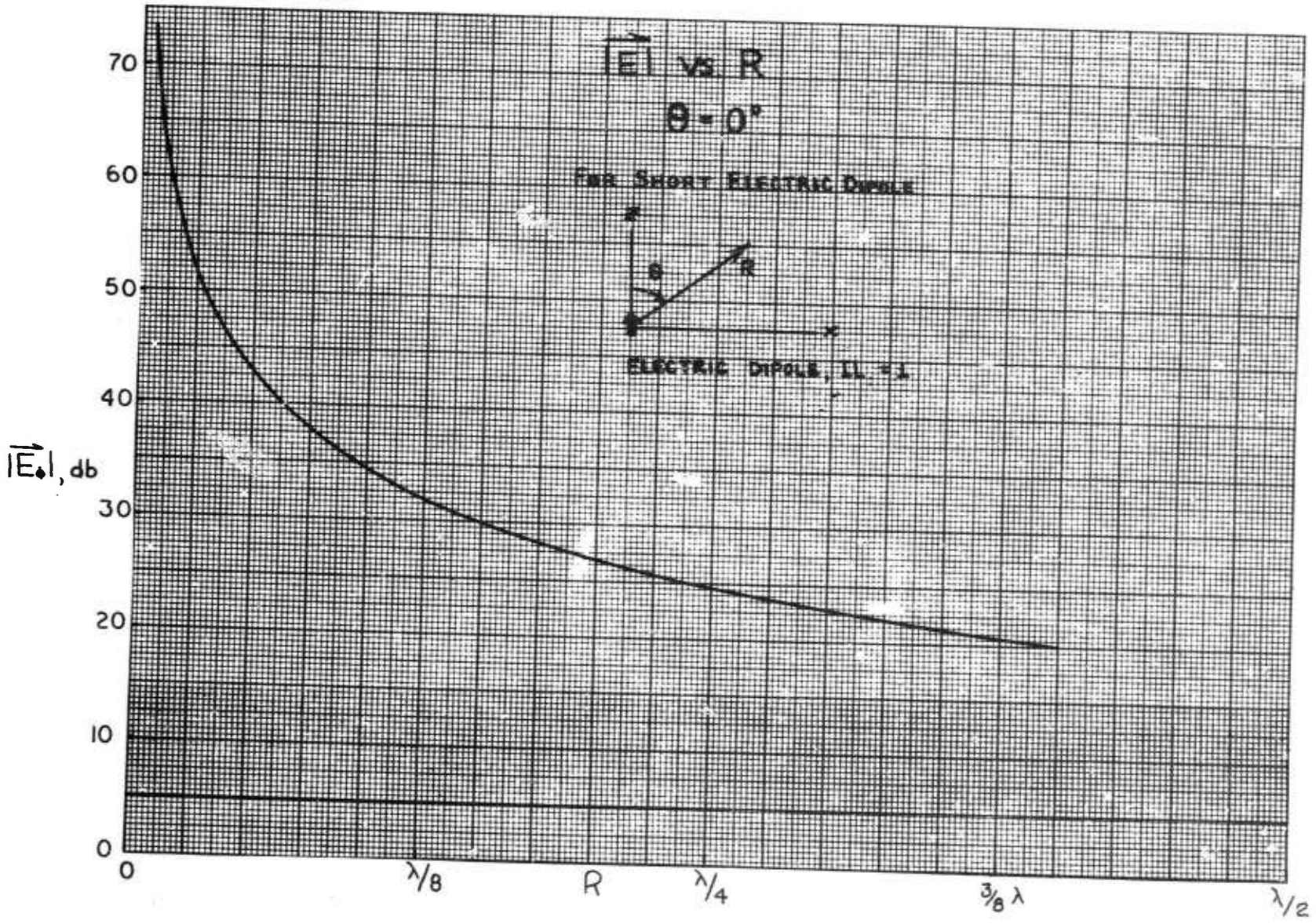

Figure 3.3.1-3. Expanded View of Figure 3.3.1-2 for $0 < R \leq 3/8\ \lambda$

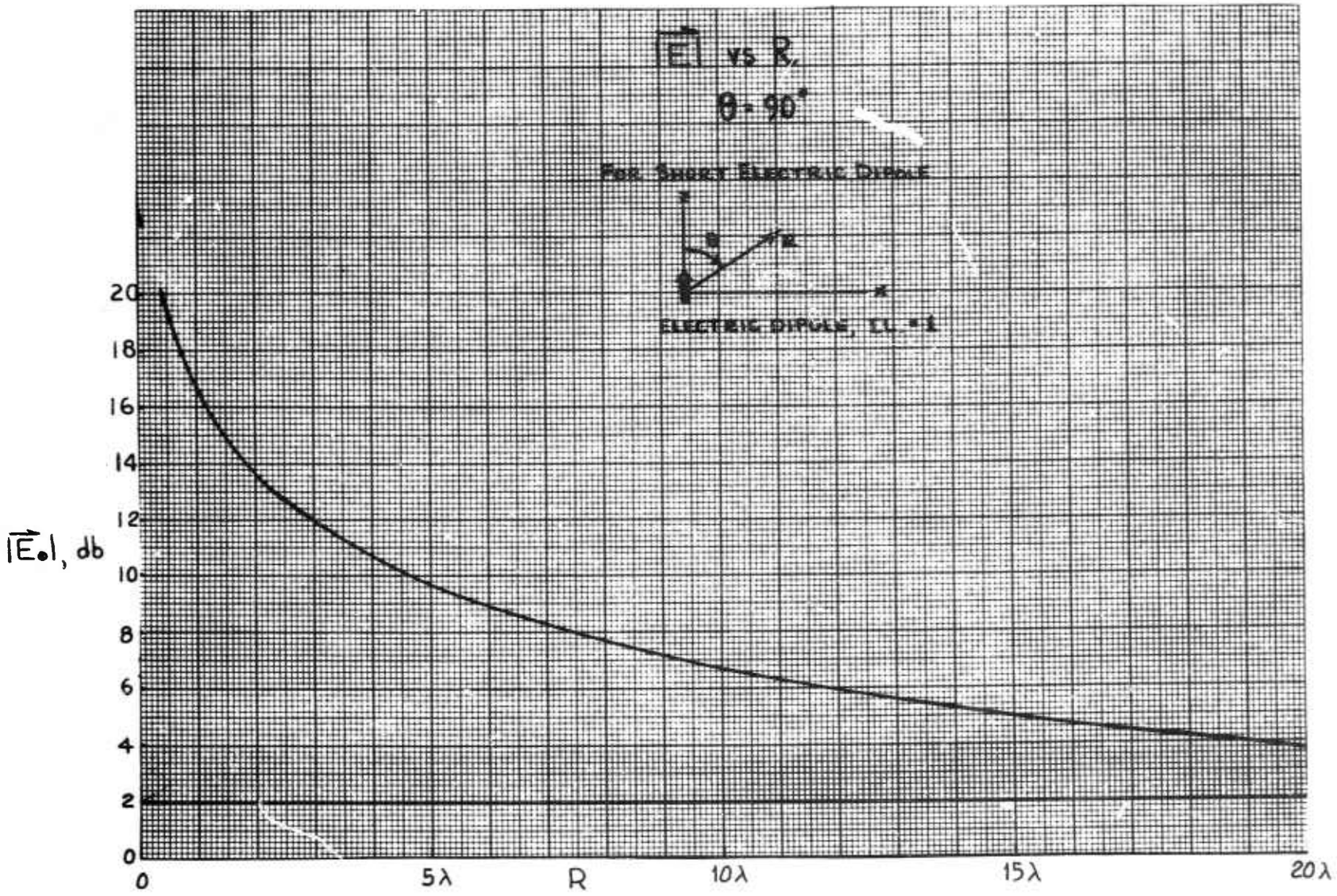

Figure 3.3.1-4. Magnitude of Electric Field of Short Electric Dipole, Normalized to Magnitude of Field at $R = \lambda\sqrt{2}$, $|E| = \sqrt{E_r^2 + E_\theta^2}$; Broadside Radiation

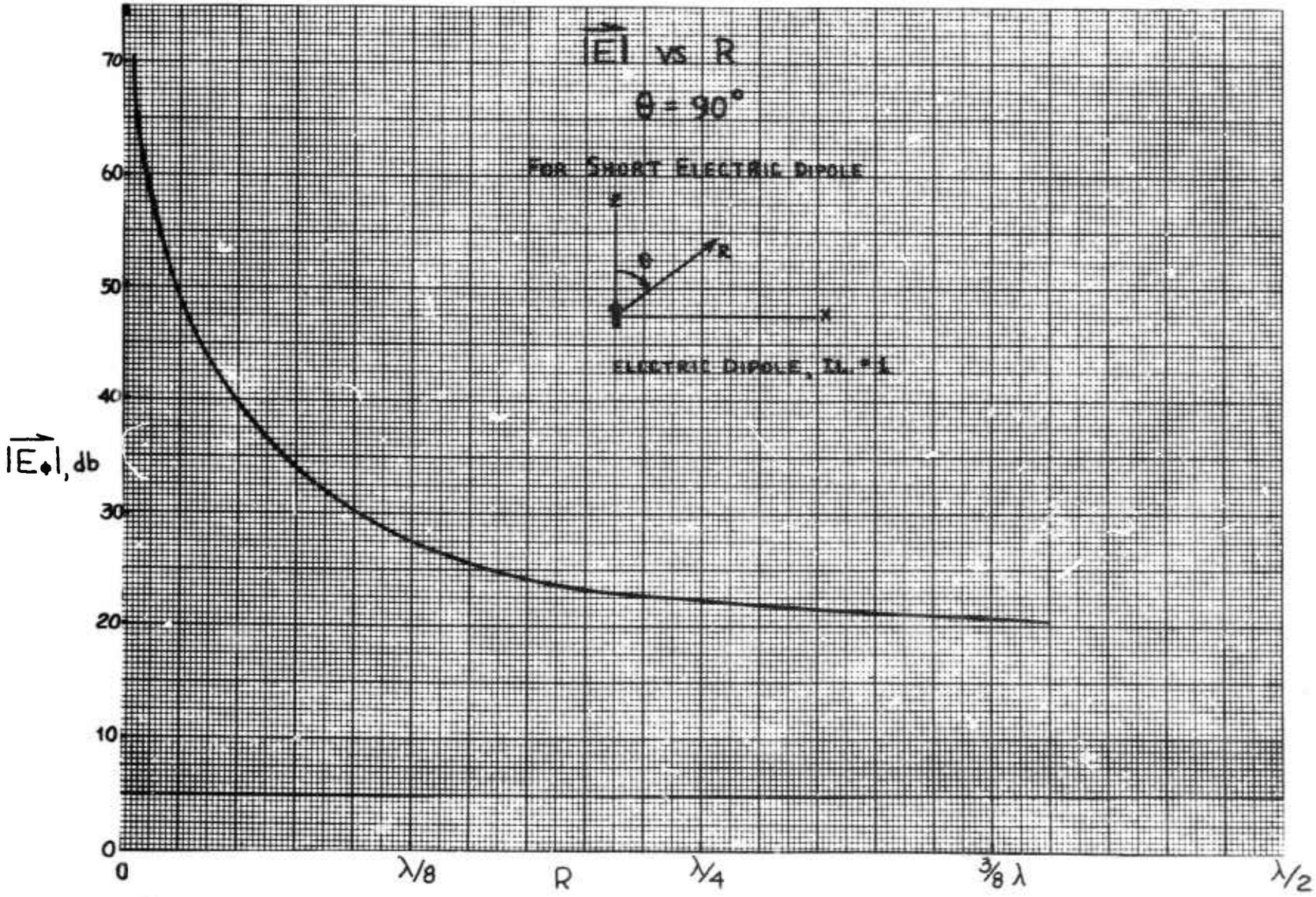

Figure 3.3.1-5. Expanded View of Figure 3.3.1-4 for $0 < R \leq 3/8\ \lambda$

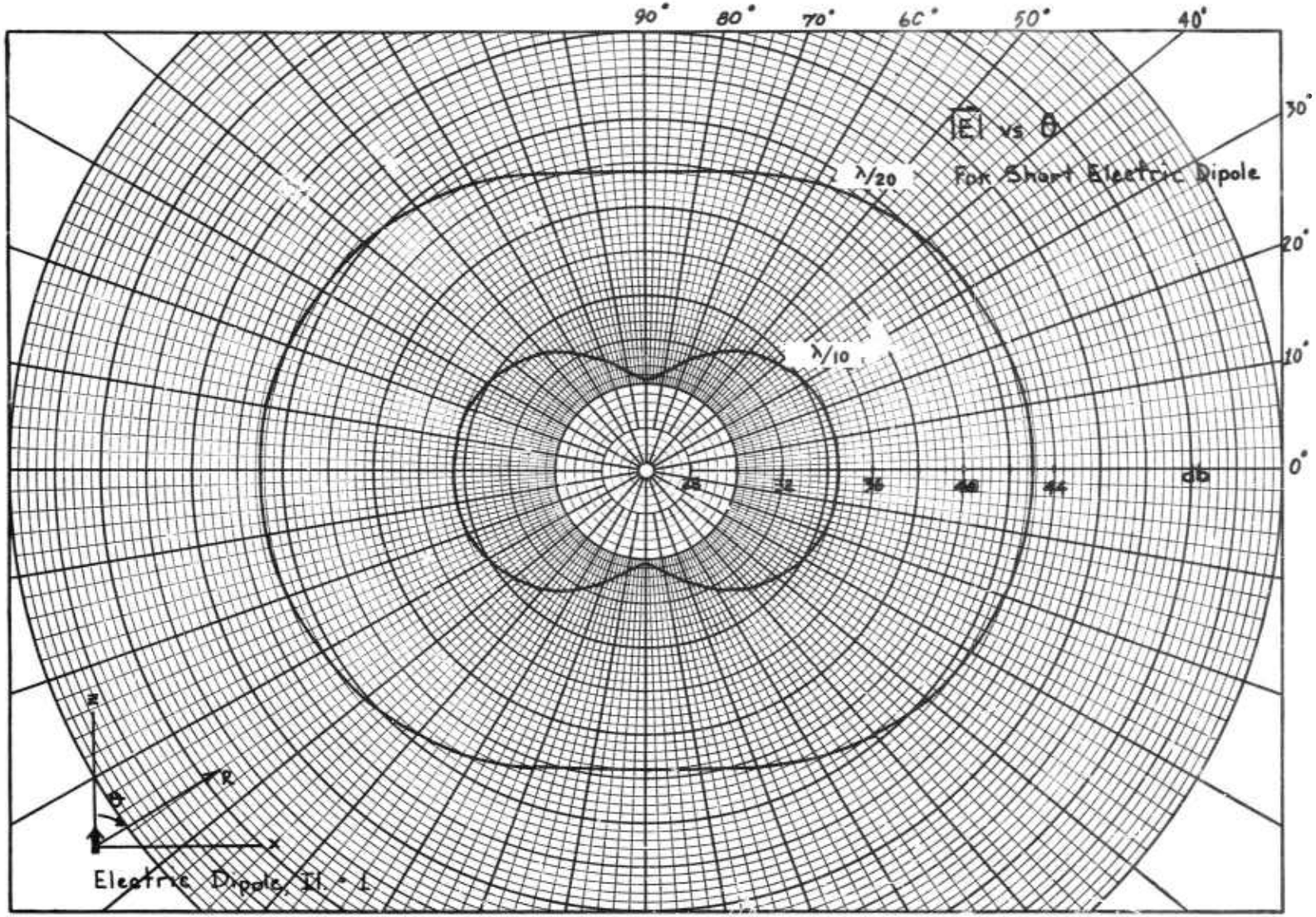

Figure 3.3.1-6. Polar Plot of |E| for Short Electric Dipole, Normalized to |E| at $R = \lambda\sqrt{2}$

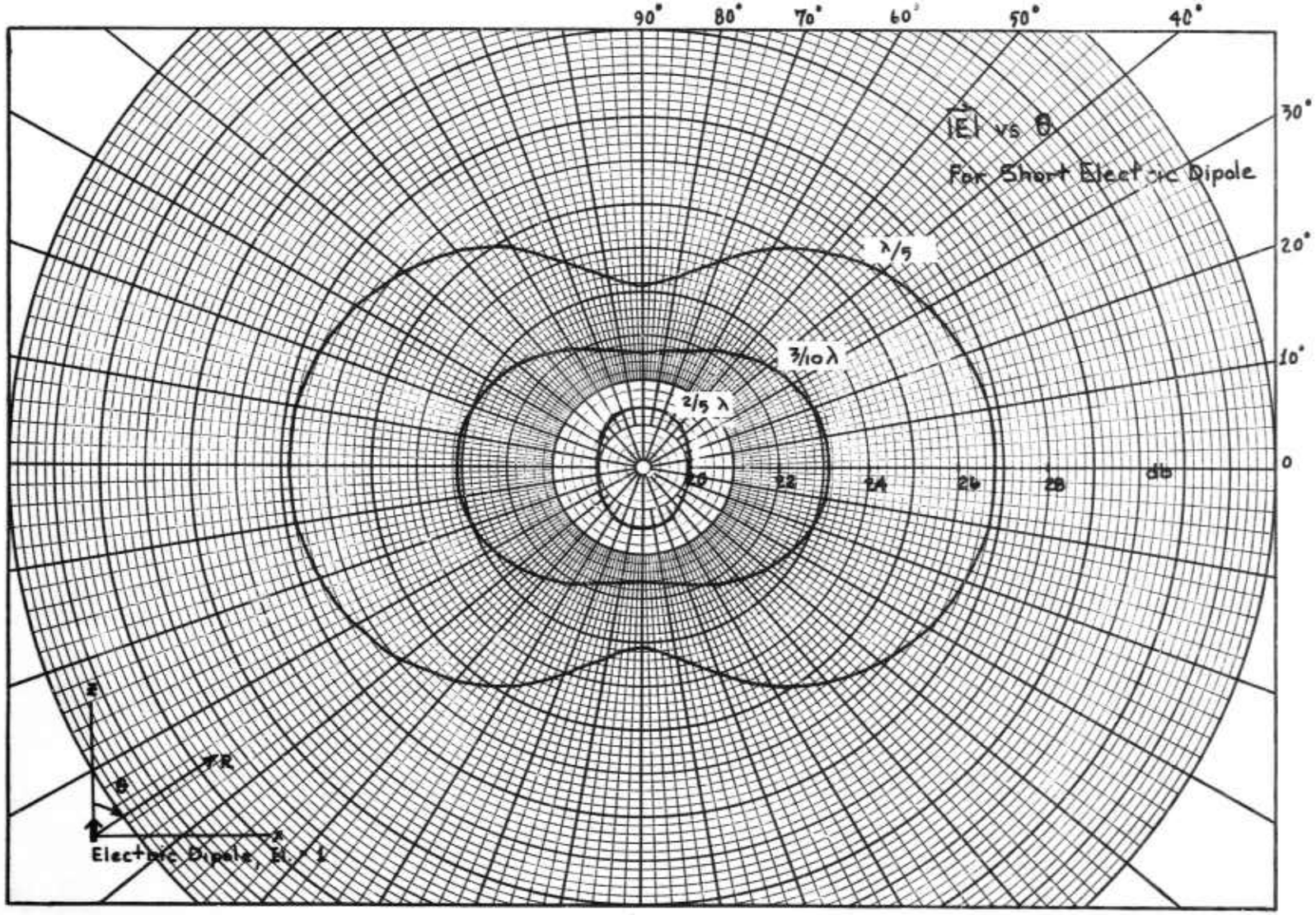

Figure 3.3.1-7. Polar Plots of $|E|$ for Short Electric Dipole, $R = \lambda/5,\ 3\lambda/10,\ 2\lambda/5$

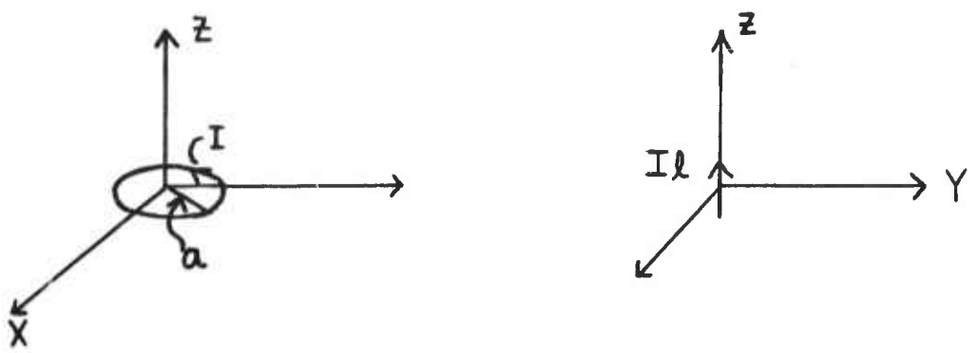

Figure 3. 3. 1-8. Configuration of Magnetic Dipole (Equivalent to a Small Electric Current Loop) Relative to the Electric Dipole of Figure 3. 3. 1-1

The field strength E_ϕ vs r and θ is plotted in Figures 3.3.1-9 through 3.3.1-17.

The CESA has been analyzed theoretically by solving the integral Equation 3.3.1-3 for the antenna current distribution[37]. The radiation patterns are well known. Extensive measurements have been made[36,41] of the radiation patterns and near-fields. These are reproduced in Figures 3.3.1-18 and 3.3.1-19. The antenna current J in general has three components, so that the near-fields

$$\vec{J} = \hat{r} J_r + \phi J_\phi + \theta J_\theta \qquad (3.3.1\text{-}12)$$

will contain both radial and azimuthal nonuniformities. The field expressions are thus complicated infinite series in terms of Bessel and Legendre functions[40].

A practical approach to obtaining approximate values for the diffusion length of typical antennas might utilize measured values of the near-field[41] in the following way. For a 10 degree conical spiral, the width of the active region is approximately 0.45λ if the length of the near-field is taken between 10 db points of Figure 3.3.1-18. The impedance measurements of Figure 3.3.1-19 indicate a 10 to 1 bandwidth is possible. Other investigators[36] have not achieved such wide bandwidth, possibly due to their narrow band balun. The active region shown in Figure 3.3.1-18 is the effective radiating aperture of the antenna. That is, although the CESA is an end fire antenna as shown in Figure 3.3.1-19, the peak fields occur in the active region. We therefore make the approximation that the CESA may be treated as a slot of width b where we equate b to the length of the active region. Using this approximation we may obtain an order of magnitude diffusion length for the conical equiangular spiral by using the well known result for a slot of width b, namely $\Lambda = b/(2\pi)$. Thus we estimate $\lambda = 14\Lambda$.

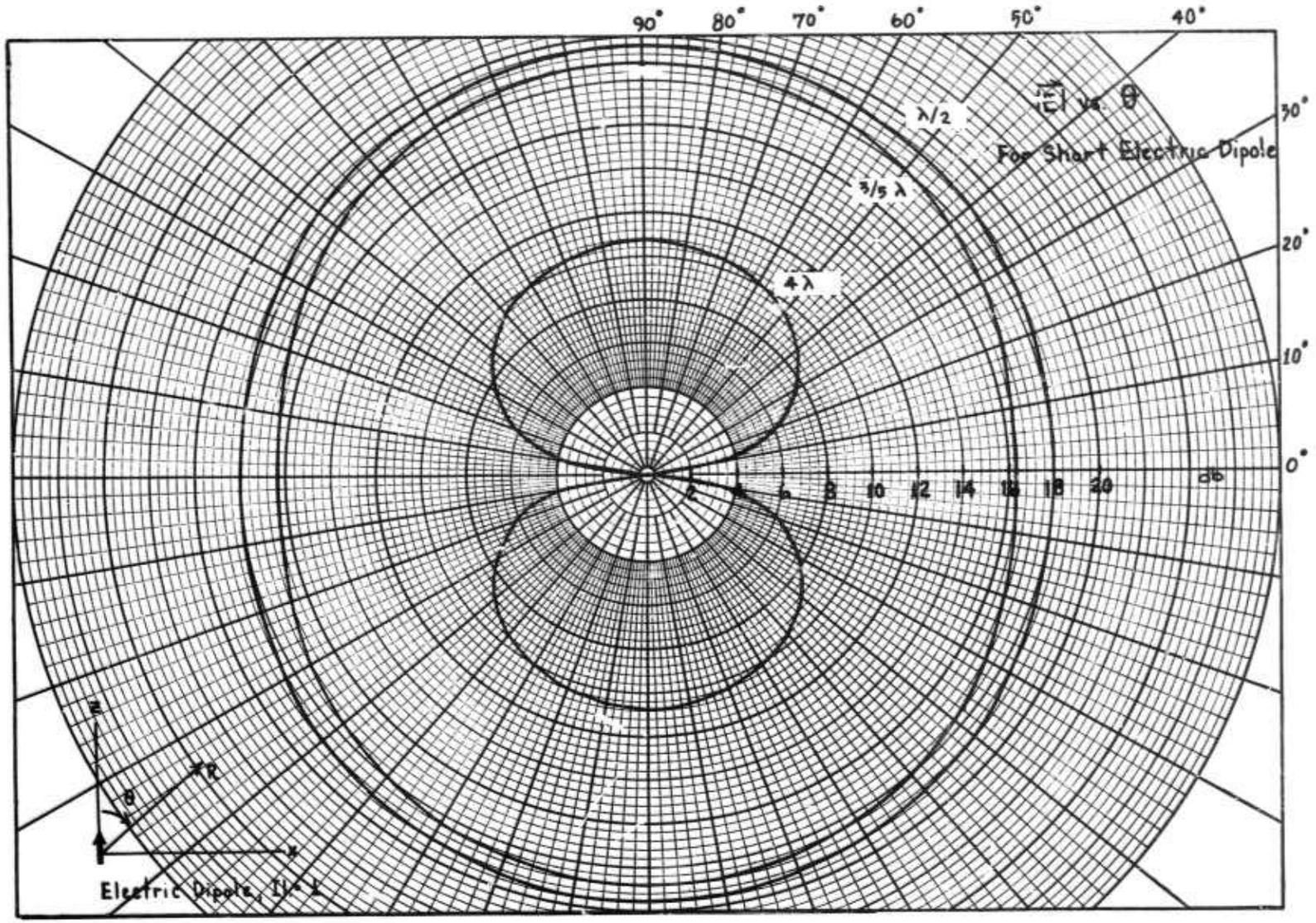

Figure 3.3.1-9. Polar Plots of $|E|$ for Short Electric Dipole, $R = \lambda/2,\ 3\lambda/5,\ 4\lambda$

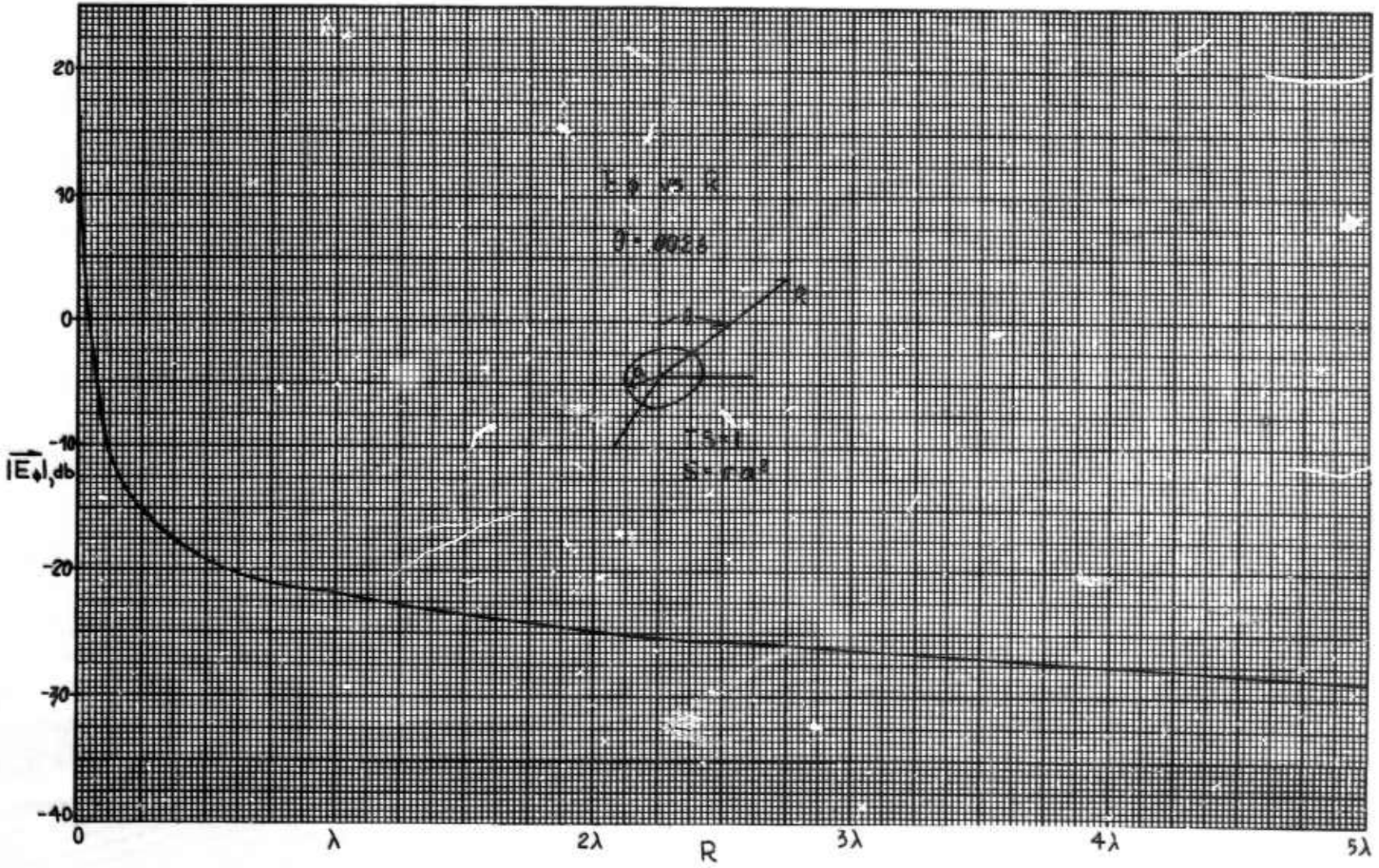

Figure 3. 3. 1-10. Magnitude of Electric Field of Small Current Loop, Normalized to Magnitude of Field at R = λ/30; Near-Axial Radiation

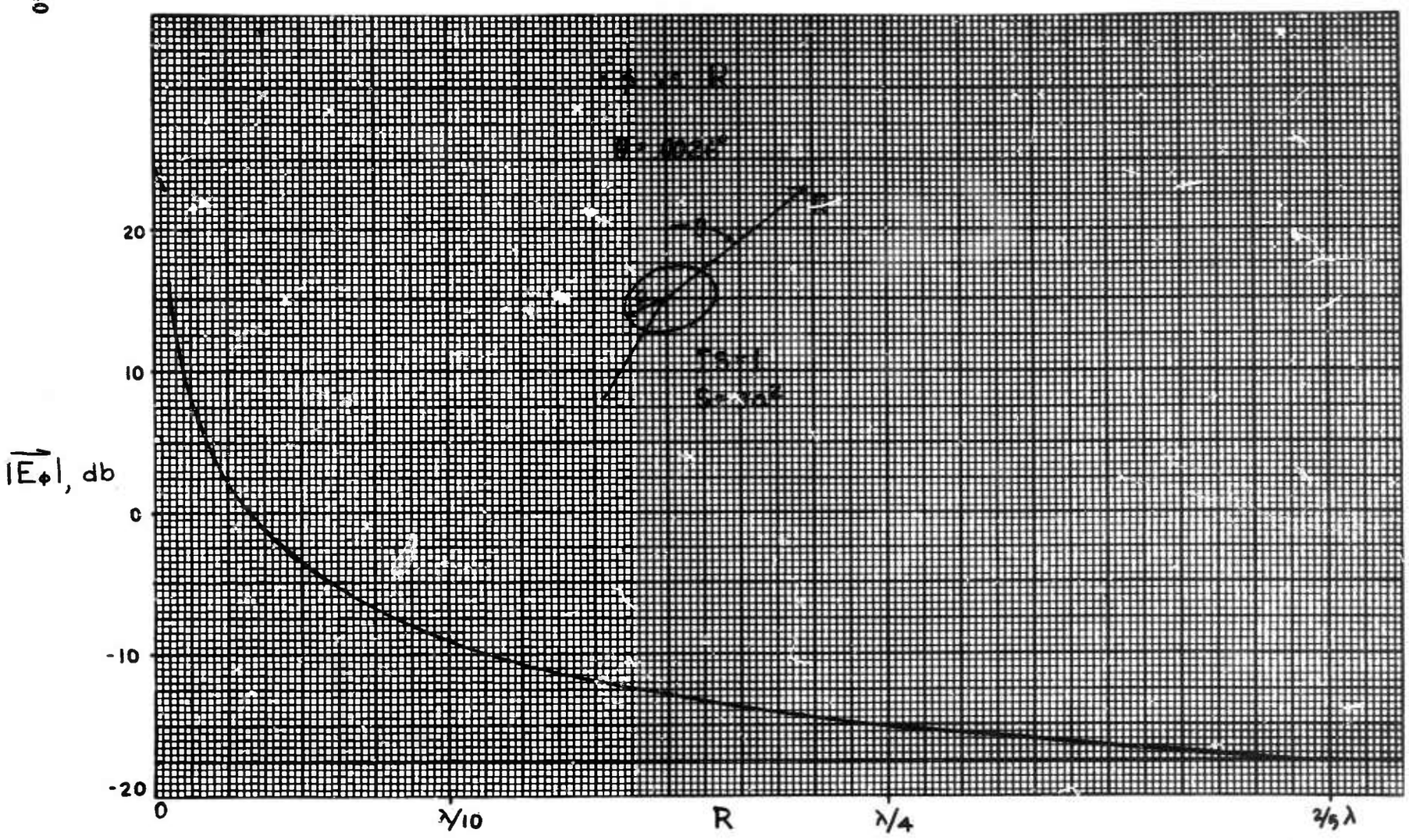

Figure 3.3.1-11. Expanded View of Figure 3.3.1-9 for $0 < R \leq 2\lambda/5$

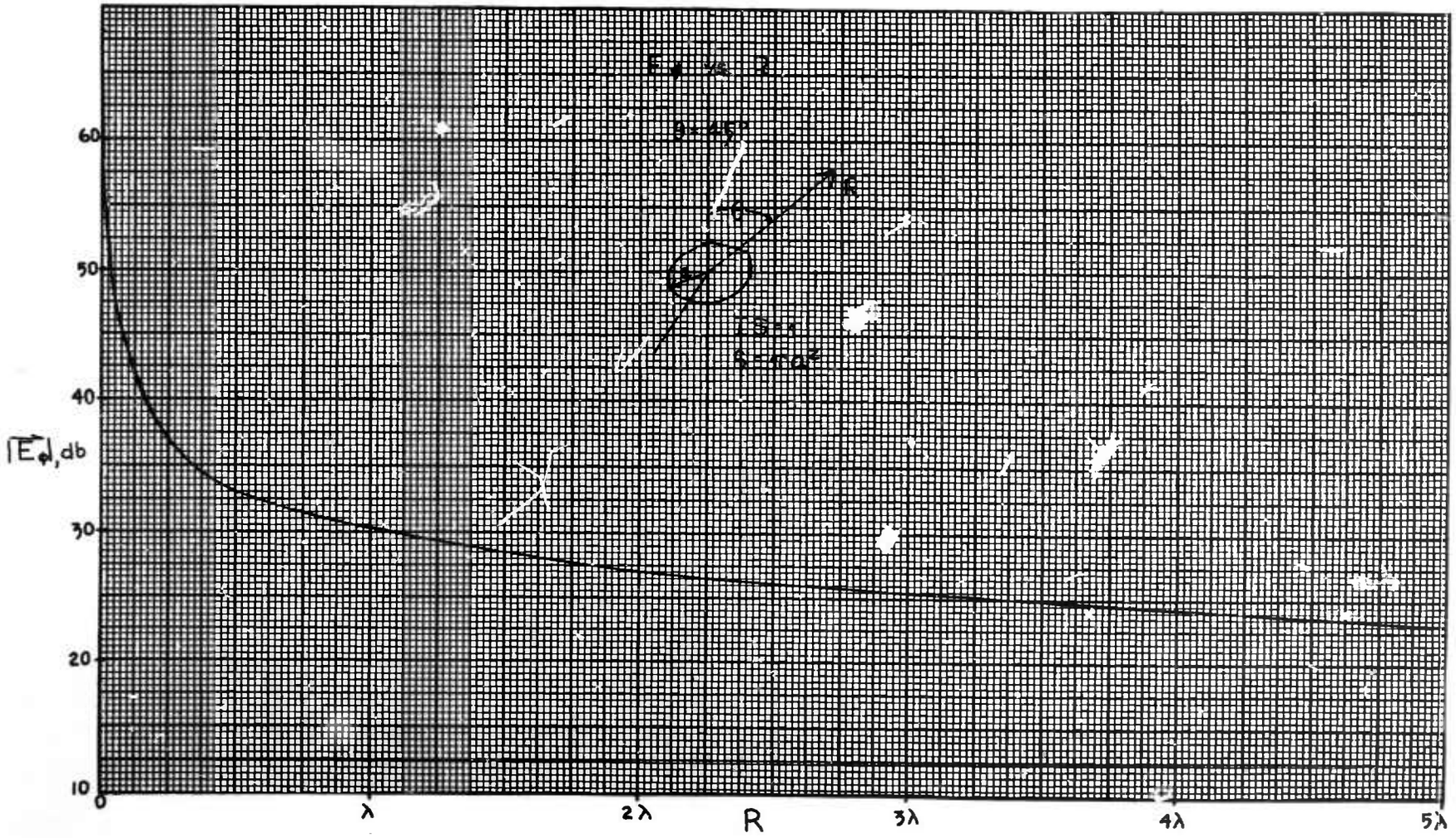

Figure 3.3.1-12. Magnitude of Electric Field of a Small Current Loop, Normalized to Magnitude of Field at R = λ/50; Oblique Radiation

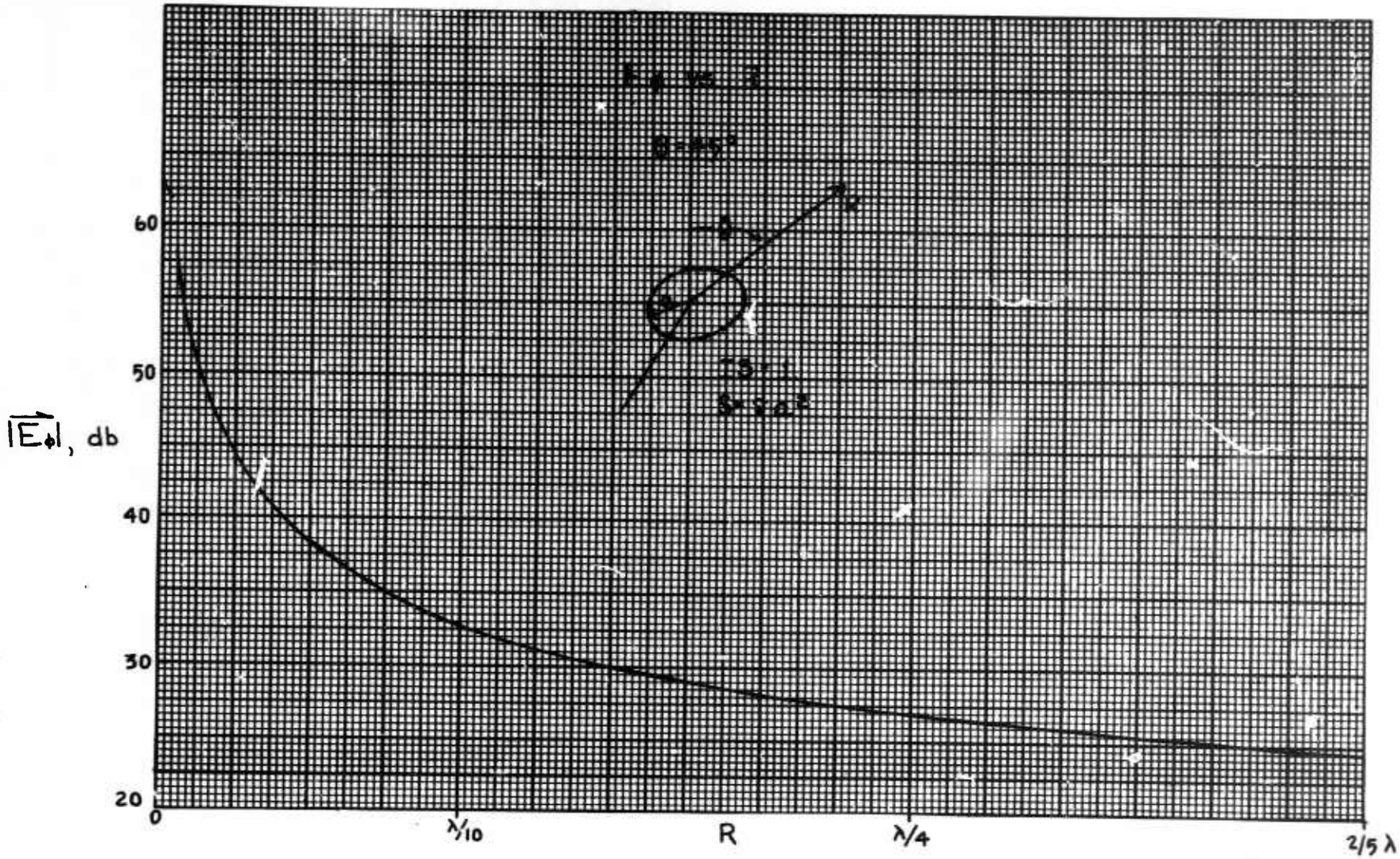

Figure 3. 3. 1-13. Expanded View of Figure 3. 3. 1-12 for $0 < R \leq 2\lambda/5$

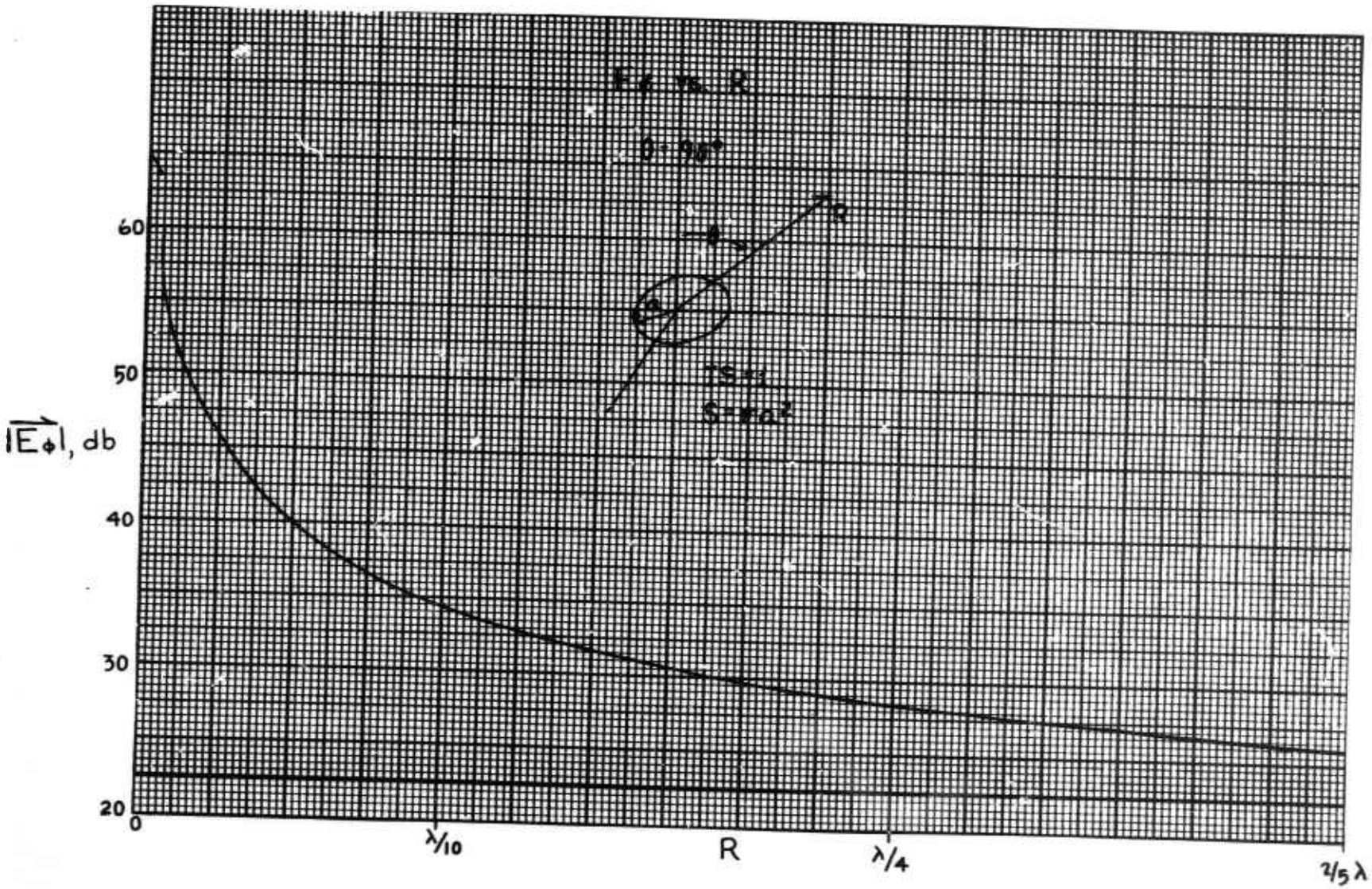

Figure 3.3.1-14. Magnitude of Electric Field of Small Current Loop, Normalized to Magnitude of Field at $R = \lambda/30$; Broadside Radiation

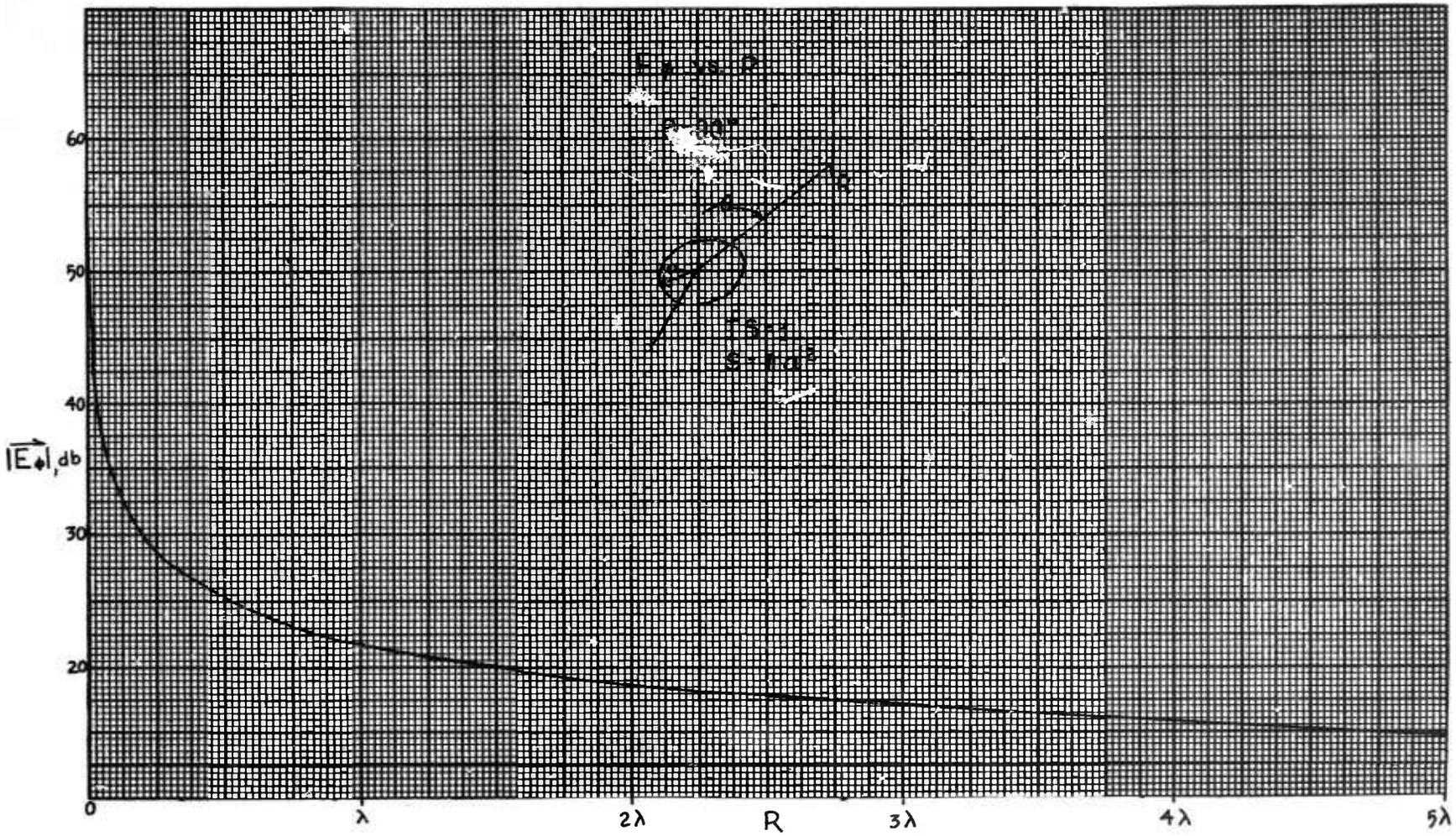

Figure 3.3.1-15. Expanded View of Figure 3.3.1-14 for $0 < R \leq 2\lambda/5$

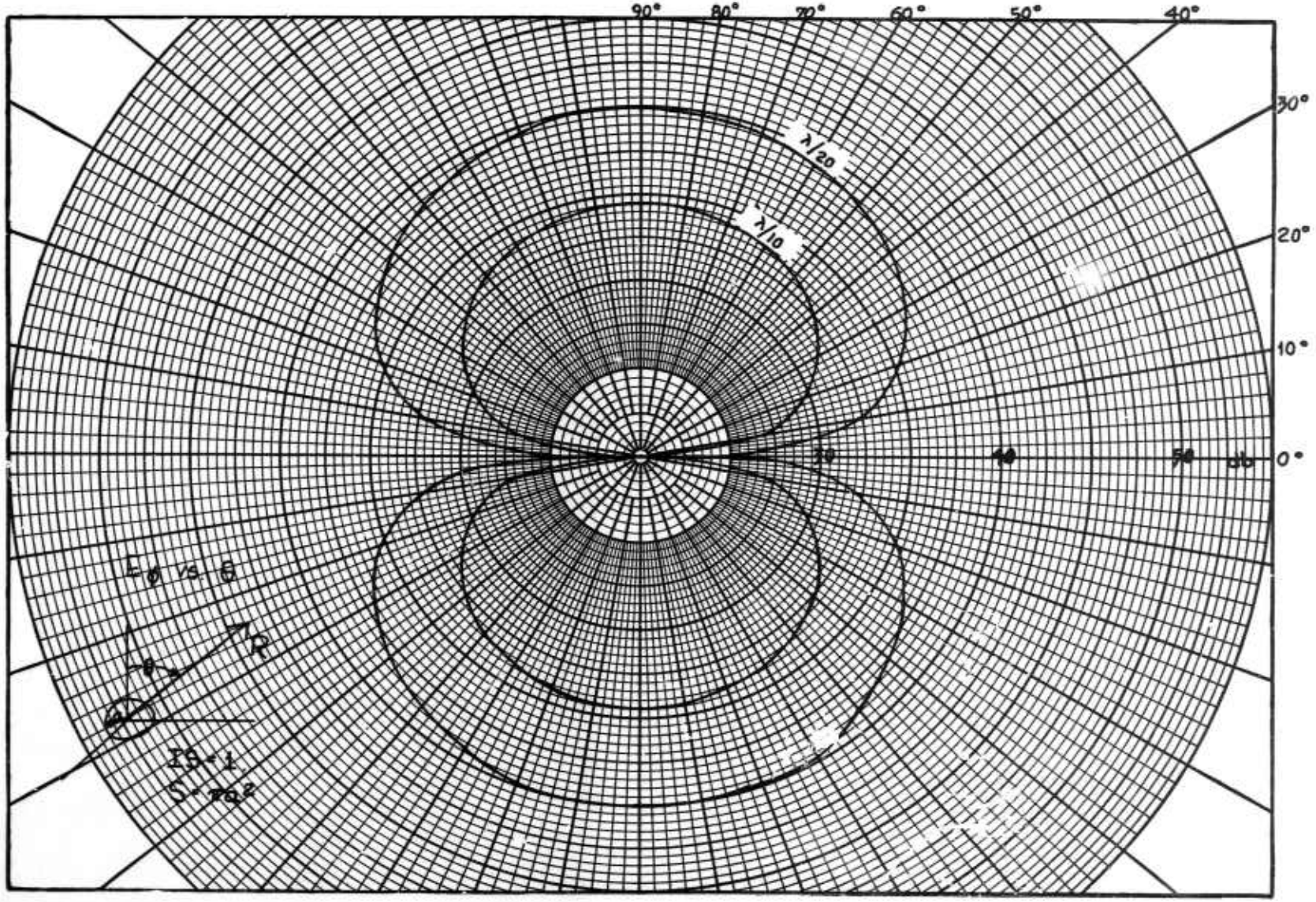

Figure 3.3.1-16. Polar Plots of $|E|$ for Small Electric Current Loop, $R = \lambda/20, \lambda/10$

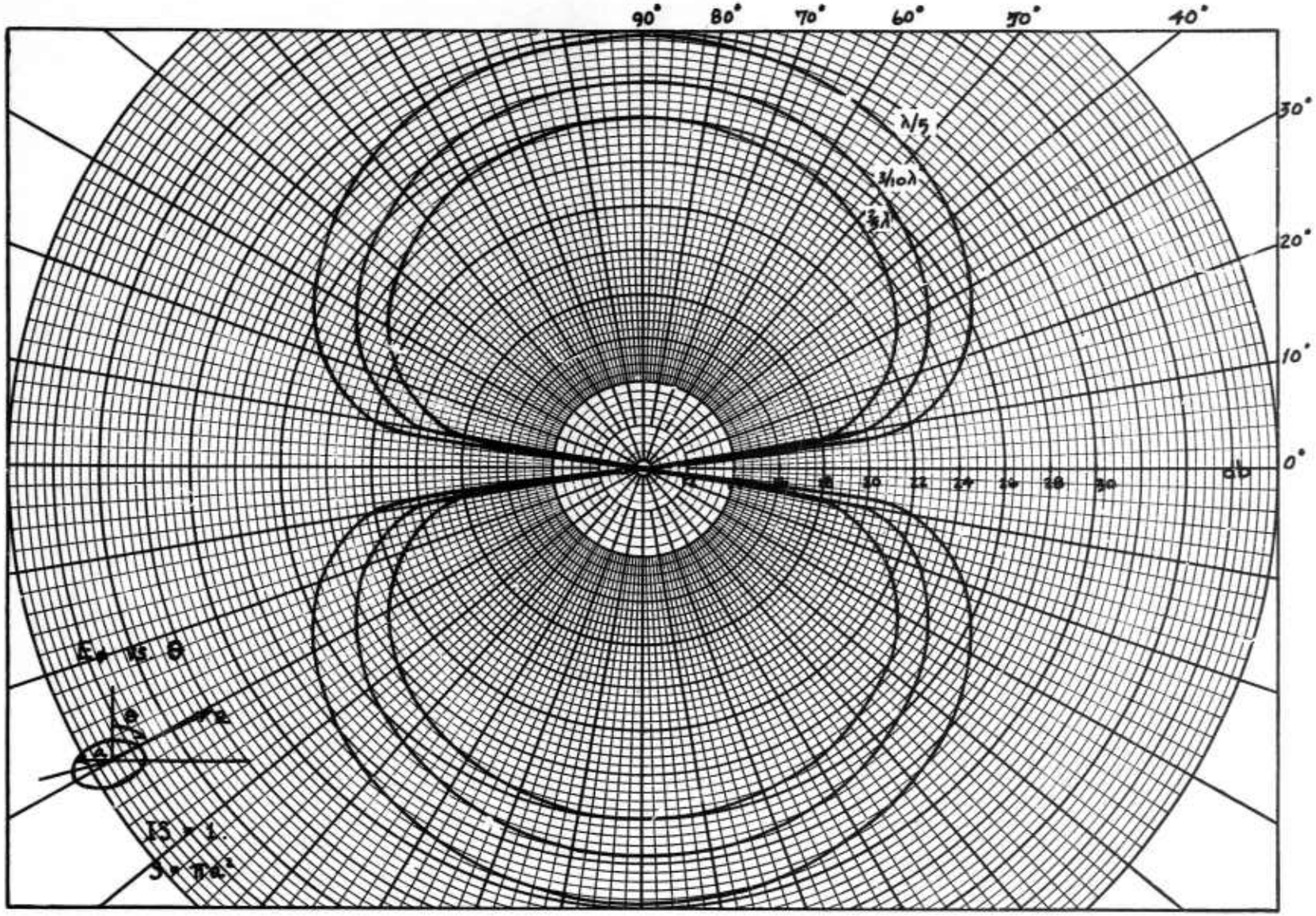

Figure 3.3.1-17. Polar Plots of $|E|$ for Small Electric Current Loop, R = 2λ/5, 3λ/10, λ/5

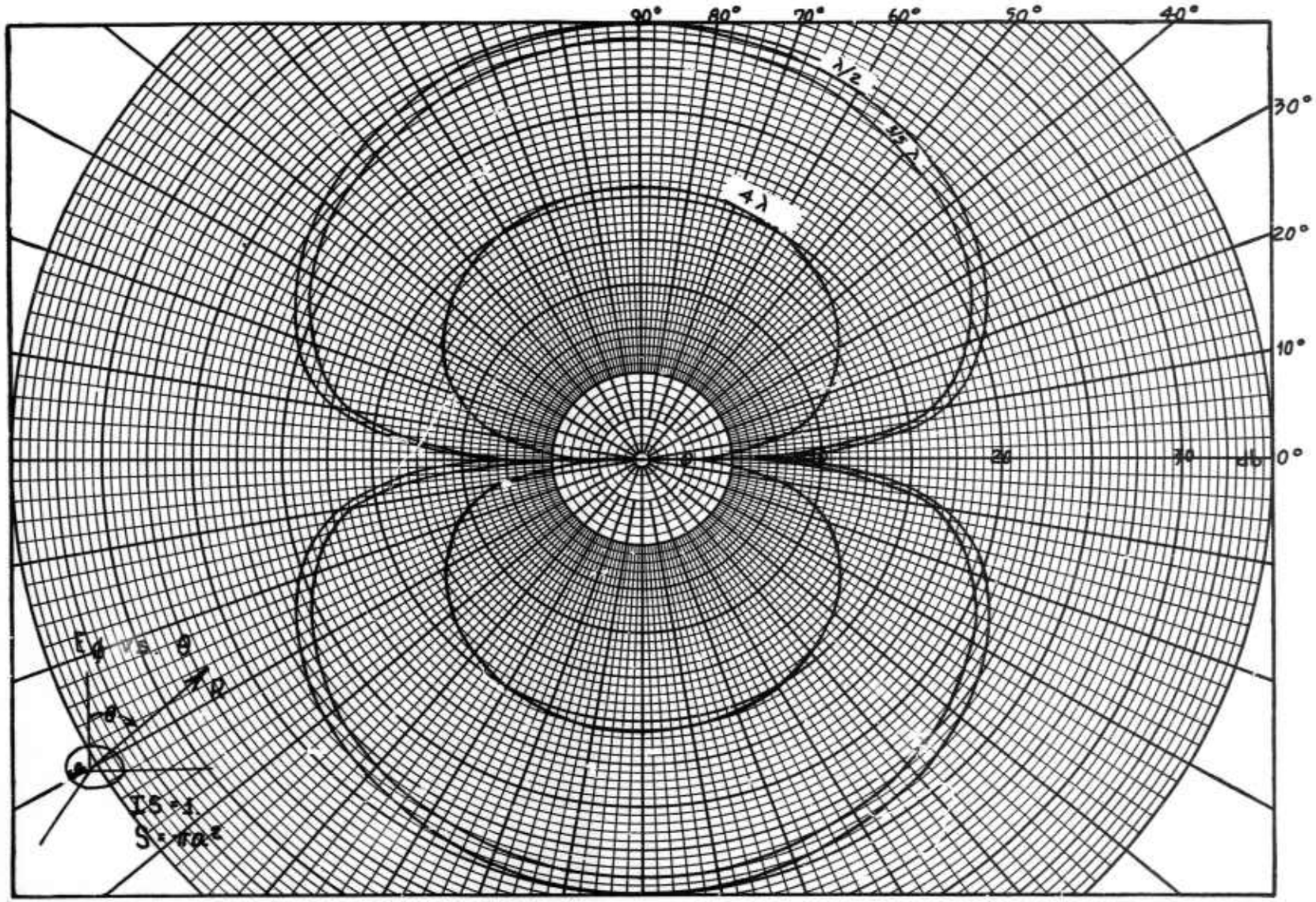

Figure 3. 3. 1-18. Polar Plots of $|E_\phi|$ for Small Electric Current Loop, R = λ/2, 3λ/5, 4λ

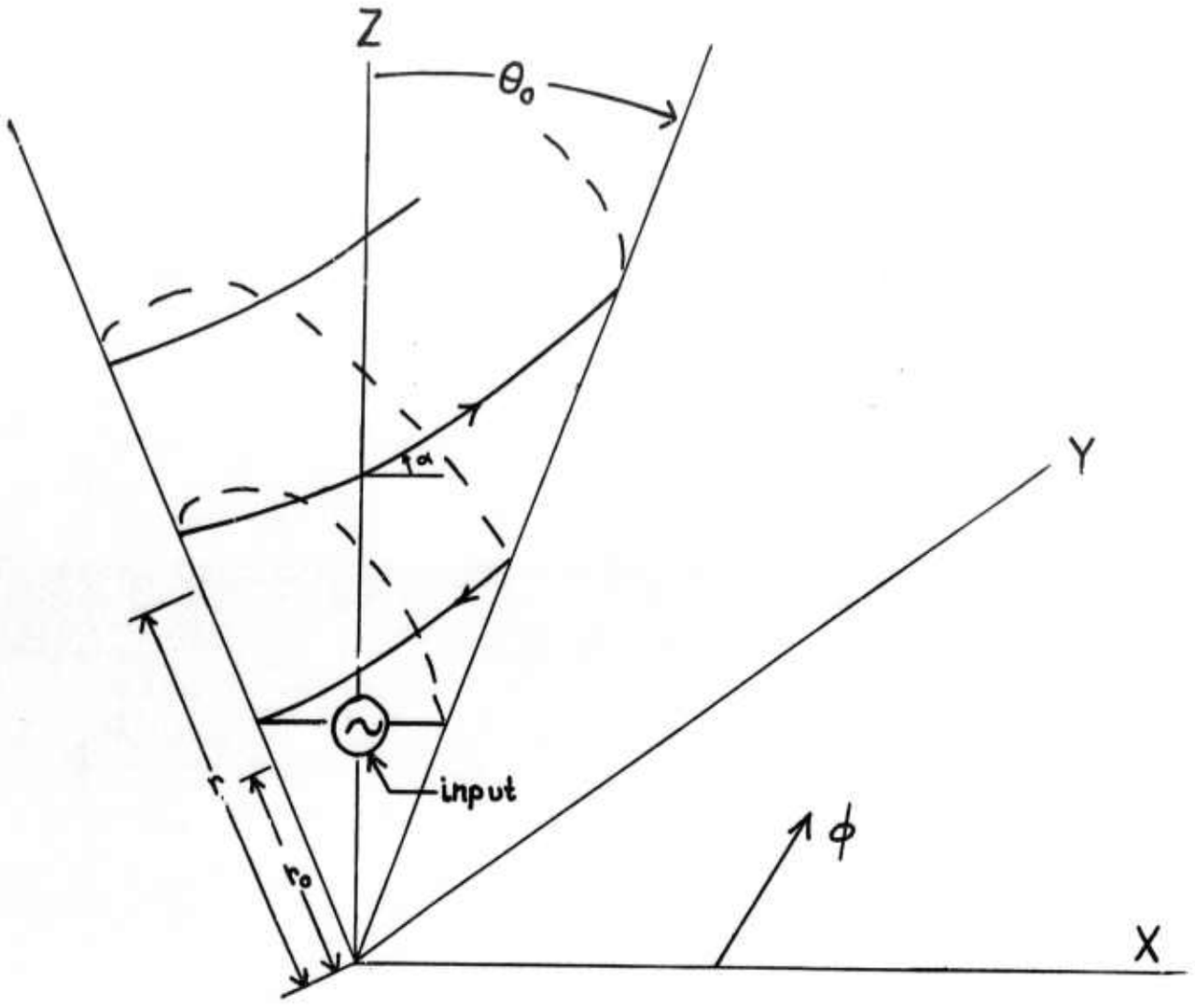

Figure 3.3.1-19. Configuration of Conical Equiangular Spiral Antenna (CESA) of Cone Angle θ_o and Pitch Angle α

3.3.2 FLOW FIELD GRADIENTS

The above discussion indicates the importance of field gradients in antenna breakdown. It is possible to consider such gradients as equivalent to an additional electron loss mechanism. In a similar way, the nonuniform flow field around a reentry vehicle can be effectively an electron loss mechanism. Among these effects are gradients of gas density, convective velocity, temperature, composition, and electron density. Thus, all the terms in the coefficient of ψ in the continuity equation are subject to gradients. The complete solution of the reentry breakdown problem must consider these nonuniform properties, as Fante[10] has indicated in an approximate analysis using a two-layered model.

3.4 ILLUSTRATIVE CALCULATIONS

The continuity equation in the reentry environment can be written in the following form as a breakdown condition*:

$$\nu_n = \frac{D_s}{\Lambda_e^2} + \frac{1}{\tau} \ln\left(\frac{n_B}{n_1}\right) + \frac{V^2}{4D_s} \qquad (3.4\text{-}1)$$

assuming an effective diffusion length Λ_e, transitional diffusion coefficient D_s, effective velocity V, and initial flow field electron density n_1 can be defined. A convenient set of proper variables is $(p^*\lambda)$, (λ/Λ), and the number N of rf cycles in a pulse of duration τ.

$$\frac{\nu_n}{p^*} = \frac{(D_s p^*)}{(p^*\lambda)^2}\left(\frac{\lambda}{\Lambda_e}\right)^2 + \frac{c}{N(p^*\lambda)} \ln\left(\frac{n_B}{n_1}\right) + \frac{V^2}{4(D_s p^*)} \qquad (3.4\text{-}2)$$

Now the reentry effects can be written in terms of a number of parameters, including (p/p^*), (D_s/D_-), (Λ/Λ_e), γ_o, and γ_1, where Λ is the diffusion length of the antenna in the absence of flow field gradients.

*As pointed out above, this form of velocity effect may be conservatively large, but it is easily changed by dropping the last term and changing τ to L/V, whichever is smaller.

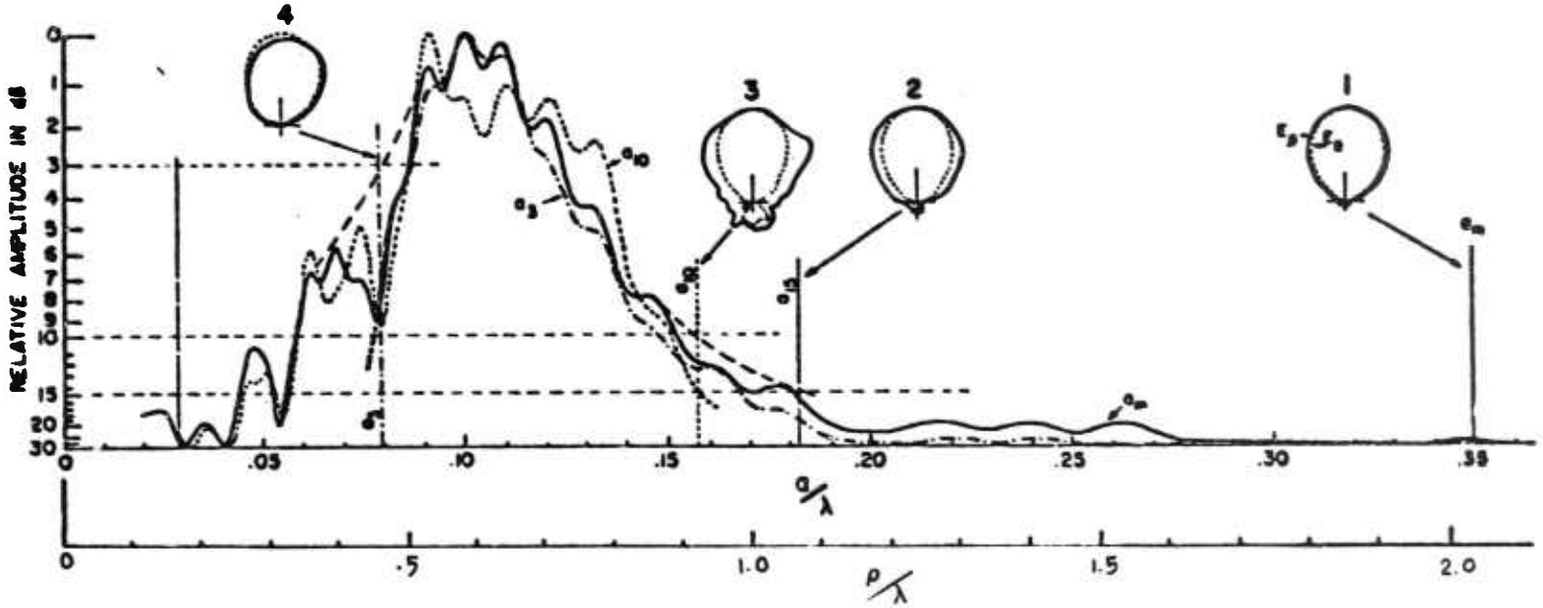

Figure 3.3.1-20. Amplitude of Near-Fields Measured With a Small Shielded Loop Probe Along the Surface of One Cone and Electric Far-Field Radiation Patterns Corresponding to a Truncation at Indicated Points (From J. D. Dyson, Trans. IEEE, Ant. and Prop., Vol AP-15, Page 488, July 1965)

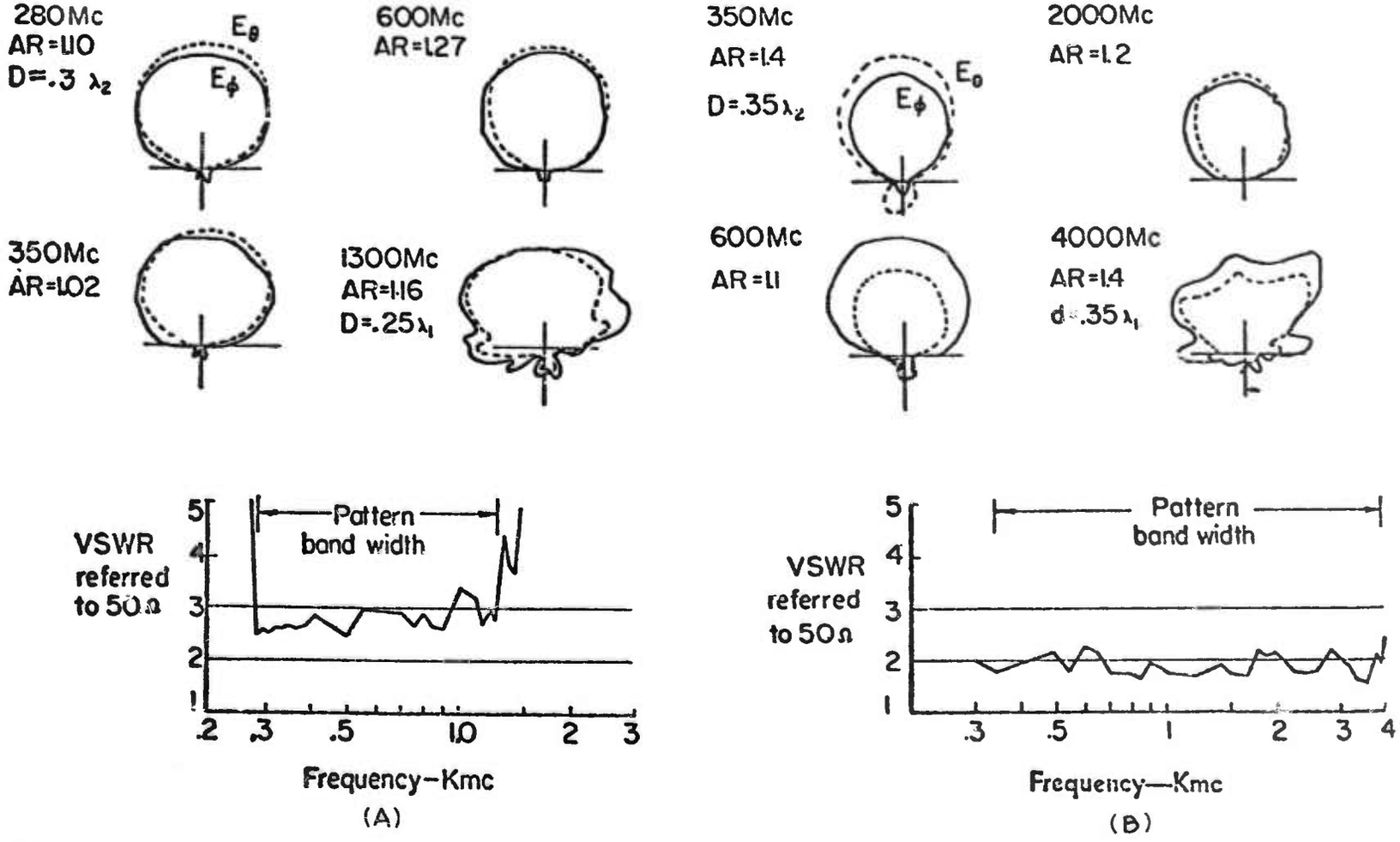

Figure 3.3.1-21. Electric Field Radiation Patterns and VSWR of (A) Wire Antenna and (B) Conical Antenna With RG 141/U Arms. $\theta = 10^{o}$, b = 0.053, D = 30 cm, $\alpha = 73^{o}$ $\phi = 0^{o}$, K = Not Constant, AR = Axial Ratio on Axis (From J. D. Dyson, Trans. IEEE, Ant. and Prop., Vol AP-7, Page 329, October 1959)

$$\gamma_o = \frac{c}{N(p\lambda)} \ell n\left(\frac{n_B}{n_o}\right) \tag{3.4-3}$$

$$\gamma_1 = \frac{c}{N(p\lambda)} \ell n\left(\frac{n_1}{n_o}\right) \tag{3.4-4}$$

where c is the speed of light, p is the free stream pressure ($p \cong p^*$), and n_o is the initial electron density in the ordinary pulse breakdown criterion.

$$\frac{\nu_n}{p^*} = \left(\frac{p}{p^*}\right)\left[\frac{(D_- p)}{(p\lambda)^2}\left(\frac{\lambda}{\Lambda}\right)^2\left(\frac{\Lambda}{\Lambda_e}\right)^2\left(\frac{D_s}{D_-}\right) + \gamma_o - \gamma_1 + \frac{V^2}{4(D_- p)}\left(\frac{D_s}{D_-}\right)\right] \tag{3.4-5}$$

A little manipulation gives the result in the following form:

$$\frac{\nu_n}{p^*} = \frac{p}{p^*}\left[\left(\frac{\nu_n}{p^*}\right)_o \left\{\left(\frac{D_s}{D_-}\right)\left(\frac{\Lambda}{\Lambda_e}\right)^2 + \left(\frac{D_-}{D_s}\right)\left[\frac{V(p\lambda)}{2(D_- p)}\left(\frac{\Lambda}{\lambda}\right)\right]^2\right\} + \gamma_o - \gamma_1\right] \tag{3.4-6}$$

where the CW breakdown ionization frequency without reentry effects is

$$\left(\frac{\nu_n}{p^*}\right)_o = \frac{(D_- p)}{(p\lambda)^2}\left(\frac{\lambda}{\Lambda}\right)^2 \tag{3.4-7}$$

This equation shows the effects of reentry directly in each of its terms. The first term shows that diffusion is affected by the transitional diffusion coefficient and by gradients. The second term shows that the convection effect is important at high pressure and when diffusion is inefficient. The last two terms show that flow field ionization tends to decrease the effect of pulsed signals.

The effects of reentry on the breakdown power of an antenna can be related to the ionization frequency by using Equation 3.2.1-2. Consider a simple illustrative case, using $\lambda/\Lambda = 2\pi$, $N = 10^3$, $n_B/n_o = n_1/n_o\ 10^8$, $p^*/p = 4.5$, $v = 2 \times 10^4$ feet/second, and $\Lambda/\Lambda_e = 3$. In the presence of ionization we reduce D_s to 0.01 D_-. (Note that in the finite time theory of convection the pulse length used in this example is equivalent to an antenna length of 0.02 λ.) Table 3.4-1 shows the results for $p\lambda$ = 36 cm torr.

These results show that the effect of convection is weak in the absence of ionization, except in the space charge coupled theory, in which case it represents the largest effect shown. The latter theory is not shown for the case of ionization (ambipolar diffusion), since it is then identical with the conventional theory.

In addition to the effects shown in the table, the effects of gas temperature and composition on the net ionization frequency must be considered. As shown in Figure 3.2.2-1, the gas temperature effect can be on the order of 6 db in the shock layer. At any rate, the gas temperature effect will tend to reduce the numbers shown in the last column of Table 3.4-1. Gas composition may have either kind of effect.

This type of table is useful in predicting where breakdown will occur, by searching for the lowest db values. For example, if the conventional convection theory is correct, then CW breakdown will occur in the free stream, assuming that the antenna field does not fall off too rapidly. Pulse breakdown may be affected by gas temperature enough to cause breakdown in the shock layer. If the space charge coupled theory is true, then the presence of shock layer ionization (there, conventional convection theory is equivalent to space charge coupled theory) will make the free stream and shock layer roughly equivalent. High gas temperature will then cause breakdown in the shock layer.

The above discussion applies only to one value of $p\lambda$, which has been chosen near the normal breakdown minimum. The results are more generally useful if we consider the net ionization frequency as a measure of the importance of a given effect, keeping in mind that, relative

Table 3.4-1. Typical Effects of Reentry on Antenna Breakdown

Conditions	ν_n/p^* (sec torr)$^{-1}$	Breakdown Power, db
Free stream:		
CW	4.9×10^4	0
Pulse	1.5×10^7	+8.1
CW, v	1.1×10^5	+0.8
CW, v*	5.9×10^8	+14.1
Pulse, v	1.5×10^7	+8.1
Pulse, v*	5.9×10^8	+14.1
Shock layer:		
CW	1.1×10^4	+9.5
CW, n_1	1.1×10^2	+9.3
CW, n_1, Λ_e	1×10^3	+9.3
CW, n_1, Λ_e, v	1.3×10^6	+14.2
CW, Λ_e, v	1.1×10^5	+10.8
CW, Λ_e, v*	1.2×10^8	+21.5
Pulse	3.4×10^6	+15.7
Pulse, n_1	1.1×10^2	+9.3
Pulse, n_1, Λ_e	1×10^3	+9.3
Pulse, n_1, Λ_e, v	1.1×10^5	+14.2
Pulse, Λ_e, v	3.5×10^6	+15.7
Pulse, Λ_e, v*	1.2×10^8	+21.5

NOTE: In the Conditions column, n_1 refers to ionization effects, Λ_e refers to gradients, v refers to convection, and v* is convection in the space charge coupled theory.

to the diffusion effect, the convection effect scales as $(p\lambda)^2$ and the pulse effect as $p\lambda$. For example, on the low pressure side of the breakdown curve the breakdown power is proportional to the square of the net ionization frequency and there is a 13 db increase in free stream breakdown field over the shock layer values. It is easily seen then that at one-tenth of the pressure discussed above, the diffusion effect would dominate over all others and the only significant reentry effects would be ionization and gradients.

3.5 RECOMMENDATIONS

From the above discussions it is evident that the theoretical prediction of antenna breakdown in a reentry environment presents a number of problems at the present time. The most serious theoretical problem is the effect of high gas temperature, where theoretical models are practically nonexistent and experimental data cover only a narrow range of conditions. Therefore effort is needed in the following areas of development:

a. Breakdown data at high temperature is needed over a wider range of laboratory experiment conditions.

b. Phenomenological models need to be developed and checked against the data.

c. Crucial experiments are needed to verify the models once they have been derived.

The convective effect is important only in view of the widely different theoretical approaches presently extant. The older theories can be shown to be approximately equivalent in the broad sense, and on the basis of these alone the effect of convection would not be significant in reentry. However, the coupled convection-diffusion-space charge theory predicts much stronger effects. More theoretical work is needed in formulating breakdown criteria and resolving inconsistencies among the theories. Laboratory experiments over an extended range of conditions of velocity, electron density, and diffusion length are needed to settle the observational facts and to give crucial tests of the theory. At the present time it appears that some experimenters see one effect and others see the other.

Careful theoretical analyses are needed in order to predict the breakdown of an antenna in the reentry environment in terms of a solution of the continuity equation. The factors which need careful attention are breakdown criteria in terms of effects of ionization and convection, near-field gradients, and gradients of flow field properties.

The fact that many flow field parameters in addition to ionization tend to affect breakdown means that the effects of reentry will be difficult to isolate in a flight experiment. In view of the fact that flight experiments should be conducted as a final step in verifying the importance of various reentry effects, it is a necessity to take all possible steps to design such flight experiments to give the needed isolation of the various important effects of reentry. This consideration is just as important as doing a straightforward system test experiment by flying a given antenna and vehicle system, since the system test results are difficult to extrapolate to other situations.

SECTION 4
EXPERIMENT DESIGN REQUIREMENTS

This section is intended to give the general relationships between the design requirements and the objectives of antenna breakdown experiments. It derives requirements on the signal characteristics (pulse length) and the field geometry (antenna design) needed to meet various experiment objectives. A decision to design an experiment for a given set of detailed objectives would then lead to specific requirements on the pulse length and antenna design. Requirements on pulse amplitude automatically result from these two requirements.

Various possible objectives of antenna breakdown experiments can be anticipated, but these are generally of two types, namely system tests and basic data experiments. The objective of a system test is to obtain data on the extent to which the reentry environment changes the antenna power handling capability relative to that in a static environment, for a given antenna, signal, and vehicle system. This type of experiment gives only a single "system data point" in that its results cannot rightfully be extrapolated to other systems. On the other hand, the general objective of a basic data type of experiment is to yield data which can be extrapolated to other systems, because it gives basic data on the magnitude and form of the effect which a given specific feature of the reentry environment has on antenna breakdown.

The technical requirement of a system test type of experiment is that it simulate all of the reentry effects without compromising the ability to obtain usable data. The technical requirement of a basic data experiment is that it provide data on the effect of only one of the reentry environmental factors at a time.

The basis for the establishment of experiment requirements can be derived from the equations of Section 3.4, in which the quantities N and λ/Λ enter as controllable parameters. N is proportional to the pulse length and within limits λ/Λ is a function of the antenna geometry. The object of this section is to obtain the condition on these two parameters for which each of the various reentry effects dominates. The result will be expressible in terms of a graph of N versus λ/Λ showing regions in which each of these effects dominates.

The equation which we use as the basis for these calculations is

$$\frac{\nu_i}{p} = \frac{\nu_a}{p} + \frac{(D_- p)}{(p\lambda)^2}\left(\frac{\lambda}{\Lambda}\right)^2\left(\frac{D_s}{D_-}\right) + \frac{c}{N(p\lambda)}\ln\left(\frac{n_B}{n_o}\right) + \frac{V^2}{4(D_s p)}\left(\frac{D_s}{D_a}\right) \qquad (4\text{-}1)$$

where ν_i and ν_a are the ionization and attachment frequencies, respectively. In order to give realistic representation of the attachment we use MacDonald's[23] value of 2.12×10^4 $(\text{sec torr})^{-1}$ for ν_a/p.

Before proceeding to the specification of requirements on the controllable parameters N and ν/Λ, it is helpful to take account of the fact that transmitter power output is always a practical consideration. Thus it is necessary to conduct experiments in an altitude regime near the breakdown minimum, which we assume to correspond to a value of 36 cm torr for $p\lambda$. The boundaries of the regions in which each of the terms in this equation dominates over the sum of all of the others are then given by simple equations between N and λ/Λ, which are plotted in Figure 4-1. In this figure the regions of the N versus λ/Λ space marked by arrows are dominated by the different effects indicated. In general, the shapes of these boundaries will be the same regardless of what part of the breakdown curve is considered. As is evident, the value of the diffusion coefficient has a strong effect. Note also that the slight separation between the convection boundary and the pulse and diffusion boundaries is caused by attachment being nearly equal to convection in the free diffusion regime.

It is possible to construct similar boundaries for the breakdown control regions for other values of velocity and $p\lambda$, but it is more convenient to consider only the asymptotes of these curves, keeping in mind the general shapes as modeled by Figure 4-1. Different conditions merely move these asymptotes around the graph without rotation.

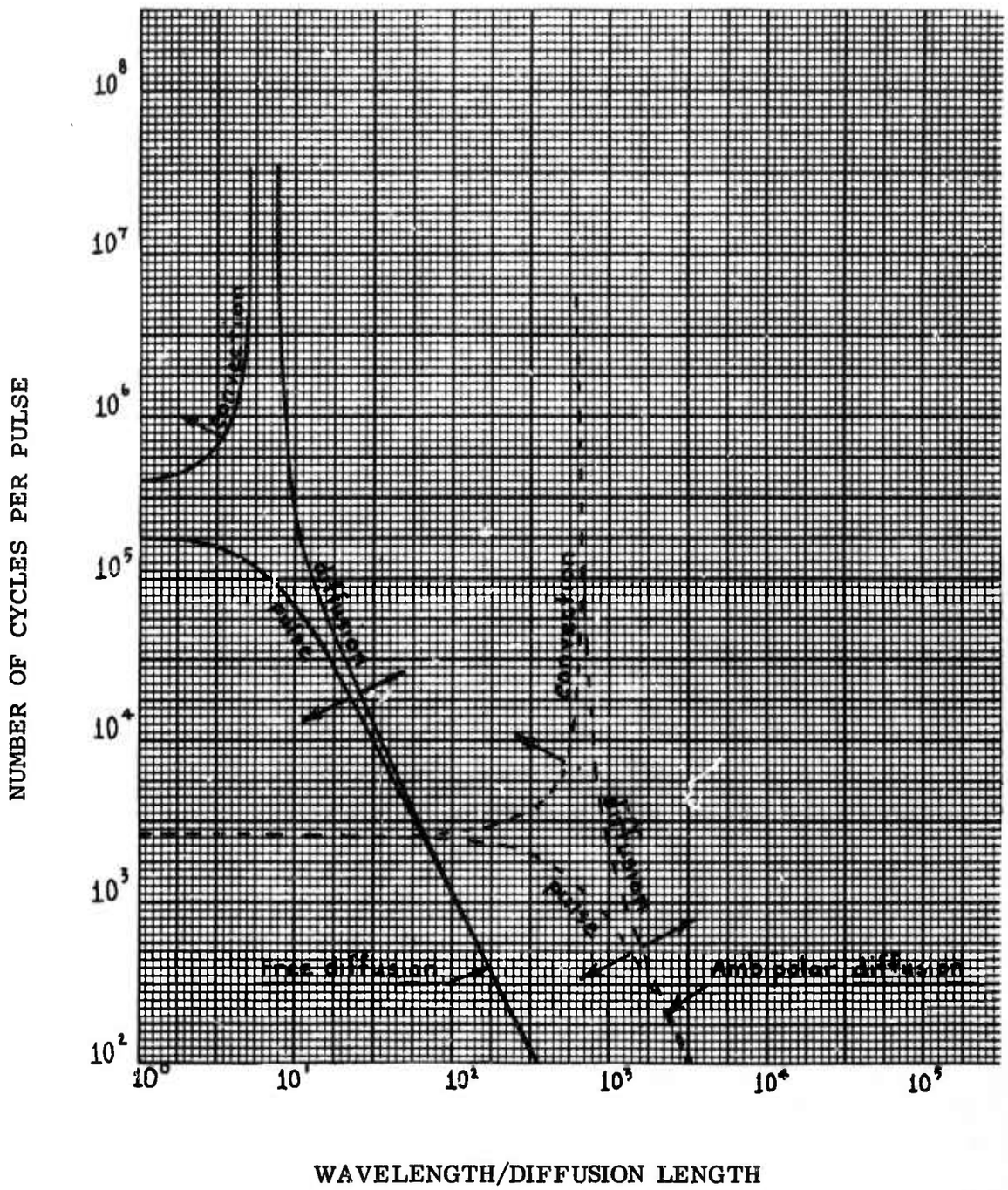

Figure 4-1. Breakdown Control Regions, p = 36 cm torr, V = 2×10^4 Feet/Second

The pulse-diffusion control boundary has the asymptotic form of

$$N\left(\frac{\lambda}{\Lambda}\right)^2 = \frac{c\,(p\lambda)}{D_- p}\left(\frac{D_-}{D_s}\right) \ell n\left(\frac{n_B}{n_o}\right)$$

$$= 3.45 \times 10^5\,(p\lambda)\left(\frac{D_-}{D_s}\right) \qquad (4\text{-}2)$$

The convection effect dominates over attachment at velocities of 12,000 and 1200 feet/second for free and ambipolar diffusion, respectively. (The space charge coupled theory would give a value of 120 feet/second for free diffusion.) The diffusion-convection boundary is

$$\frac{\lambda}{\Lambda} = \frac{V\,(p\lambda)}{2\,(D_- p)}\left(\frac{D_-}{D_s}\right)$$

$$= 3.1 \times 10^{-7}\,V\,(p\lambda)\left(\frac{D_-}{D_s}\right) \qquad (4\text{-}3)$$

and the diffusion-attachment boundary is

$$\frac{\lambda}{\Lambda} = (p\lambda)\sqrt{\left(\frac{\nu_a}{p}\right)\left(\frac{1}{D_- p}\right)\left(\frac{D_-}{D_s}\right)}$$

$$= 0.115\,(p\lambda)\sqrt{D_-/D_s} \qquad (4\text{-}4)$$

The pulse-convection boundary is

$$N = \frac{4c\,D_-\,p}{(p\lambda)\,V^2}\left(\frac{D_s}{D_-}\right)\ell n\left(\frac{n_B}{n_o}\right)$$

$$= \frac{3.5 \times 10^{18}}{(p\lambda)\,V^2}\left(\frac{D_s}{D_-}\right) \qquad (4\text{-}5)$$

and the pulse-attachment boundary is

$$N = \frac{c}{(p\lambda)\,(\nu_a/p)}\,\ell n\left(\frac{n_B}{n_o}\right)$$

$$= \frac{2.6 \times 10^{7}}{(p\lambda)} \qquad (4\text{-}6)$$

Note that the space charge coupled convection theory reduces N at the pulse-convection boundary by a factor of 10^4.

In order to extend the conditions for these criteria beyond the breakdown minimum, consider the high pressure side of the curve, which is dominated by the effective field effect:

$$(p\lambda) = 36\sqrt{2p/p_o - 1} \qquad (4\text{-}7)$$

where p/p_o is the breakdown power relative to the minimum value. Thus, for example, the value of $p\lambda$ is increased by 4.35 when the breakdown power is 10 db above the minimum on the high pressure side, increasing $N\,(\lambda/\Lambda)^2$ at the pulse-diffusion boundary by the same factor. Also λ/Λ at the attachment or convection-diffusion boundary is increased by the same amount. The value of N at the attachment or convection-pulse boundary is reduced by this factor.

On the low pressure side of the curve, only diffusion or pulse effects can be important and the attachment/convection region does not exist. The effective field on this side of the curve is given by

$$\frac{E_e}{p} = \frac{E\lambda}{36} \tag{4-8}$$

while at the minimum breakdown field,

$$\left(\frac{E_e}{p}\right)_o = \frac{E_o\lambda}{36\sqrt{2}} \tag{4-9}$$

Thus, if we use the power law for the ionization frequency,

$$\left(\frac{\sqrt{2}\,E}{E_o}\right)^{5.34} = \frac{\dfrac{D_s p}{(p\lambda)^2}\left(\dfrac{\lambda}{\Lambda}\right)^2 + \dfrac{c}{p\lambda N}\,\ell n\left(\dfrac{n_B}{n_o}\right)}{\dfrac{D_s p}{(36)^2}\left(\dfrac{\lambda}{\Lambda}\right)^2 + \dfrac{c}{36N}\,\ell n\left(\dfrac{n_B}{n_o}\right)} \tag{4-10}$$

Simultaneous solution of Equations 4-2 and 4-10 gives

$$N(\lambda/\Lambda)^2 = 18c\left(\frac{D_-}{D_s}\right)\frac{\ell n\left(\dfrac{n_B}{n_o}\right)}{D_- p}\left[\sqrt{1 + 8\left(\frac{E_o}{\sqrt{2}E}\right)^{5.34}} - 1\right] \tag{4-11}$$

$$= 6.2 \times 10^6\left(\frac{D_-}{D_s}\right)\left[\sqrt{1 + 8\left(\frac{E_o}{\sqrt{2}E}\right)^{5.34}} - 1\right]$$

$$\cong 2.5 \times 10^7\left(\frac{D_-}{D_s}\right)\left(\frac{E_o}{\sqrt{2}E}\right)^{5.34}$$

The pulse-diffusion boundary at 10 db up from the minimum is then given by

$$N\left(\frac{\lambda}{\Lambda}\right)^2 = 8.5 \times 10^3 \left(\frac{D_-}{D_s}\right) \qquad (4\text{-}12)$$

If we consider 5 and 2 as the smallest practical values of N and λ/Λ, respectively, then solving for E/E_o, we find that for free diffusion pulse, controlled breakdown can be maintained only up to 18 db above the minimum (8 times the minimum field) on the low pressure side. Similar practical limitations appear in other factors involving diffusion controlled or pulse controlled breakdown on the high pressure side. However, it is generally true that an approach like that given above is necessary and useful to the design of meaningful experiments.

The following general considerations enter into the generation of experimental requirements on pulse length and antenna design. As indicated in Figure 4-2, an experiment designed to isolate one of the six phenomena listed requires the experiment design to lie in the region indicated. Regions 2 and 3 are pulse and diffusion regions, respectively, and region 1 is either convection or attachment. (Gas density experiments are less interesting than the others, because this effect is well understood.) A gas temperature experiment would best be done in region 2. Ionization experiments could be done in either region 3, using diffusion as an indicator, or region 1, using convection as an indicator. Effects of additives on attachment and ionization frequency could be isolated by doing an experiment with both long and short pulses, provided convection were eliminated from region 1. The short pulse would isolate the effects on the ionization frequency and the long pulse would give the additional effect on attachment. Gas temperature would have to be either minimized or accounted for by "turning off" the additive injection.

The design of a system test experiment is made more meaningful by the above techniques also. Generally it is necessary to conduct antenna breakdown experiments with a train of pulses of various amplitudes, the pulses which break down indicating the breakdown power level. But care must be taken so as not to change the effects of reentry by using pulses

EXPERIMENT	REQUIRED REGION
CONVECTION	1
DENSITY	2
GRADIENTS	3
TEMPERATURE	2
IONIZATION	3 (OR 1)
ADDITIVES	1* (AND 2)

1 = CONVECTION REGION
1* = ATTACHMENT REGION

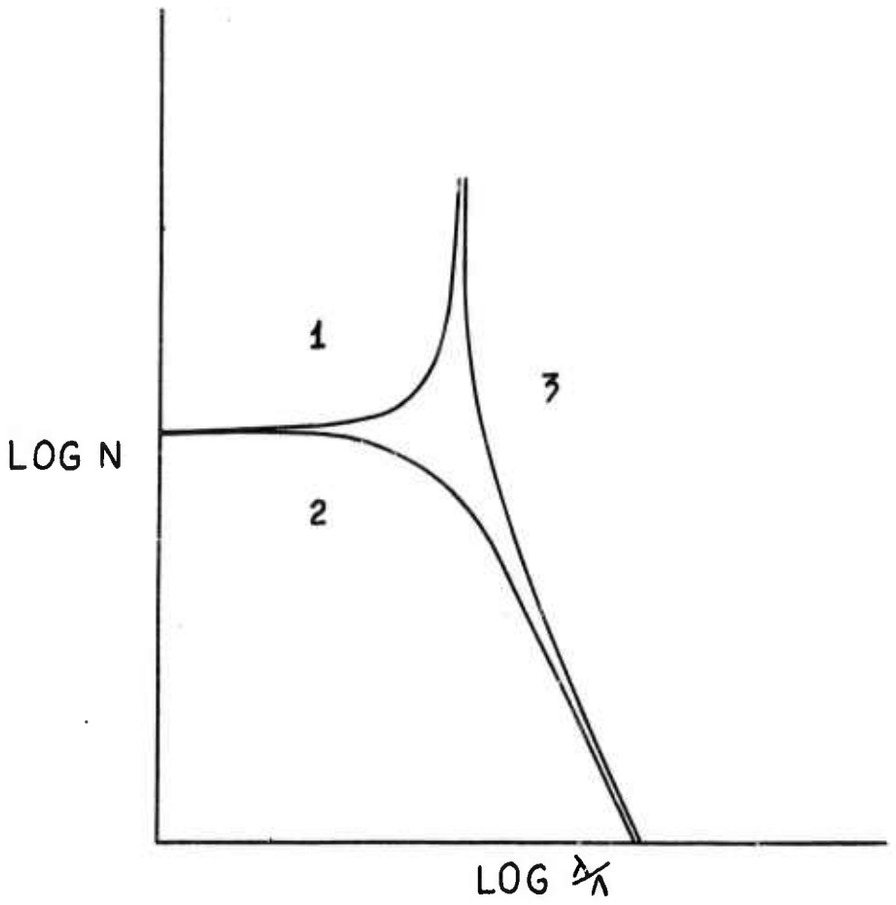

Figure 4-2. Pulse Length and Antenna Geometry Requirements for Basic Data Experiments

which are too short. Thus the experimental system must lie on the same side of the pulse control boundary as the actual system being tested. If the system lies in region 2, then the experiment must be designed with the same pulse length as the system itself.

To summarize the results of this section, we tabulate numerical values for the boundaries of the various control regions, using a flow velocity of 20,000 feet/second. For the diffusion-convection/attachment boundary we get the following results for the value of λ/Λ above which diffusion dominates:

	Breakdown Minimum	10 db Above Minimum at High Pressure
Convection, with free diffusion	6.8	30
Convection, with ambipolar diffusion, or with free diffusion in the space charge coupled theory	680	3000
Attachment, with free diffusion	4.1	18
Attachment, with ambipolar diffusion	41	180

For the pulse-convection/attachment boundary, the value of N below which the pulse length dominates is as follows:

	Breakdown Minimum	10 db Above Minimum at High Pressure
Convection, with free diffusion	2.6×10^4	6×10^3
Convection, with ambipolar diffusion	260	60
Convection, with free diffusion in the space charge coupled theory	2.6	0.6
Attachment	7.2×10^5	1.7×10^5

For the diffusion-pulse boundary the value of $N(\lambda/\Lambda)^2$ above which diffusion dominates is as follows:

Breakdown minimum: 1.2×10^7

10 db above minimum at high pressure: 5.4×10^7

10 db above minimum at low pressure: 8.5×10^3

The values of these last three results are increased by a factor of 100 by ambipolar diffusion.

The following list summarizes the values of N and λ/Λ needed to maintain the various control regions discussed above.

	N	λ/Λ
Convection	$> 2.6 \times 10^4$	< 6.8
Pulse	< 60*	$< 92/\sqrt{N}$
Diffusion**	$> 6 \times 10^5$	> 30

*Much lower values are required in the space charge coupled convection theory.

**This applies only to free diffusion. Much higher values apply with ambipolar diffusion or in the space charge coupled convection theory.

SECTION 5
CONCLUSIONS

The vibrational nonequilibrium effect on the flow field of a hypersonic, slightly blunt body has been found to be significant at 250,000 feet altitude. This conclusion has been reached through results of calculations using a superpositional technique. It is found that once the stagnation region streamlines expand around the conical region of the body, the vibrational temperature tends to freeze and approaches the equilibrium state only after a long distance. The vibrational temperature tends to be higher than the equilibrium temperature near the body and vice versa, away from the body. If high vibrational temperature decreases the breakdown field as suggested by Light and Taylor[16], then vibrational nonequilibrium may have an important effect on antenna breakdown, especially near the vehicle surface. However, boundary layer effects may change this conclusion.

Sufficient knowledge presently exists on the phenomena of reentry which affect antenna breakdown to permit an evaluation of their relative importance and to allow diagnostic experiments to be designed. But the effects of high gas temperature are not well understood theoretically, and more data are needed over a wider range of parameters. The effects of convection are important in terms of the conflicting theories, each of which can be supported by some form of experimental data. The effects of slender reentry vehicle flow fields on the solution of the electron continuity equation need to be examined more carefully in terms of breakdown criteria in order to resolve the convection conflict and provide a meaningful definition of pulse breakdown in the presence of flow field ionization.

BLANK PAGE

SECTION 6
REFERENCES

1. McMenamin, D. L., Jr., and O'Brien, M. E. "The Finite Difference Solution of Multicomponent Non-Equilibrium Steady Influscid Streamtube Flows Using a Novel Stepping Technique. Part I: Analysis and Applications." General Electric Company, TIS 67SD241, April 1967.

2. Burke, A. F.; Curtis, J. T.; and Boyer, D. W. "Non-Equilibrium Flow Considerations in Hypervelocity Wind Tunnel Testing." Cornell Aeronautical Laboratory, Report Number AA-1632-Y-1, May 1962.

3. Storer, E. M. "A Simple Method for Calculating the Stagnation Point Shock Detachment of Spherical Bodies in Supersonic Flow." General Electric Company, RSD ATCFM 64-2, May 1964.

4. Blottner, F. G. "Chemically Reacting Boundary Layer with Ablation Products and Nose Bluntness Effects (U)." General Electric Company, TIS R67SD14 (Confidential), April 1967.

5. Millikan, R. C. and White, D. R. "The Systematics of Vibrational Relaxation." General Electric Research Laboratory, Report Number 63-RL-(3411C), August 1963.

6. Bisbing, P. E.; McMenamin, D. L.; and Scherer, P. "Study to Obtain Design Data for Reentry ECM Antenna Systems (U)." Second Quarterly Technical Report, AFCRL-67-0585, General Electric Report No. 67SD7170, September 1967.

7. Kelly, D. and Margenau, H. "High Frequency Breakdown of Air." Journal of Appl. Phys., Vol. 31, No. 9, pp. 1617-1620, September 1960.

8. Covert, E. E. and Boedecker, L. R. "Studies of Antenna Breakdown in the Presence of a Plasma Sheath Including the Effects of Forced Convection." MIT Aerophysics Laboratory Report 135, AFCRL 670190, February 1967.

9. Romig, M. F. "Steady State Solutions of the Radiofrequency Discharge With Flow." Phys. of Fluids, Vol. 3, No. 1, p. 129, January 1960.

10. Fante, R. L. "Mathematical Analysis of Microwave Breakdown in Flowing Gases." IEEE Trans. on Antennas and Propagation, pp. 781-788, September 1965.

11. Allis, W. P. and Rose, D. J. "The Transition from Free to Ambipolar Diffusion." Phys. Rev., Vol. 93, No. 1, 1 January 1954.

12. Allis, W. P. "Motions of Ions and Electrons." Handbuch der Physik, Vol. XXI, Springer Verlag, Berlin (1956).

13. Gould, L. and Roberts, L. W. "Breakdown of Air at Microwave Frequencies." J. Applied Phys., Vol. 27, No. 10, p. 1162, October 1956.

14. Whitmer, R. F. and MacDonald, A. D. "RF Antenna Breakdown Conditions in the Presence of the Plasma Sheath." Proceedings of the First Plasma Sheath Symposium, W. Rotman and G. Meltz, ed., Pergamon Press, 1961.

15. Reilly, J. P. "Microwave Breakdown of the Air Around a Conical Re-Entry Vehicle." AVCO Research Report 214, BSDTR65157, April 1965.

16. Light, G. C. and Taylor, E. C. 'Antenna Breakdown in High Temperature Air." Aerospace Report No. TR1001 (2220-10), SSDTR67118, June 3, 1967.

17. Bisbing, P. E. "Analysis of an Antenna Breakdown Experiment in a Re-Entry Environment (U)." AMRAC Proceedings, Vol. XIII, November 1965.

18. Nanevicz, J. E.; Chown, J. B.; Vance, E. F.; and Martin, J. A. "SRI Participation in Voltage Breakdown and Rocket Charging Experiments on Nike Cajun Rocket," AFCRL66-588, August 1966.

19. MacDonald, A. D.; Gaskell, D. U.; and Gitterman, H. N. "Microwave Breakdown in Air, Oxygen, and Nitrogen." Phys. Rev., Vol. 130, No. 5, pp. 1841-1850, 1 June 1963.

20. Mentzoni, M. H. "Ambipolar Diffusion in an Isothermal Oxygen Plasma at Elevated Temperatures." Phys. Rev., Vol. 134, No. 1A, pp. A80-A85, 6 April 1964.

21. Epstein, M. "Antenna Breakdown in a Hypersonic Re-Entry Environment." ASTIA AD 473936, September 1965.

22. Cottingham, W. B. and Buchsbaum, S. J. "Electron Ionization Frequency in Hydrogen." Phys. Rev., Vol. 130, No. 3, pp. 1002-1006, 1 May 1963.

23. MacDonald, A. D. "High-Frequency Breakdown in Air at High Altitudes." Proc. IRE, pp. 436-441, March 1959.

24. Herlin, M. A. and Brown, S. C. "Breakdown of a Gas at Microwave Frequencies." Phys. Rev., Vol. 74, pp. 291-296, August 1948.

25. Scharfman, W. and Morita, T. "Focused Microwave Technique for Measurement of the Ionization Rate and Collision Frequency." J. Applied Phys., Vol. 35, No. 7, pp. 2016-2020, July 1964.

26. Sharbaugh, A. H.; Watson, P. K.; White, D. R.; Lee, T. H.; and Greenwood, A. "An Investigation of the Breakdown Strength of Nitrogen at High Temperatures with Use of a Shock Tube." Trans. AIEE (Power Apparatus and Systems), Vol. 80, pp. 333-344, June 1961.

27. Lee, T. H.; Greenwood, A. N.; and White, D. R. "Electrical Breakdown of High-Temperature Gases and Its Implications in Post-Arc Phenomena in Circuit Breakers." IEEE Trans. on Power Apparatus and Systems, Vol. PAS-84, No. 12, pp. 1116-1125, December 1965.

28. Taylor, W. C.; Chown, J. B.; and Morita, T. "Measurements of RF Ionization Rates in High Temperature Air." Stanford Res. Inst., AFCRL-67-028, March 1967.

29. Brown, S. C. and MacDonald, A. D. "Limits for the Diffusion Theory of High Frequency Gas Discharge Breakdown." Phys. Rev., Vol. 76, pp. 1629-1633, December 1949.

30. Herlin, M. A. and Brown, S. C. "Electrical Breakdown of a Gas Between Coaxial Cylinders at Microwave Frequencies." Phys. Rev., Vol. 74, No. 8, pp. 910-913, 15 October 1948.

31. Herlin, M. A. and Brown, S. C. "Microwave Breakdown of a Gas in a Cylindrical Cavity of Arbitrary Length." Phys. Rev., Vol. 74, No. 11, pp. 1650-1656, 1 December 1948.

32. MacDonald, A. D. and Brown, S. C. "Electron Diffusion in a Spherical Cavity." Can. J. Res., Vol. A28, pp. 168-174, 1950.

33. MacDonald, A. D. Microwave Breakdown in Gases. Wiley, New York (1966).

34. Samaddar, S. N. "Study of ECM Antenna Optimization." Report AFCRL-67-0348, Raytheon Company; March 1967.

35. Lyon, J. A. M., et al. "Study and Investigation of a UHF-VHF Antenna." University of Michigan, May 1966, AD 485835.

36. Andre, S. "Study of Antenna Voltage Breakdown in a Shock Tunnel (U)." Cornell Aeronautical Laboratory Report No. UB-2394-E-Z; July 1967. (Confidential)

37. "Electronic Warfare Technology Techniques (U)." Syracuse University Research Corporation, Report No. SPL-997; September 30, 1966 (Secret).

38. Bisbing, P. E., et al. "Study to Obtain Design Data for Reentry ECM Antenna Systems." First Quarterly Report, GE Report No. 67SD5232, AFCRL-67-0473, Volume 1, June 1967.

39. Yeh, Y. S. and Mei, K. K. "Theory of Conical Equiangular Spiral Antennas. Part I - Numerical Technique." IEEE Trans. Ant. & Prop., Vol. AP-15, p. 634; September 1967.

40. Chatterjee, J. S. "Radiation Field of a Conical Helix." J. Appl. Phys., Vol. 24, p. 550, May 1953; see also R. Mittra and P. W. Klock, "A Theoretical Study of the Conical Spiral Antenna." Antenna Lab., University of Illinois; AD 483194.

41. Dyson, J. D. "The Characteristics and Design of the Conical Log-Spiral Antenna." IEEE Trans. Ant. & Prop., Vol. AP-13, p. 488; July 1965. Also "The Unidirectional Equiangular Spiral Antenna." op. cit., Vol. AP-9, p. 329; October 1959.

Security Classification Unclassified

DOCUMENT CONTROL DATA - R&D

(Security classification of title, body of abstract and indexing annotation must be entered when the overall report is classified)

1. ORIGINATING ACTIVITY *(Corporate author)*
General Electric Company
Reentry Systems Dept. Missile & Space Div.
Box 8555, Philadelphia, Pennsylvania 19101

2a. REPORT SECURITY CLASSIFICATION
Unclassified

2b. GROUP

3. REPORT TITLE
STUDY TO OBTAIN DESIGN DATA FOR REENTRY ECM ANTENNA SYSTEMS

4. DESCRIPTIVE NOTES *(Type of report and inclusive dates)*
Scientific Interim

5. AUTHOR(S) *(First name, middle initial, last name)*
Paul E. Bisbing,
Daniel L. McMenamin
Arthur K. Jordan

6. REPORT DATE
December 1967

7a. TOTAL NO. OF PAGES

7b. NO. OF REFS

8a. CONTRACT OR GRANT NO.
F 19(628)-67-C-0210 ARPA Order

b. PROJECT, TASK, WORK UNIT NOS.
8671-00-01 Amed. No. 1

c. DOD ELEMENT
6250301R

d. DOD SUBELEMENT
None

9a. ORIGINATOR'S REPORT NUMBER(S)
GE Report No. 67SD7343
Third Quarterly Technical Report
Vol. 1 of 2

9b. OTHER REPORT NO(S) *(Any other numbers that may be assigned this report)*
AFCRL-68-0037

10. DISTRIBUTION STATEMENT
2 - This document is subject to special export controls and each transmittal to foreign governments or foreign nationals may be made only with prior approval of AFCRL (CRDM), L.G. Hanscom Field, Bedford, Massachusetts 01730

11. SUPPLEMENTARY NOTES
This research was sponsored by the Advanced Research Projects Agency

12. SPONSORING MILITARY ACTIVITY
Air Force Cambridge Research Laboratories (CDR)
L. G. Hanscom Field
Bedford, Massachusetts 01730

13. ABSTRACT

This report presents survey material on the effects of the reentry environment on the voltage breakdown characteristics of antennas. Enough is presently known about these effects to indicate their relative importance and to allow meaningful experiments to be designed to diagnose them. Effects of convection are not well understood because of conflicts among various theories and experimental data. High gas temperature effects are not adequately explained and insufficient data presently exist to allow extrapolation with confidence.

Results of some illustrative calculations of flow fields about a typical slightly blunt-nosed body are presented, including an assessment of the vibrational nonequilibrium effect, which is found to be important.

DD FORM 1 NOV 65 1473

Unclassified
Security Classification